A NUMERICAL STUDY OF THE RESPONSE OF BLAST LOADED THIN CIRCULAR PLATES, WITH BOTH CLAMPED AND INTEGRAL BOUNDARY CONDITIONS

by

MARK ERNEST GELMAN

1996

Submitted to the University of Cape Town
in partial fulfilment of the requirements for the
Degree of Master of Science

To my friend Tracey.

ABSTRACT

This report sets out the results of a numerical investigation into the response of thin circular plates subjected to impulsive loads, using the commercial finite element code ABAQUS.

Previous theoretical and numerical predictions of plate response have assumed a fully constrained boundary condition, while experiments have involved the use of both clamped and integral (fully built-in) boundary conditions. The current analysis employs 4-noded continuum elements in the finite element model, that allow the experimental boundary conditions to be modelled closely. Fully built-in plates are modelled by the inclusion of a material boundary, and clamped plates by the use of rigid clamping elements and a simple friction condition between the clamps and the plate surface.

The inclusion of fillet radii at the integral boundary, and an edge radius at the clamped boundary, have been reported in additional experiments. These modifications are also modelled in the current investigation.

The finite element model incorporates non-linear geometry and material effects, and strain rate sensitivity is included in the viscoplastic material definition. Impulsive loading is implemented through short duration pressure pulses, while the use of a uniform initial velocity profile is also shown to give good results. An explicit time integration scheme is used for the dynamic structural response.

Results are presented for Mode I response (large inelastic deformations) for a range of boundary conditions. Criteria for comparison include mid-plate deflections, deformed profiles and response times, and good correlation is observed with experimental data and previous theoretical and numerical predictions. It is predicted that the effect of boundary condition on the global Mode I response is not significant. The incremental nature of the finite element solution also allows the transient plate response to be observed, and the 2-

dimensional mesh allows detailed observations of plate thinning. Thinning is shown to occur primarily at the plate centre and boundary, and this is related to the occurrence of large plastic strains in these region, and is supported by microstructural evidence.

A material rupture model is included in an attempt to predict Mode II failure (ductile tearing at the boundary). The model is based on a criterion of maximum equivalent plastic strain. Correlation with experimental data for the onset of tearing is found to be poor, and several possible causes are discussed, including the need for reliable material parameters. However the effect of boundary condition on tearing behaviour is demonstrated.

DECLARATION

I, MARK ERNEST GELMAN, declare that this thesis is essentially my own work and has not been submitted in this or in any similar form for a degree at any other university.

ACKNOWLEDGEMENTS

I wish to thank the following :

- Professor G N Nurick my supervisor, for his guidance and support throughout this project.
- Messrs. H Bowles, G Starke, and G Mitchell of CERECAM, whom I often approached for advice and assistance.
- The Department of Mechanical Engineering which provided financial assistance, and whose members have been my colleagues and friends throughout.
- My friends and family who are ever loyal, and especially Tanya, who stood by me.

Your contribution to this report is noted with my gratitude.

TABLE OF CONTENTS

LIST OF FIGURES

NOTATION

UPPER CASE

I	Impulse
M	Mass
T	Period of ballistic pendulum
R	Plate radius
W_f	Plate mid-point deflection
V_0	Initial velocity of plate
D	Material constant
F	Force vector
M	Lumped mass matrix
L_{min}	Smallest element dimension
E	Youngs Modulus
G	Elastic shear modulus
K	Elastic bulk modulus
G_d	Damaged shear modulus
K_d	Damaged bulk modulus
P	Applied pressure
A	Area of plate
V(r)	Velocity distribution over plate
$P_{contact}$	Clamping contact pressure

LOWER CASE

$\dot{x}_0$	Initial velocity of ballistic pendulum
x_1, x_2	Displacement functions for ballistic pendulum
t	Plate thickness
n	Strain rate sensitivity factor

q	Material constant
l	Length of plastic hinge
r_0	Boundary radius of plate
$\mathbf{u}$	Displacement of material point
$\dot{\mathbf{u}}$	Velocity of material point
$\ddot{\mathbf{u}}$	Acceleration of material point
i	Increment counter
c_d	Dilational wave speed
t_b	Burn time of explosive

GREEK

β	Damping constant for ballistic pendulum
ϕ	Dimensionless impulse
ρ	Density
σ_0	Initial yield stress
σ_f	Flow stress
$\dot{\varepsilon}$	Strain rate
ε_{max}	Maximum total strain
ε_m	Membrane strain
ε_b	Bending strain
κ	Curvature of plastic hinge
θ	Rotation of plastic hinge
ε_{rup}	Total rupture strain
τ_{avg}	Average shear stress
τ_{ult}	Ultimate shear stress
Δt	Time increment
ω_{max}	Highest eigenvalue of dynamic system
λ, μ	Lame constants

ν	Poissons ratio
δ	Damage number
$\bar{\varepsilon}^p$	Equivalent plastic strain
$\bar{\varepsilon}_0^p$	Offset equivalent plastic strain (at first necking)
$\bar{\varepsilon}_f^p$	Rupture equivalent plastic strain
$\dot{\varepsilon}^p$	Plastic strain rate tensor
σ_{yd}	Damaged yield surface
τ_{eq}	Equivalent frictional shear stress
τ_1, τ_2	Principal frictional shear stresses
τ_{crit}	Critical frictional shear stress
μ	Coefficient of friction

1. INTRODUCTION

Prediction of the response of engineering structures to loads of very high magnitude and very short duration (impact and impulsive loads), is increasingly important in design for safety. Typically, impact loads originate in situations where impact occurs between two bodies, such as a high speed car accident or in some types of metal forming process, and impulsive loads where a body is in the vicinity of an explosion. There are thus many situations within the field of engineering where an understanding of such behaviour is crucial, and which provide motivation for the study of response of structures to impulsive and impact loading. Examples include the blast resistance and crashworthiness of road vehicles, aircraft and shipping, and similarly the integrity to impact and blast damage of high risk installations such as nuclear power plants.

1.1 IMPULSIVE LOADING

The nature of the blast problem is complex. The duration of any impulsive loading event is measured in the order of microseconds, and in the particular case of a detonating explosive involves a complex decaying pressure-time history, which impinges on the loaded structure and causes elastic and plastic stress waves to propagate. The blast is followed by a relatively long term structural dynamic response, often one or more orders of magnitude slower than the load duration, but involving rates of strain high enough that material properties such as flow stress are in general no longer consistent with the quasi-static values. Inertia effects, due to the mass of the structure, become significant, and large plastic deformations frequently occur that dissipate the energy of the blast as irrecoverable strain energy and heat. In general these large deformations cannot be treated as infinitesimal - an assumption that may often be valid for the case of purely elastic response problems.

To further complicate the study of blast loaded structures, the rapid transient response of such structures is normally difficult to observe. Thus hypotheses about transient behaviour must often be formulated and tested based solely on observations made before and after loading occurs. This renders the outcome of anything but

geometrically simple and repeatable impact or blast situations difficult to predict, using closed form analytic methods.

The impulsive loading response of both beams and shells is an area that has received considerable attention, due to the widespread occurrence of these basic design elements in most complex engineering structures. In particular the consideration of thin circular and rectangular plates provides a platform upon which the fundamentals of shell behaviour are researched. Numerous experimental investigations have been conducted on the response of both circular and rectangular plates, subjected to various types of loading and boundary fixation conditions. Large quantities of data thus exist for the deformation of plates of various geometries, and phenomena such as three distinct modes of failure have been widely observed [1,2]. These have been defined as

Mode I - Large inelastic deformation
Mode II - Tearing (tensile failure) at or over the support
Mode III - Transverse shear failure at the support

These failure modes are illustrated schematically in figure {1.1}.

Analysis of the experimental data has allowed trends to be established that relate dependent global quantities such as mid point deflections, deflected shapes and impulse magnitude at failure, to independent parameters such as plate thickness, material properties, and applied impulse. Purely analytical solutions for plate response have also been formulated, utilising for example mode approximation and energy techniques.

In this era of increased computer processing power, the use of numerical methods is becoming common and often preferable as a means of solving structural response problems, both static and dynamic, but in particular those where the solution sought is highly non-linear, as is typical of the structural response of plates to impulsive loading.

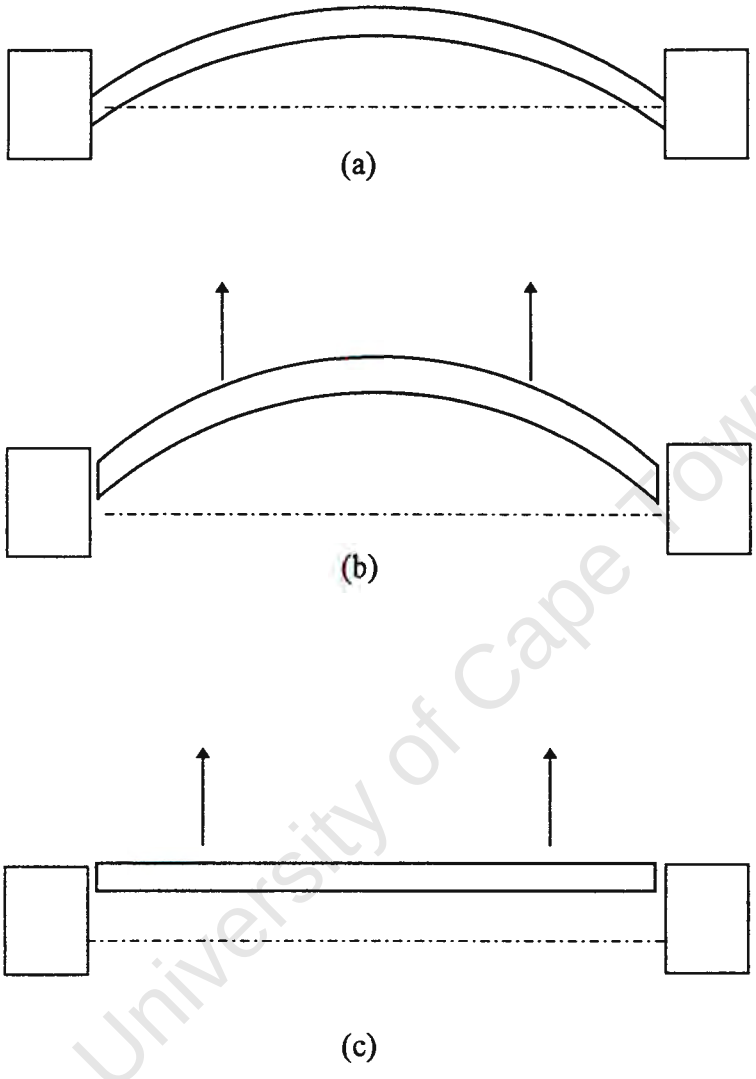

Figure {1.1} The three modes of failure exhibited by impulsively loaded plates: (a) Mode I - large inelastic deformations.
(b) Mode II- ductile tearing.
(c) Mode III - shear failure.

1.2 THIS STUDY

1.2.1 Aim

It is the primary aim of this study to investigate the use of a general purpose, commercial finite element code (ABAQUS) in the modelling of the blast loading of thin circular plates, using the available element, material, loading and failure formulations. The effect of boundary conditions on the response of the plates will be sought.

The study will extend recent work into the response and failure of blast loaded mild steel plates using ABAQUS, in which the use of simple shell type elements has already provided good correlation with experiments for the global response. In this thesis the use of the code is extended to a model that utilises a continuum quadrilateral element. Experimental work conducted to date has incorporated a variety of boundary fixation methods and the use of a continuum element allows these to be realistically modelled.

The new model still accurately predicts the general global response, when compared to extensive experimental data, and the 2-dimensional axisymmetric element also allows localised behaviour to be observed, such as the distribution of strain through the thickness of the plate.

A secondary aim of the investigation is to attempt to predict Mode II failure by incorporating a tearing model based on a simple plastic strain failure criterion.

1.2.2 Scope

The scope of the study covers several methods of boundary fixation used in experimental work, including a clamped boundary, and an integral (fully built-in) boundary. The use of radii to reduce stress concentration and localisation at both of these boundary supports is also modelled. Applied impulses are in the range experimentally shown to cause both Mode I failure (large inelastic deformation) and

Mode II failure (ductile tearing). Impulses that have been shown to cause Mode III (transverse shear) failure, are not considered.

The report begins with a general overview of the literature supporting this area of research, in which details of experimental, analytical and numerical work are considered, and further motivation for this study is developed. Details of the experimental procedure are also presented.

This is followed by a description of the ABAQUS finite element code including details of the solution scheme and material constitutive behaviour used. Details of meshing, load application, and the boundary conditions are also presented.

The overall performance of ABAQUS is reported in terms of the cost of solution, and convergence of the finite element mesh for displacements and stresses is established.

Global deformation results in the range of Mode I failure (large inelastic deformations with no tearing) are presented first, for clamped plates of diameter 120mm, 100mm, and 80mm, and for 100mm diameter plates with a fully built-in method of boundary fixation. Results are also presented for analyses where the boundary condition has been relaxed by the inclusion of radii. Schematic representations of the various boundary conditions considered in this report are given in figure {1.2}. Comparisons are made for these results with available experimental data, and also with limited analytically predicted values.

The ability of the numerical model to provide visualisation of transient plate behaviour is demonstrated. In particular the deformation of the plate by the propagation of a plastic hinge from the plate boundary toward the centre is discussed. Localised behaviour is observed in particular at the plate boundary where a stationary plastic hinge forms and strain values are highest. Attention is paid to the occurrence of localised necking in the boundary region, and the effect of boundary condition on this necking behaviour, is observed.

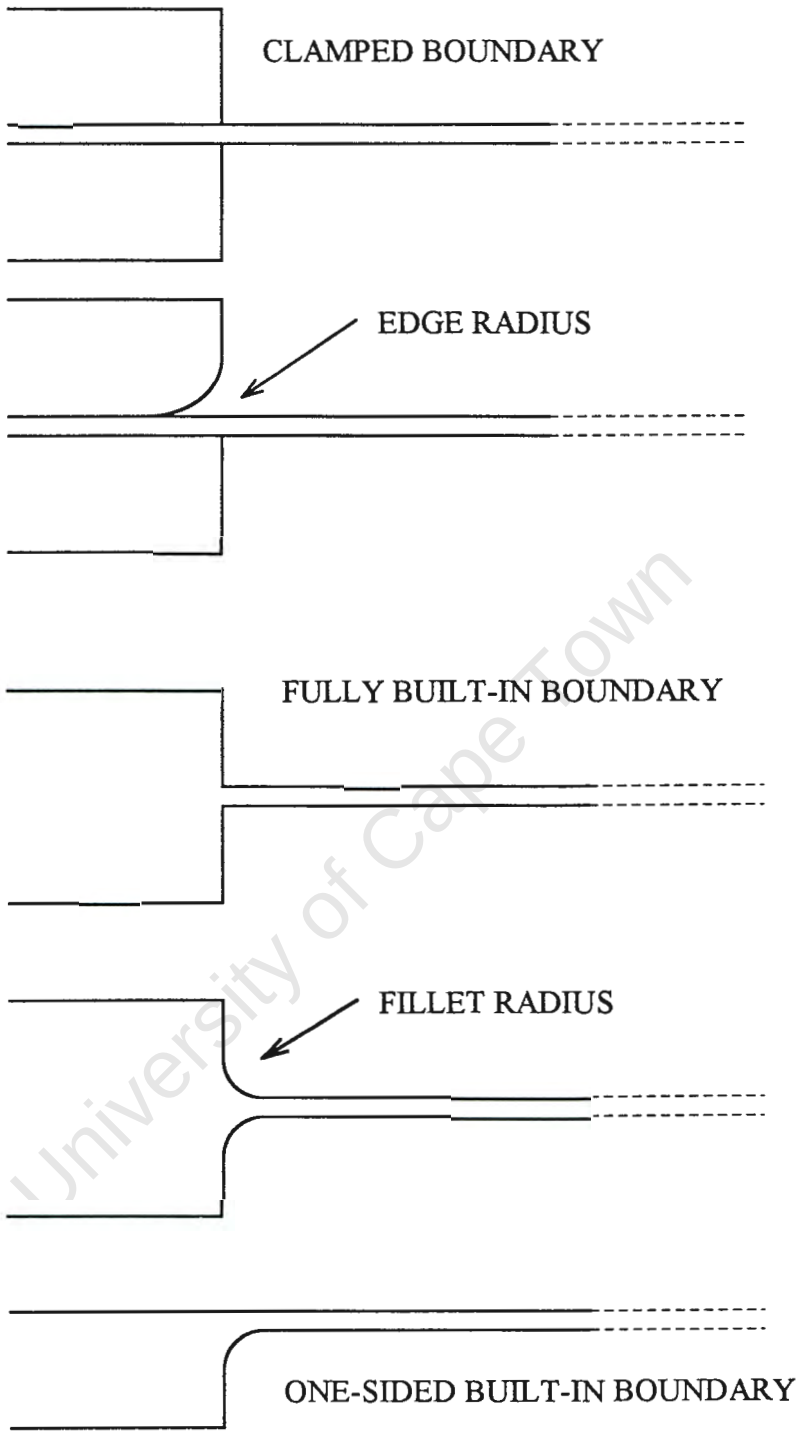

Figure {1.2} Schematic representation of the various boundary conditions encountered in the experimental study of blast loaded plates.

A preliminary attempt to model Mode II tearing is reported, that utilises a criterion of maximum equivalent plastic strain to predict material rupture. While correlation to experiments is not as favourable as with the case of Mode I, the model allows the sensitivity of factors that contribute to plate tearing to be investigated. The scope of this attempt is limited by problems encountered with the finite element code, but some useful results are presented, and observations are thus made concerning the appropriateness of the failure criterion chosen.

Finally a summary discussion of the findings of this investigation is undertaken, from which conclusions are drawn and recommendations made for future research.

2. LITERATURE REVIEW

2.1 INTRODUCTION

Interest in the field of impulsively loaded plates is reflected by numerous references in the literature, covering studies that are both experimental and theoretical in nature. In the latter case, an increasing amount of work has been done utilising numerical and computer based techniques. This chapter summarises some relevant aspects of the literature and while not exhaustive, aims to put the current study into context.

As early as 1950, Taylor [3] described an experimental study involving the effect of underwater explosions on large steel plates, and in 1955, Hoffman [4] investigated the magnitude of the permanent deformation of plate specimens due to pressure waves generated by the explosion of spherical charges in air. Humphreys [5] in 1965, used sheet explosives and a ballistic pendulum to generate and measure the impulsive loading of beams, thus laying the groundwork for the majority of experimental work since conducted. Later in this chapter the experimental techniques adopted by more recent researchers will be reviewed.

There have also been numerous analytical solutions proposed for the response of blast loaded plates,and these have been supported by experimental evidence. Initially these solutions took only bending effects into account but later both membrane and shear effects have been considered. The use of mode shapes to approximate the transverse motion of the plates has allowed predictions of deflections in the range of 4 to 9 plate thicknesses, and where the lateral as well as transverse motion of the plate is considered, even larger deflections are well predicted.

Numerical studies into impulsively loaded plates also occur in the literature [6,7], and include the use of both dedicated and general purpose codes. Several of these studies will be mentioned in this chapter.

2.2 EXPERIMENTAL WORK

2.2.1 Background

In 1988, Nurick and Martin [8], gave an overview of references to experimental studies on blast loaded plates and prepared a resume of experimental techniques listing plate dimensions, specimen type and material, deflection to thickness ratio and response time for each study. The methods of loading include underwater blasts, air blasts, inertial forming and sheet explosive blasts, for both circular and rectangular plates. Of most relevance to this report are studies that combine the use of sheet explosives with circular steel plates, and these are used later for comparative purposes.

Florence and Wierzbicki [9] used sheet explosive separated from the specimen by a layer of Neoprene, and estimated the impulse generated by calibration of the actual explosive. Duffey and Key [10] also used the mass of explosive to estimate impulse, and used a high speed camera to measure the displacement-time history. Bodner and Symonds [11] made use of a condenser microphone placed near the centre of the plate to establish a displacement-time history. Nurick et al [12] used annular rings of explosive to approximate a uniform blast load, in conjunction with a ballistic pendulum for the measurement of impulse, and employed a light-interference technique to record transient behaviour. Deflections of up to 20mm during a time period of 200 microseconds were observed in over 100 experiments on fully clamped circular, square and rectangular plates. These results span a larger range of deflection-thickness ratios than do those from other experimental studies.

2.2.2 Experimental technique modelled in this study

The same experimental technique and apparatus used by Nurick was later used by a series of other researchers to gather most of the data against which comparisons are drawn in this thesis. While this data has been compiled over a number of years by independent researchers, variations in the experimental approach have been minor and it is sufficient here to present a very general explanation of the apparatus and associated measuring techniques.

The plate specimens used in most of the experimental work referred to in this report were of cold rolled mild steel. In most preliminary studies, clamping of the plates was used to provide constraint at the boundary and in these cases the plates were cut from sheet nominally 1.6mm in thickness. Later studies attempted to better approximate a truly integral (fully built-in) boundary, and here the 1.6mm plate was machined out of a block nominally 20mm thick. These fully built-in plates were annealed after preparation to remove residual stresses associated with machining.

This report deals only with circular plates of different diameters, but similar experiments have been carried out on square and rectangular plates, having comparable loaded areas. A typical value of static yield stress for the mild steel used was 290MPa, determined from uniaxial tensile tests conducted on specimens of the steel stock used.

Small quantities (typically 4 - 25 grams) of plastic explosive (Metabel), having a burn velocity of 6500 - 7500 ms^{-1} were detonated to approximate the impulsive load. The explosive was arranged in two concentric rings in order to approximate a uniform pressure pulse. The sheets of explosive were separated from the plate specimen by a 16mm polystyrene pad to attenuate the shock transmitted to the plate and to prevent localised damage of the surface. While careful measurement of the explosive mass allowed the required impulse to be approximated, the use of a ballistic pendulum was required to accurately determine the actual magnitude of the impulse.

The ballistic pendulum consists of an I - beam suspended by four wires from a rigid ceiling. Onto the pendulum is mounted the plate specimen, and known masses are applied to ensure a balance of load through the suspending wires. A pen is also carried that traces the path of the swinging pendulum once it has been set into motion by the impulse of the explosion. The layout of the ballistic pendulum is given in figure {2.1}.

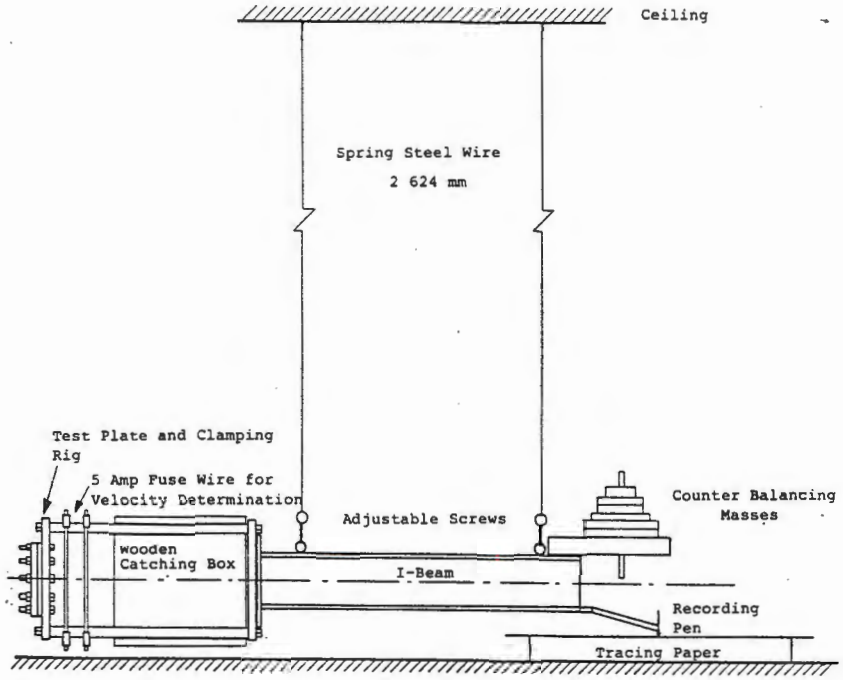

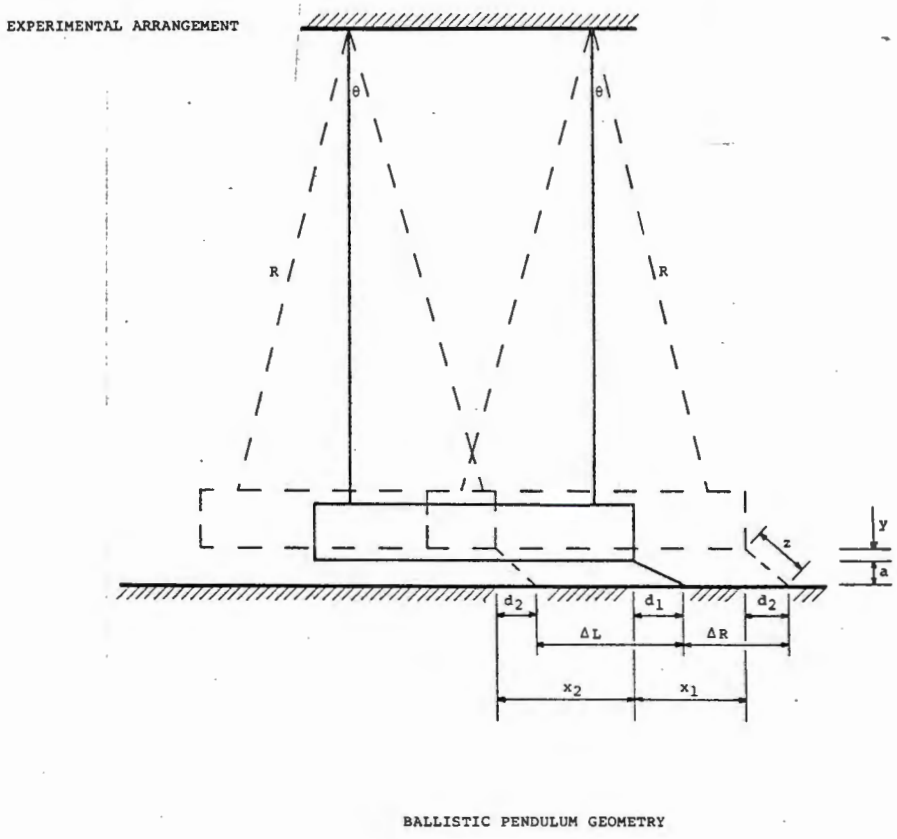

Figure {2.1} Schematic layout of the ballistic pendulum, used to experimentally determine the magnitude of applied impulse.

It can be shown that the impulse I created by the detonation of the sheet explosive, can be calculated as

$$I = M\dot{x}_0 \quad . \quad . \quad . \quad . \quad . \quad . \quad . \quad 2.1$$

where M is the mass of the entire pendulum and $\dot{x}_0$ is the initial velocity of the pendulum calculated from

$$\dot{x}_0 = \frac{2\pi}{T} x_1 e^{(1/4)\beta t} \quad . \quad . \quad . \quad . \quad . \quad . \quad 2.2$$

with T the period of the pendulum, and β a damping constant of the form

$$\beta = \frac{2}{T} \ln\left(\frac{x_1}{x_2}\right) \quad . \quad . \quad . \quad . \quad . \quad . \quad . \quad 2.3$$

T is easily measured by timing several oscillations of the pendulum; x_1 and x_2 are displacement functions that are easily evaluated from other direct measurements. The interested reader is referred to reference [12].

Nurick used a light interference technique [13] in order to quantify the deflection-time history of the plate specimen. Response times of the order of 150μs were found to be typical. The final mid-point deflections of the plates were measured using a vernier and the use of a reflex metrograph allowed points on the plate surface to be digitised, interpolated and plotted as deflected profiles.

This basic experimental technique has been utilised several times since the apparatus was commissioned, to provide a large base of essentially standardised experimental data covering plates of various geometries and boundary conditions. Observations and data from much of this experimental work is used for purposes of comparison in this thesis.

Teeling-Smith [14, 15] conducted experiments on fully clamped circular plates to observe Modes I, II and III failure. A method was devised that allowed the residual velocity of the failed plate to be measured and hence an analysis of the energy balance was performed in each case. The plates were all 100mm in diameter and 1.6mm thick, and clamping was by the same method used by Nurick. Little attention was paid to the effect of the boundary condition on any of the modes of failure. For Mode I response, results obtained were very similar to those obtained by Nurick [12], demonstrating good repeatability. A threshold impulse of around 25Ns was identified for Mode II failure which was considerably higher than the 15.6Ns reported by Nurick..

The influence of the nature of the clamped boundary condition and of plate diameter was investigated by Marshall [16], who used sharp edged clamps as well as clamps with different edge-radii (nominally 1.6mm and 3.2mm), and also varied the dimensions of the plate specimens to include diameters of 80mm and 120mm. In this investigation, three distinct modes were identified within Mode I failure:

Mode I - No visible necking around the plate boundary.
Mode Ia - Necking of the plate around part of the boundary.
Mode Ib - Necking around the entire boundary.

Marshall further concluded that the effect of increasing plate diameter was to increase the range of Mode I failure, causing the onset of tearing to occur at a higher applied impulse, and with correspondingly higher deflections, although tearing of 120mm plates was not actually reached.

For 100mm plates of thickness 1.6mm, it was reported that an increased radius on the clamp edge caused the transition from Mode I to Mode II failure to occur at higher impulse. Marshall found the threshold impulse for Mode II in the case of a sharp edge to be 11.75Ns, which is considerably lower than those reported by both Nurick and Teeling-Smith (less than 50% of the latter). The onset of tearing was retarded by as much as 87% when a 3.2mm edge radius was introduced, with the threshold impulse increased to 22.0Ns. A slight decrease in plate stiffness was also noted with increasing

edge radius. Similarly at the onset of necking near the plate boundary, a decrease in stiffness was noted, since larger rotations occur.

Further use of the experimental apparatus was undertaken by Thomas [17, 18]. This work was motivated by concern that while the majority of analytic solutions to plate response are based on the assumption that the plate boundary is fully constrained, most experimental work utilises some form of clamping which only approximates full constraint and involves certain errors. For example Teeling-Smith [14] reported signs of material draw-through from the clamped region of plates being tested, observed as elongation of the clamping bolt holes, and noted that the extent of this was dependent on the failure mode. The stretching occurred during Mode I response and was at a maximum when partial tearing occurred at the plate edge. Once full tearing occurred the stretching phenomenon disappeared. This clearly indicates that clamping does not provide a fully constrained boundary. In order to measure the effect of this, Thomas used plates formed by machining out the plate diameter from a much thicker piece of material, resulting in a good approximation to an integral (fully built-in) boundary condition. The plates used were also 100mm in diameter and nominally 1.6mm thick.

Thomas found that for Mode I, the response of clamped and integral plates were similar, but that tearing failure in the integral plates corresponds to necking in the clamped plates. He concluded that shear effects play a more significant role in integral plate rupture and that solutions for rupture based on clamped plate research are not valid for such fully built-in boundaries. A threshold for Mode II failure of around 17Ns was identified. In the recommendations of his report he suggests the use of finite element methods to better understand detailed behaviour at the plate boundary.

Loumeau [19] carried the work of Thomas further by investigating the effect of machining a fillet radius at the integral boundary, in order to reduce the effect of stress concentrations caused by the previously sharp machined corner. In general he found that the inclusion of a fillet radius allowed the plates to reach higher values of deflection before the onset of Mode II tearing failure, thus extending the range of

Mode I response. However in terms of deflections and deflected profiles, the form of the Mode I response was not significantly affected

The combination of the work described above leads to several observations and hypotheses:

- Mode I response is based on the *global* stiffness of the plate, and is little affected by *localised* changes to boundary fixation, provided that excessive rotations and translations are not allowed. Clamped and fully built-in plates meet this criterion, which is not affected by the inclusion of edge or fillet radii. This is illustrated by figure {2.2} that shows all the experimental data mentioned above plotted in dimensionless form. It can be seen that all the deflection-thickness ratio points fall into a narrow band, and there are no immediately obvious trends in the scatter.

- The global stiffness in terms of deflection for a given impulse is a function of plate dimensions. Deflections decrease with both increasing thickness and diameter.

- It appears that Mode II tearing in clamped plates is as a result of strain localisation (necking), whereas for fully built-in plates, the stress concentrations due to the sharp corners lead to a shear type failure before necking can occur, or possibly a combination of both types of failure.

- For clamped plates the initiation of necking is assisted by localised indentation of the plate by the clamping surfaces, which are substantially thicker and resist deformation. The effect of a radius on the clamp edge is to reduce this indentation and so necking and ductile tearing occur at higher applied impulse.

- The use of a clamped boundary allows draw-through of the plate from within the clamp. The extent of this has not been quantified but the effect on Mode I response does not appear to be significant.

- The extent of draw-through is likely to be affected by clamping parameters such as friction and clamping pressure, and may influence necking behaviour and subsequent rupture. This may explain why Mode II failure in clamped plates occurs over a wide range of applied impulse. (11.75 Ns to 25 Ns reported by Marshall and Teeling-Smith respectively for 100mm clamped plates)
- For fully built-in plates, the effect of a fillet radius is to reduce the extent of stress concentration and thus retard the onset of a shear type failure. Failure by strain localisation (necking followed by rupture) may then occur at a higher threshold impulse.

The various boundary conditions discussed are all modelled in this study and thus the hypotheses upon which the above observations are based, may be tested.

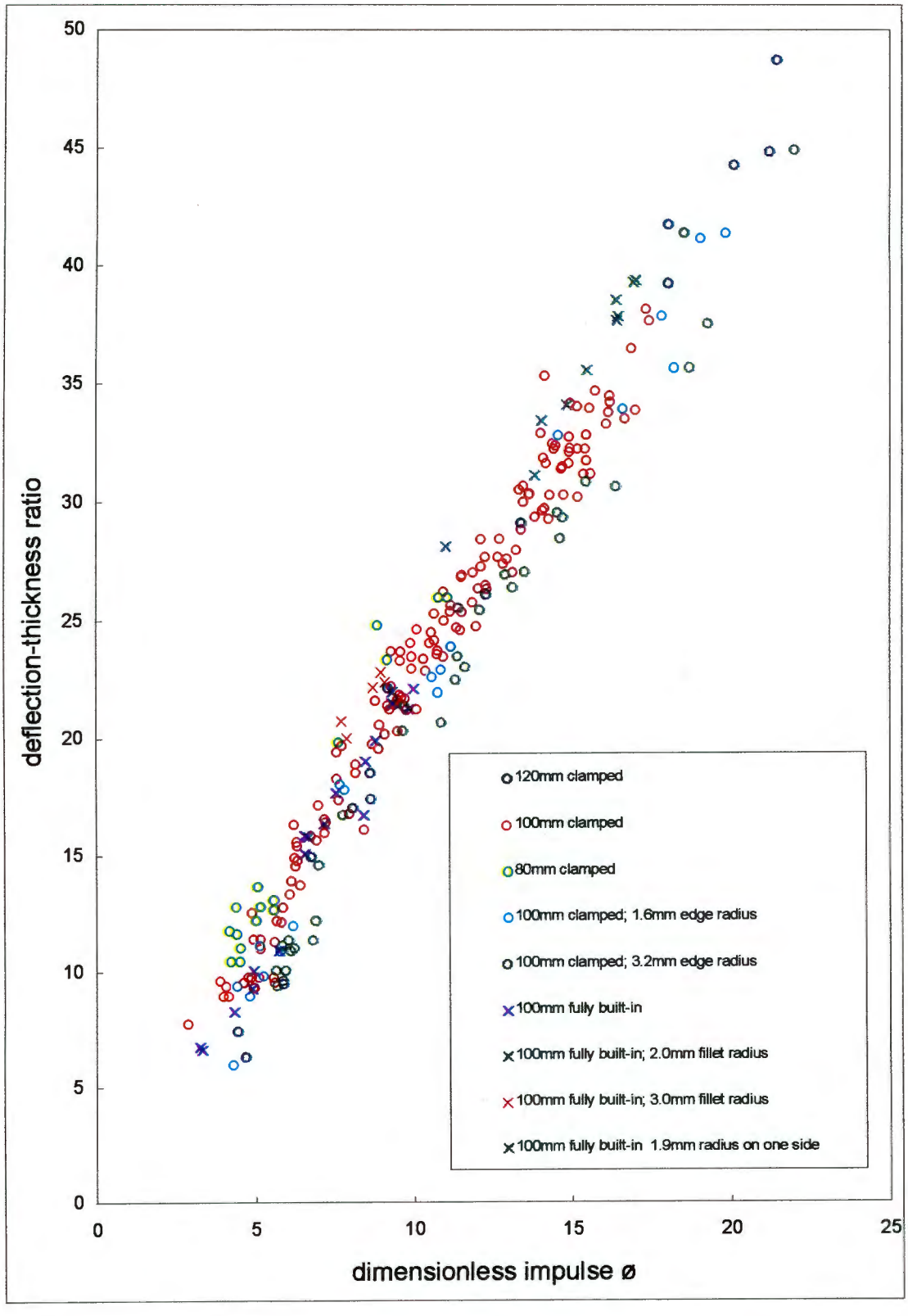

Figure {2.2} Deflection-thickness ratio against dimensionless impulse ø for all the experimental results used in comparisons.

2.3 THEORETICAL WORK

Theoretical models of the dynamic response of thin plates far outnumber experimental studies. Simple closed form solutions can often provide a rapid and sufficiently accurate design estimate to, for example, plate deflections, deformed profiles, and residual strains, but normally provide little insight into areas such as transient behaviour and tearing failure.

2.3.1 Mode I predictions

Nurick and Martin [20] list numerous approximate methods for predicting the dynamic global response of thin plates, assuming a uniform load distribution. The earliest studies predicted only small deformations due to bending effects, but in later analyses membrane effects were included, and by assuming a deformed shape, such methods were very successful. Several proposals using energy methods are also listed as are mode approximation techniques. The predictions are tabulated in terms of deflection-thickness ratio related to a dimensionless damage number ϕ proposed by Nurick, which takes the form

$$\phi = \frac{I}{\pi R t^2 \sqrt{\rho \sigma_0}} \qquad . \quad . \quad . \quad . \quad . \quad . \qquad 2.4$$

The various predictions are also plotted against the experimental data of Nurick et al [7] and while many of the predictions are poor, good correlation is noted in some cases. For example Lippman [21] used an approximate method that included both bending and membrane effects in a model that assumed a deformed shape with a radial thickness variation to predict mid-point deflection as

$$W_f = \frac{0.132I}{tR(\rho\sigma_0)^{1/2}} \qquad . \quad . \quad . \quad . \quad . \quad . \qquad 2.5$$

corresponding to a deflection-thickness ratio of

$$\frac{W_f}{t} = 0.415\phi \quad . \quad . \quad . \quad . \quad . \quad . \quad . \quad 2.6$$

Perrone and Bhadra [22] used an energy method, where kinetic energy calculated from an initial velocity profile is equated to work done by plastic stretching in order to determine a mid-point deflection of

$$W_f = \frac{0.117I}{tR(\rho\sigma_0)^{1/2}} \quad \text{and} \quad \frac{W_f}{t} = 0.368\phi \quad . \quad . \quad . \quad 2.7$$

The effects of bending and cicumferential strain were ignored and the model underestimates deflections. It can be seen that these two predictions vary only by a linear factor when related to the dimensionless damage number ϕ and this applies to a range of other predictions, where deflection-thickness ratio takes the form of $n\phi$ and n ranges from 0.252 to 1.233.

Symonds and Wierzbicki [23] formulated a membrane mode solution that takes the form

$$\frac{W_f}{t} = 1.0186 \times \left[\frac{2\rho V_0^2 R^2}{3\sigma_f t^2}\right]^{1/2} \quad . \quad . \quad . \quad . \quad . \quad 2.8$$

where σ_f is the flow stress that depends on the average rate of straining, given as

$$\dot{\varepsilon} = 0.05365 \cdot \frac{I^2}{R^5 t^2 \sqrt{\sigma_f \rho^3}} \quad . \quad . \quad . \quad . \quad . \quad 2.9$$

This is related to the strain rate obtained from the Cowper-Symonds Equation [24] and an iterative procedure results in which σ_f is determined.

Jones [25] proposes a relationship of very similar form

$$\frac{W_f}{t} = \left[\frac{2\rho V_0^2 R^2}{3n\sigma_0 t^2}\right]^{1/2} \quad . \quad . \quad . \quad . \quad . \quad . \quad 2.10$$

in which n, a strain rate sensitivity factor, can be obtained approximately and an iterative procedure avoided using the result

$$n \cong 1 + \left\{\frac{V_0^2}{3DR}\left(\frac{\rho}{3\sigma_0}\right)^{1/2}\right\}^{1/q} \quad . \quad . \quad . \quad . \quad . \quad 2.11$$

Shen and Jones [26] note that in general, a bending only analysis gives good results where overall deflection is of the order of the plate thickness, and membrane only analyses in the case where the impulse produces finite transverse deflections many times the plate thickness.

Nurick, Pearce and Martin [6] adopted a model in which the mode shape is computed at each time step. In addition to considering transverse displacements, the analysis was adapted to include the effects of lateral displacements in the plane of the plate. This allowed the prediction of in plane strains, and provided good correlation to experimental data.

It should be noted that most of the theoretical solutions presented make some form of approximation or simplification and thus the accuracy of the solutions are limited. Examples of these approximations include:

- Material behaviour. Frequently the effect of strain rate, or strain hardening, is neglected. Also very simplified yield surfaces are employed.

- Load distribution. The pressure imparted by the explosive in an experiment will impinge on the plate surface in some form of spatial distribution that is non-uniform. Most theoretical solutions ignore this fact.

- Boundary conditions. Most theoretical solutions assume that all degrees of freedom at the boundary are fully constrained.

The analytical solutions described above are compared later to the present numerical work and associated experimental data, and comments will be made on these comparisons.

2.3.2 Mode II failure

Shen and Jones [26] presented an approximate rigid-plastic analysis for dynamic plastic response, combining the effects of bending moments, membrane forces, and transverse shear forces in an interaction yield surface. Comparison of Mode I predictions to experimental results of Nurick and Teeling-Smith [15], and Bodner and Symonds [11], show excellent correlation. The analysis also included an energy density criteria for Mode II failure, but correlation in this range with the experimental data of Teeling-Smith and Nurick was found to be poor. Shen and Jones noted that further experimental results was required with particular attention paid to achieving a fully constrained boundary condition, that does not allow material draw through. Such experimental results were reported by Thomas and Nurick [18] and it was found that for fully built-in plates, correlation to the predictions of Shen and Jones was improved.

The significance of boundary condition was again noted in an investigation by Li and Jones [27] who used an extended Johansen yield criterion in a rigid, perfectly plastic analysis, to explore the effects of transverse shear on plate yielding. Li and Jones noted for example that a fully clamped circular plate resists bending deformations more effectively than a simply supported plate, though its resistance to transverse shear sliding is inferior. This analysis also showed that transverse shear failure (Mode III) may occur in some situations, as observed in experiment.

2.4 NUMERICAL PREDICTIONS

2.4.1 Dedicated analyses

The development of special purpose in-house codes that utilise numerical solution schemes has been widespread. For example Olson et al [28, 29] used the code NAPSSE (non-linear analysis of plate structures using super elements) to predict the response for both unstiffened and stiffened square plates. The super elements utilise displacement fields represented by analytical as well as polynomial functions, and only one element is required to model each beam span and plate bay. Good correlation was achieved for global deflections (Mode I) and the onset of tearing (Mode II) using a maximum strain criterion.

Olson et al [30] used a different code NAAPFE (non-linear analysis of axisymmetric plates with finite elements) to predict the response of fully clamped circular plates. This was a code developed in-house, utilising classical Kirchhoff thin plate theory with shear deformation effects neglected. The code also included geometrical and material non-linearity, and finite element equations obtained by virtual work principles. Initial dynamic yield stress was adjusted to account for strain rate effects by the Cowper-Symonds [24] relation.

Mode I response was predicted accurately by the code and several observations result that can be compared to the current work

- Permanent deflection was not dependent on the pressure-time history selected, provided the time selecetd was short compared to the overall response time of the plate.

- Mid plate deflection increased linearly to a maximum value followed by small elastic vibrations. The early part of this response is identical for rate sensitive and rate insensitive models.

- Peak displacement occurs at around 130μs, for 100mm plates.

- Radial strain at the boundary reaches a maximum at a time of around 50μs, which is consistent with the onset of tearing failure.

Mode II predictions were also made using an interaction failure model incorporating the effects of bending and membrane effects. The highly concentrated plastic deformation of the plate near the boundary was modelled using plastic hinge lines, so that bending strains in this region are estimated from rigid-plastic theory. The hinge rotation is taken simply as the slope of the plate adjacent to the boundary and hence the maximum total strain ε_{max} at the boundary where failure occurs is given by

$$\varepsilon_{max} = \varepsilon_m + \varepsilon_b \quad . \quad . \quad . \quad . \quad . \quad . \quad . \quad 2.12$$

where ε_m is the membrane strain and ε_b the bending strain, given by

$$\varepsilon_b = t\kappa / 2 \quad . \quad . \quad . \quad . \quad . \quad . \quad . \quad 2.13$$

Here t is the plate thickness and κ is the curvature of the plastic hinge defined as

$$\kappa = \theta / l \quad . \quad . \quad . \quad . \quad . \quad . \quad . \quad 2.14$$

where θ is the rotation of the plastic hinge and l is the hinge length. The membrane strain ε_m is approximated by averaging the membrane strain of the element adjacent to the boundary

$$\varepsilon_m = \frac{1}{\Delta r} \int_{r_0-\Delta r}^{r_0} \left[\partial u / \partial r + (\partial w / \partial r)^2 / 2 \right] \cdot dr \quad . \quad . \quad . \quad 2.15$$

where r_0 is the boundary radius and Δr is the length of the element nearest the boundary. The maximum strain is computed at each time step and compared to a specified ultimate rupture strain ε_{rup} to form a strain ratio $|\varepsilon_{max} / \varepsilon_{rup}|$.

Since NAAPFE does not include shear deformation, the average shear stress τ_{avg} must be estimated from the transverse force reaction per unit length at the boundary, divided by the plate thickness. A stress ratio of the form $| \tau_{avg} / \tau_{ult} |$ then provides an estimate to Mode III failure, which is beyond the scope of this discussion.

Results for Mode II failure are in general in good agreement with experiments and the following observations regarding Mode II tearing are made that provide useful comparisons for this study

- At the threshold of Mode II failure, the contributions of both the strain and stress ratios were significant. Although only the strain ratio was used in the prediction of Mode II tearing, this implies that the effect of shear may also be significant in this failure mode, which is normally characterised as a purely tensile failure.

- The time to failure decreases monotonically as impulse is increased.

- The strain based failure model provides a good prediction of Mode II tearing.

2.4.2 Previous ABAQUS investigation

Farrow [31, 32] used both the ABAQUS/Explicit and ABAQUS/Standard codes to model circular plates using simple 2-noded axisymmetric shell elements based on classical Kirchhoff thin shell theory. This resulted in a simple linear mesh, and good correlation for Mode I response was achieved using as few as four unbiased elements along the plate radius. With more refined meshes, predictions were also made for deformed plate shapes, thinning, and approximate strain distributions. A 4-noded planar shell element was also used, with similarly good results being obtained. This planar model was also used to model the response of sandwich plates, again with good correlation. Schematic representations of both meshes used are shown in figure {2.3}.

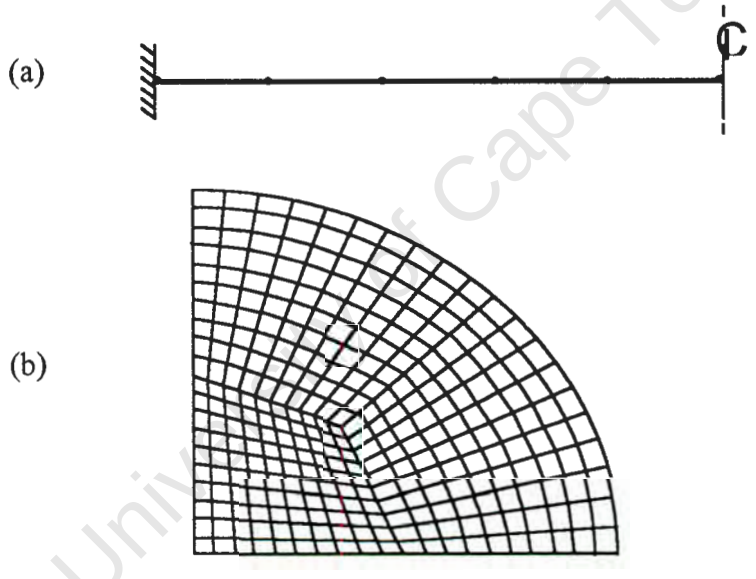

Figure {2.3} Schematic representation of the finite element models used by Farrow; (a) Axisymmetric shell elements and (b) Planar shell elements.

Important observations to emerge from this study include

- While both solution schemes had advantages and disadvantages, the explicit scheme was found to be superior in terms of the cost of solution, with CPU time sometimes an order of magnitude less than for an equivalent problem running under the implicit scheme.

- The response of the plate was found to be insensitive to the duration of the pressure load applied, in a range from 5μs to 30μs.

- Of several initial velocity loads investigated, a uniform velocity was found to give the best correlation to experiments. However anything but a *uniform* velocity load was difficult to implement and the pressure loading technique was found to be more accurate.

- Comparison criteria such as deformed shapes, plate thinning and response times were well predicted in the Mode I range.

It was noted that since tearing normally occurs at the plate boundary, a study of boundary conditions would be required in order to predict Mode II failure.

2.4.3 A note on criteria for Mode II tearing

Duffey [33] has discussed the relative lack of suitable failure criteria for dynamically loaded shell structures composed of ductile elastic-plastic materials, in many finite element codes that are otherwise well suited to the calculation of dynamic elastic-plastic response. While many commercial codes provide sophisticated models for non-linear material behaviour, the prediction of material separation is not as well catered for. In general those codes that do provide a material separation model typically base the failure criterion on equating equivalent plastic strain to failure strain in simple tension. However strains in shell structures exhibit biaxial tension and hence a multiaxial in-plane strain-based criterion for failure would seem more appropriate.

The most sophisticated approach to the prediction of material rupture encountered in the literature was developed at the Sandia National Laboratories. Bammann et al [34] develop a constitutive model for use in codes such as ABAQUS and DYNA3D that is capable of predicting deformation and failure in ductile materials, using parameters determined from simple tensile and compression tests. It is argued that failure criteria such as maximum equivalent plastic strain or maximum principal stress are inadequate, since the strain at failure is highly dependent on other factors such as strain path, strain rate and temperature history, pressure and effective stress.

A complex plasticity / failure model is thus formulated based on internal state variables such as void growth, temperature, mean stress, plastic strain rate and current damage level, that track plasticity and damage. When utilised in explicit finite element codes, the model accurately predicted ductile failure mechanisms, as benchmarked by carefully planned experiments duplicating real world problems, such as target penetration and focused blasts on plates.

3. ANALYSIS

3.1 ABAQUS OVERVIEW

All finite element analyses in this study were conducted using the ABAQUS code developed by Hibbitt, Karlsson & Sorensen, Inc. This is a large and versatile general purpose code, incorporating a wide range of material constitutive behaviours, element formulations, and model history inputs. Version 5.5 [35] was used in all analyses except where an analysis of tearing was required, where version 5.4 was used, due to a bug existing in the later version.

ABAQUS caters for both static and dynamic response, depending on whether inertial effects are significant, as is the case with the current study of plate response. The code also caters for linear and non-linear response, the latter of which deals with two sources of non-linearity. Material non-linearity allows for history dependence to enter material constitutive behaviour, such as occurs in the hardening behaviour of the mild steel plates, and geometric non-linearity allows the analysis to extend beyond the assumption of small displacements into realms where the kinematic relationships are not linearised. Both of these non-linearities are thus characteristic of the blast loaded plate problem.

In a non-linear dynamic analysis, direct integration of the system equations is used, and ABAQUS provides three approaches. ABAQUS/Standard is designed to analyse the overall dynamic response of a structure and uses the Hilber-Hughes-Taylor rule which is implicit, meaning that the non-linear dynamic equilibrium equations must be solved at each time increment, using the iterative Newton's Method. It is not unconditionally stable for dynamic problems. A second method is also provided in ABAQUS/Standard that uses the "subspace projection" method, but details of this method are not included here.

The third method which is used throughout the current investigation deals with wave propagation on a local level through the implementation of a central difference

integration scheme, and diagonal element mass matrices. This forms the basis of ABAQUS/Explicit.

In the explicit solution scheme, the equations of motion are integrated through time by using many small time increments within a central difference explicit integration rule.

$$\dot{\mathbf{u}}^{(i+1/2)} = \dot{\mathbf{u}}^{(i-1/2)} + \frac{\Delta t^{(i+1)} + \Delta t^{(i)}}{2}\ddot{\mathbf{u}}^{(i)} \quad . \quad . \quad . \quad . \quad 3.1$$

$$\mathbf{u}^{(i+1)} = \mathbf{u}^{(i)} + \Delta t^{(i+1)}\dot{\mathbf{u}}^{(i+1/2)} \quad . \quad . \quad . \quad . \quad . \quad 3.2$$

The method is explicit in that the current state is calculated based solely on values from the previous increment, and is computationally simple. This fact, alongside the use of diagonal element mass matrices, provides high computational efficiency. Using these diagonal or 'lumped' mass matrices, the accelerations at the start of a new increment are computed by

$$\ddot{\mathbf{u}}^{i} = \mathbf{M}^{-1} \cdot (\mathbf{F}^{(i)} - \mathbf{I}^{(i)}) \quad . \quad . \quad . \quad . \quad . \quad 3.3$$

where **M** is the diagonal lumped mass matrix, **F** is the applied load vector, and **I** is the internal force vector. Thus the explicit procedure requires no iterations and no tangent stiffness matrix. The explicit procedure integrates through time in increments Δt given by

$$\Delta t \leq \frac{2}{\omega_{max}} \quad . \quad . \quad . \quad . \quad . \quad . \quad . \quad 3.4$$

where ω_{max} is the highest eigenvalue of the system. This upperbound on the magnitude of the time increment is to ensure that high frequency components of the response, such as the stress waves propagated through the impulsively loaded plates, are properly resolved. Hence the maximum increment time must be smaller than the time required for a dilational stress wave to propagate across the smallest element in the finite element mesh chosen, and it can hence be approximated by

$$\Delta t \approx \frac{L_{min}}{c_d} \qquad \text{where} \qquad c_d = \sqrt{\frac{\lambda + 2\mu}{\rho}} \quad . \qquad 3.5$$

In equation (3.5), L_{min} is the smallest element dimension in the mesh and c_d is the dilational wave speed of the material, given in terms of Lame constants μ and λ and the material density ρ. ABAQUS/Explicit automatically selects an increment time of $1/\sqrt{2}$ of the critical time step for the most critical element in the mesh. Thus the performance of the code is very dependent on mesh design, as even a single element of smaller dimension than the next largest will lead to a considerable increase in solution time.

3.2 FINITE ELEMENT MODEL

3.2.1 Non-linear material model

All experimental results considered in this report were obtained from tests using plates of cold-rolled mild steel, showing linear elasticity and isotropic strain hardening plasticity. For Mode I response, where localisation and tearing are not considered, a Von Mises yield criteria was selected for the viscoplastic behaviour, which incorporates isotropic hardening and associated flow, and with the hardening behaviour being described by a typical stress versus plastic strain curve at zero strain rate, as shown in figure {3.1}.

Values of initial static yield stress σ_0 show considerable variation from study to study. Farrow [31] in his numerical model, chose a value of σ_0 = 290 MPa, and this value is retained. It is noted that the use of dimensionless impulse ϕ allows meaningful comparison of results despite the choice of value for yield stress. Other material properties specified were

$E = 210\text{GPa}$
$\rho = 7850\text{kgm}^{-3}$
$\nu = 0.3$

Mild steel shows significant strain rate sensitivity even at strain rates as low as 10^{-2}. Strain rates as high as 10^3 are encountered in the current analysis, and these were accounted for in the ABAQUS model by using the dynamic yield stress σ_y at each material point, which is obtained from the Cowper-Symonds [24, 25] power law relationship

$$\frac{\sigma_y}{\sigma_0} = 1 + \left(\frac{\dot{\varepsilon}}{D}\right)^{1/n} \quad . \quad . \quad . \quad . \quad . \quad . \quad 3.6$$

In equation (3.6), $\dot{\varepsilon}$ is the strain rate and D and n are material parameters, with values of $D = 40.4s^{-1}$ and $n = 5$. These values have been used widely in the past. It is assumed that the form of the hardening curve for mild steel is not affected by strain rate.

Heat generation due to plastic work dissipation, and the effect of subsequent temperature rise on material properties is neglected in this study due to a lack of supporting experimental results. However there is evidence that temperature effects may play a role particularly in failure at the plate boundary, [36], and a coupled temperature-displacement analysis would then be justified.

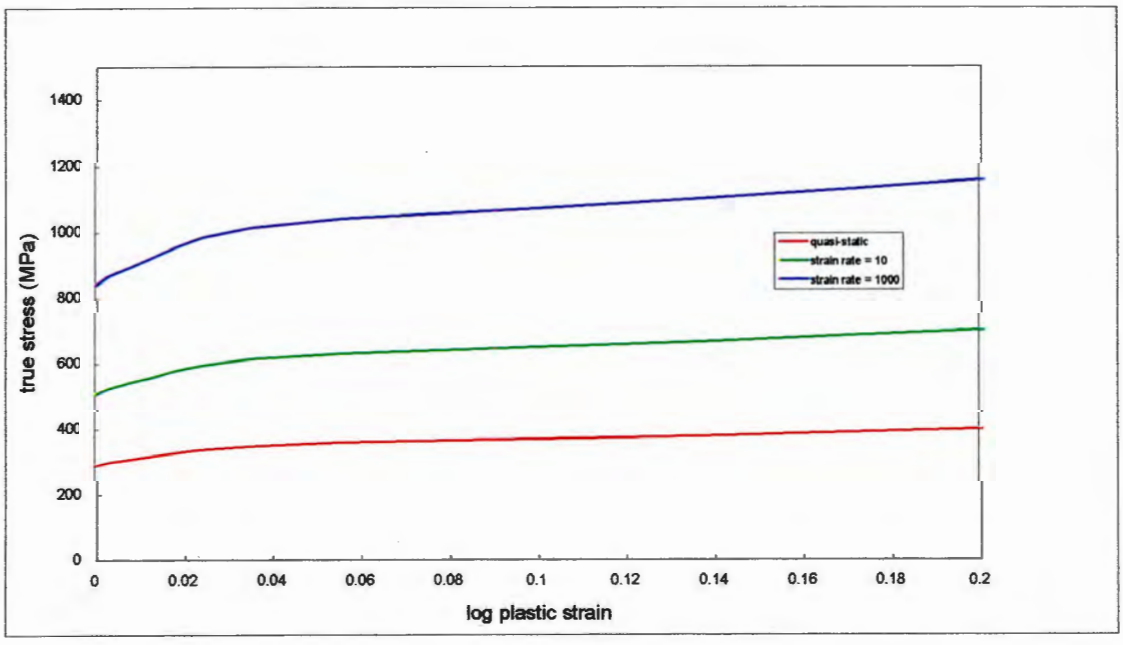

Figure {3.1} Typical strain hardening behaviour for mild steel showing the strain rate effect predicted by Cowper and Symonds.

3.2.2 Material rupture model

The Von Mises plasticity model as it stands does not account for strain localisation (necking), nor does it model the material rupture that results from such localised instability. However ABAQUS provides a failure model based on a maximum equivalent plastic strain criterion, which can be utilised in conjunction with the Von Mises plasticity. Such a model is ideally suited to the prediction of the type of failure that occurs in a standard tensile test, and the limitations of such a model [33] in a case where biaxial strains exist, have been noted. Motivation for the relevance of attempting to use this model is discussed in the chapter of results.

A damage number δ is calculated from the equivalent plastic strain and is given as

$$\delta = \frac{\bar{\varepsilon}^{p} - \bar{\varepsilon}_{0}^{p}}{\bar{\varepsilon}_{f}^{p} - \bar{\varepsilon}_{0}^{p}} \qquad 3.7$$

where $\bar{\varepsilon}^{p}$ is the current equivalent plastic strain at a material point, $\bar{\varepsilon}_{0}^{p}$ is the value of equivalent plastic strain at the point when localisation first occurs, and $\bar{\varepsilon}_{f}^{p}$ is the value at rupture. $\bar{\varepsilon}^{p}$ is defined as

$$\bar{\varepsilon}^{p} = \int_{0}^{t} \sqrt{\frac{2}{3}\dot{\varepsilon}^{p} : \dot{\varepsilon}^{p}}\, dt \qquad 3.8$$

where $\dot{\varepsilon}^{p}$ is the plastic strain rate tensor. The elastic response of the material is then degraded linearly according to the following relationships

$$\begin{aligned} G_{d} &= (1-\delta)\cdot G \\ K_{d} &= (1-\delta)\cdot K \end{aligned} \qquad 3.9$$

where G and K are the initial, and G_d and K_d are the damaged, shear and bulk modulii, respectively. The damaged plastic yield surface is defined as

$$\sigma_{yd} = (1-\delta)\cdot\sigma_y\cdot(\bar{\varepsilon}^p) \quad . \quad . \quad . \quad . \quad . \quad 3.10$$

The yield surface is reduced to a single point in stress space as damage reaches unity. Elements are regarded as failed when the stiffness at all integration points becomes zero, and these elements are removed from the mesh. The degradation of the material is as a result only of deviatoric processes; and the isotropic component of stress plays no role in the determination of damage, even though the bulk modulus K is itself degraded. The failure behaviour is represented in figure {3.2}.

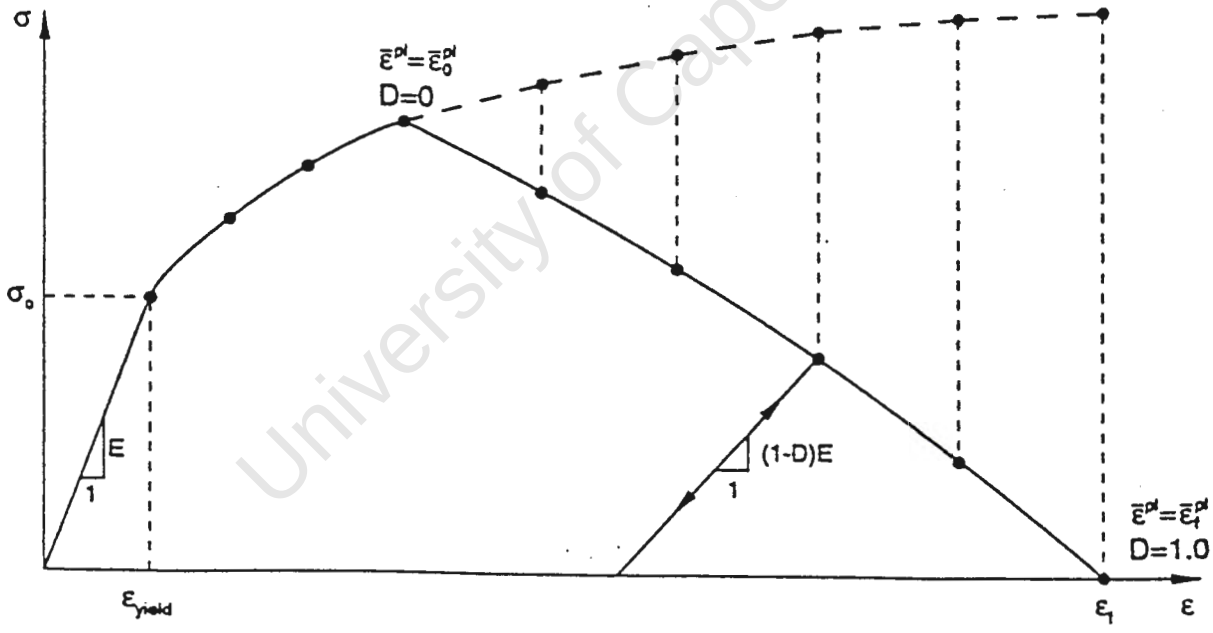

Figure {3.2} The ABAQUS equivalent plastic strain based material rupture model.

3.2.3 Blast load modelling

The impulsive blast load, generated by the use of plastic sheet explosives in the experiments, was simulated in the finite element model by the application of a pressure load of short duration. This is a simpler load condition to specify as compared to an applied initial velocity profile, most commonly used in previous analytical models. Furthermore, Farrow [31] found that the use of an initial velocity field sometimes led to numerical instability within the explicit scheme, and that the use of a pressure load also gave good correlation. The duration t_b of the pressure load P is taken to be the actual burn time of the explosive, and hence the magnitude of the pressure is calculated by

$$P = \frac{I}{(t_b \cdot A)} \quad . \quad . \quad . \quad . \quad . \quad . \quad . \quad 3.11$$

where A is the plate area. The burn time is typically 15 μs as determined from the burn velcoity of the plastic explosive, and Farrow reported that even doubling this time to 30 μs produced results for Mode I response that were insignificantly different.

For reasons of comparison, a small number of analyses were repeated using a simple initial velocity profile applied to the plate as a load condition. The initial velocity V_0 is assumed to be constant across the plate and its magnitude is calculated using the relationship

$$I = \int_0^R m \cdot V(r) \cdot dr \quad . \quad . \quad . \quad . \quad . \quad . \quad 3.12$$

yielding simply

$$V_0 = \frac{I}{M} \qquad \text{where} \qquad M = \frac{\pi d^2 t \cdot \rho}{4} \quad . \quad . \quad 3.13$$

is the mass of the plate. The two forms of load model are represented schematically in figure {3.3}.

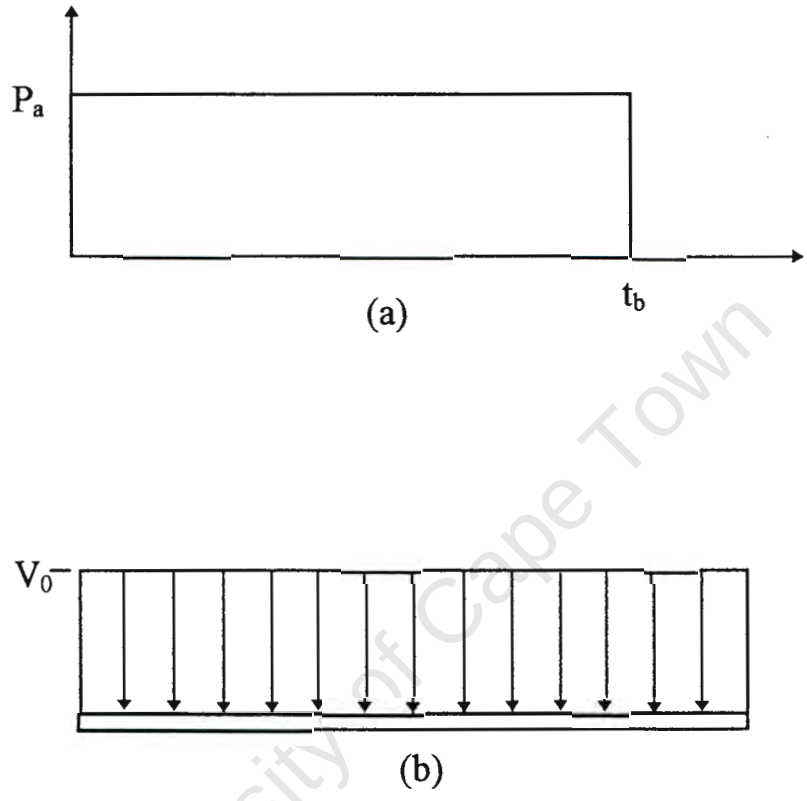

Figure {3.3} Schematic of the two methods of simulating the impulsive load; (a) pressure - time history and (b) applied initial velocity profile

3.2.4 Elements and meshing

The element selected for the analyses was a general reduced integration 4-noded axisymmetric continuum element (CAX4R). This element is not specifically designed to cater for shell analysis (as is the SAX1 element used by Farrow), but has the advantage of allowing more accurate representation of boundary conditions, and yielding far more detailed results of stress and strain through the thickness of the plate. The disadvantage of the continuum element as compared to the simpler 2-noded shell element, is that a large number of elements are needed at critical parts of the mesh in order that stress concentrations are fully resolved. Up to 3000 elements were used in some of the analyses, leading to solution times of several CPU hours. In a commercial environment the number of elements may have been reduced, but for the purposes of research, the solution times were not considered too costly.

While the use of an axisymmetric element forces the simplifying assumption that the behaviour of the plates is indeed axisymmetric, the cost of the analysis is greatly reduced due to the decreased number of elements required, and mesh design is also simplified. However it is to be noted that an asymmetric response has been reported in many experiments, particularly in the transition from Mode I to Mode II failure.

The meshing of the plate itself is straightforward due to the simple geometry of the axisymmetric cross section. Element density is increased toward the plate boundary where stress concentrations and the formation of a plastic hinge are anticipated. Up to 16 elements through the plate thickness are used at the boundary, whereas only 4 elements are required through the thickness at the plate centre where deformations follow a more gradual radius.

3.2.5 Boundary fixation

Several different boundary configurations were implemented using the same basic mesh. The configurations for which results are presented in this report are given in figure {3.4}.

FULLY BUILT-IN BOUNDARY			
Diameter		100mm	
Sharp edge		*t = 1.6mm*	
3.0mm fillet radius		*t = 2.75mm*	
2.0mm fillet radius		*t = 2.0mm*	
2.0mm fillet radius (one side)		*t = 1.9mm*	
CLAMPED BOUNDARY			
Diameter	120mm	100mm	80mm
Sharp edge	*t = 1.6mm*	*t = 1.6mm*	*t = 1.6mm*
3.2mm edge radius		*t = 1.6mm*	
1.6mm edge radius		*t = 1.6mm*	

Figure {3.4} Table of the various plate configurations modelled in this investigation.

3.2.5 (a) FULLY BUILT-IN

In order to simulate the fully built-in boundary assumption, on which most analytic solutions have been based, two approaches were undertaken. Initially all degrees of freedom of those nodes corresponding to the plate edge were fixed, allowing no rotations and no translations. However such a boundary condition is entirely theoretical, and to more closely model the experiments of Thomas [17], the finite element mesh was extended to include the actual material boundary, having the same material properties as the plate itself.

3.2.5 (b) CLAMPED

Most experimental work has been conducted on plates that have been fixed between steel clamps at the boundary, where the thickness of these clamps is considerably greater than that of the plate and consequently any deformations in the clamps have been considered negligible. Nurick [12] reports that clamping pressure was applied evenly by the use of eight high tensile bolts tightened to a predetermined torque. However no reports of the magnitude of the clamping pressure were found.

In the finite element model, the clamps are approximated as perfectly rigid, rough surfaces to which either a pressure or fixed displacement can be applied. A simple Mohr-Coulomb friction model is applied between the rigid clamping elements, that assumes no relative motion between the contacting surfaces will occur if the equivalent frictional stress

$$\tau_{eq} = \sqrt{\tau_1^2 + \tau_2^2} \quad . \quad . \quad . \quad . \quad . \quad . \quad 3.14$$

is less than the critical stress τ_{crit}, which is proportional to the contact pressure, $P_{contact}$, in the form $\tau_{crit} = \mu P_{contact}$ where μ is the coefficient of friction prescribed. Values ranging from 0.2 to 0.7 were used for μ in order to gauge the sensitivity of the response.

Clamping pressure was achieved through the application of a fixed displacement to one of the rigid clamps. An initial value of 5×10^{-3} mm was selected that would correspond to a strain through the thickness of the clamped region of the plate of approximately 0.003, implying a clamping pressure of around 600MPa. This value was confirmed by the analysis. However different values were also used in order to gauge the sensitivity of the response to the magnitude of clamping pressure, and the results are reported in the following chapter.

The four basic meshes are represented schematically in figure {3.5}.

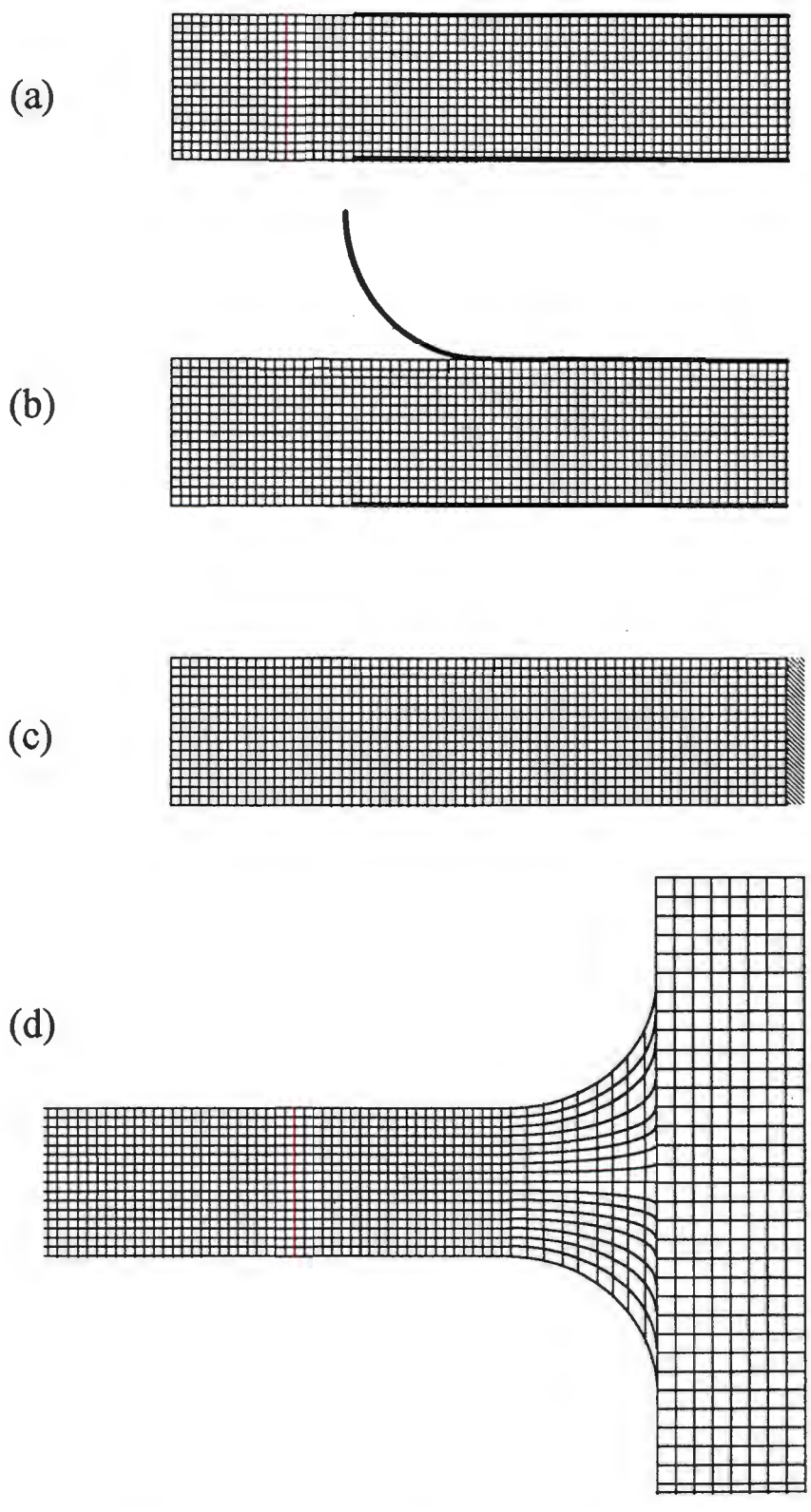

Figure {3.5} Schematic representation of the meshing of the various boundary conditions; (a) clamped; (b) clamped with edge radius; (c) fully built-in and (d) built-in with fillet radius.

4. RESULTS

4.1 MODE I RESPONSE

Establishing the level of correlation between the current model and experiments for the range of impulses causing only permanent plastic deformations, is essential before more complex behaviour, such as failure through rupture, can be considered. For the investigation of this Mode I response, results were obtained from the ABAQUS model for a range of five impulses from 4Ns to 20Ns for all the geometries and boundary conditions described, and at higher impulses in some cases, such as where the inclusion of fillet radii has been shown to increase the magnitude of the impulse required to cause tearing. A variety of criteria are used for comparison with experimental data and selected analytic predictions.

4.1.1 Convergence

Farrow [31] reported that the use of just 4 axisymmetric shell elements was sufficient for the convergence of mid-point deflection, and that 10 to 20 elements ensured convergence of stresses. In the case of general planar shell elements, a mesh containing 300 elements ensured convergence. In this study, a comparative analysis was undertaken using 80 axisymmetric shell elements, with the density of elements biased toward the plate boundary, as compared to the 20 element unbiased mesh reported by Farrow. Figure {4.1} indicates that while deflections for the 20 element mesh had converged, the concentration of plastic straining at the plate boundary had not. This demonstrates the need for adequate mesh refinement in such critical areas. However it is noted that the cost of solution for the more refined mesh was an order of magnitude greater, due to the decreased critical length of the elements.

For the axisymmetric continuum elements used in this study, convergence of mid-point deflection was found to occur for a coarser mesh than the final mesh used. However the refinement of the mesh is to ensure full convergence of stresses, especially in areas of high stress concentration, and to better resolve phenomena such as the indentation of the steel clamps at the plate boundary. The mesh sensitivity of the ABAQUS tearing

the ABAQUS tearing model was also considered and this is discussed further in the section covering Mode II failure. In the final mesh used, areas of high strain were modelled with 16 elements through the plate thickness, and as many as 4000 in the entire mesh. Comparisons of runs using meshes with increasing degrees of refinement indicate that in the final mesh used, stresses have converged fully. The time cost of the solution is variable depending on the nature of the boundary condition, in which region the smallest elements occur, and is also increased for the case of clamping, due to the use of an extra step in the analysis. Typical solution times vary from 30 to 200 minutes of CPU time on an IBM RS600 computer.

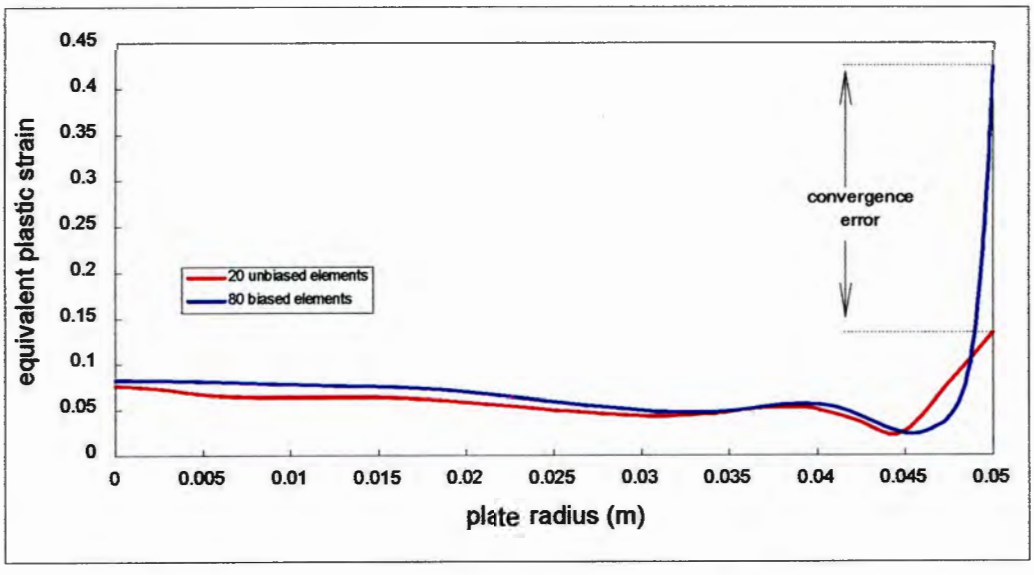

Figure {4.1} Convergence of equivalent plastic strain on the loaded surface for the axisymmetric shell finite element model of Farrow.

4.1.2 Response time

The time taken for the plate to reach its final deformed shape during a Mode I response is difficult to measure experimentally. However Bodner and Symonds [11] and Nurick [12] report response times in the region of 100 to 200μs, with 150μs as an average, for 100mm diameter mild-steel circular plates. These observations are included in figure {4.2} which shows the mid-plate deflection-time response for a fully built-in plate at I = 12Ns. The path of the response is seen to be independent of the element and loading method used and is essentially linear. However the overall response times show a small variation with these parameters. In general the shell

element model shows a slightly slower response time as compared to the continuum element model used throughout the current study, and this is in closer agreement with the more recent experimental results of Nurick, and also with predictions of Olson et al [30] using NAAPFE. The use of an initial velocity profile to approximate loading, leads to a marginally reduced response time. However all the predicted response times for plates of 100mm diameter fall within the bounds of experimental observations.

The yellow line in figure {4.2} is the response path of the same plate where the Cowper-Symonds relationship (equation 3.6) has been replaced by Jones's [25] n-value approximation (equation 2.11) for strain rate sensitivity. This modification is necessary in the prediction of Mode II failure that is documented later on in the report. It is seen that both the overall midpoint deflection and response time are increased, but that the early part of the response follows the same path as the original model. Olson et al predicted that early plate response was independent of strain rate sensitivity effects and this trend appears to be supported.

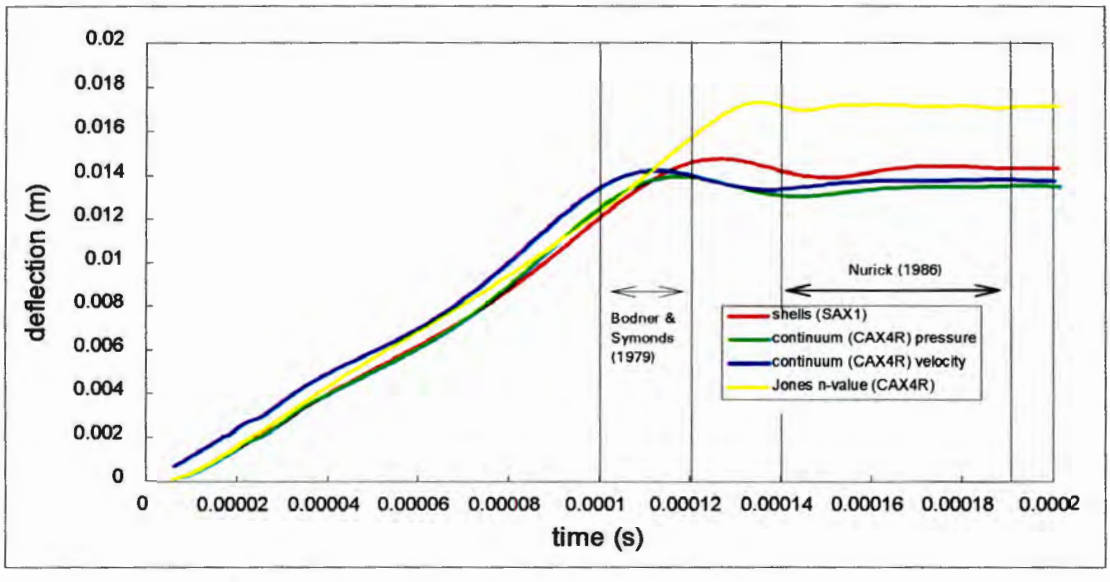

Figure {4.2} Response path of the plate centre for a 100mm fully built-in plate, showing the influence of element type and loading method.

For plates of different dimensions, the response time is seen to increase with diameter, as shown in figure {4.3}. The experimental observations of Bodner and Symonds (100 - 110μs) were for 64mm mild steel plates, whereas those of Nurick (140 - 190μs) where for 100mm plates, and so it is clear that the limited experimental evidence supports this finding. Furthermore it is consistent with the hypothesis that the mechanism of plate deformation is through the propagation of a zone of bending that originates near the plate boundary at the start of the global response and arrives at the plate centre at the end of this response. Additional evidence in support of this hypothesis is presented later.

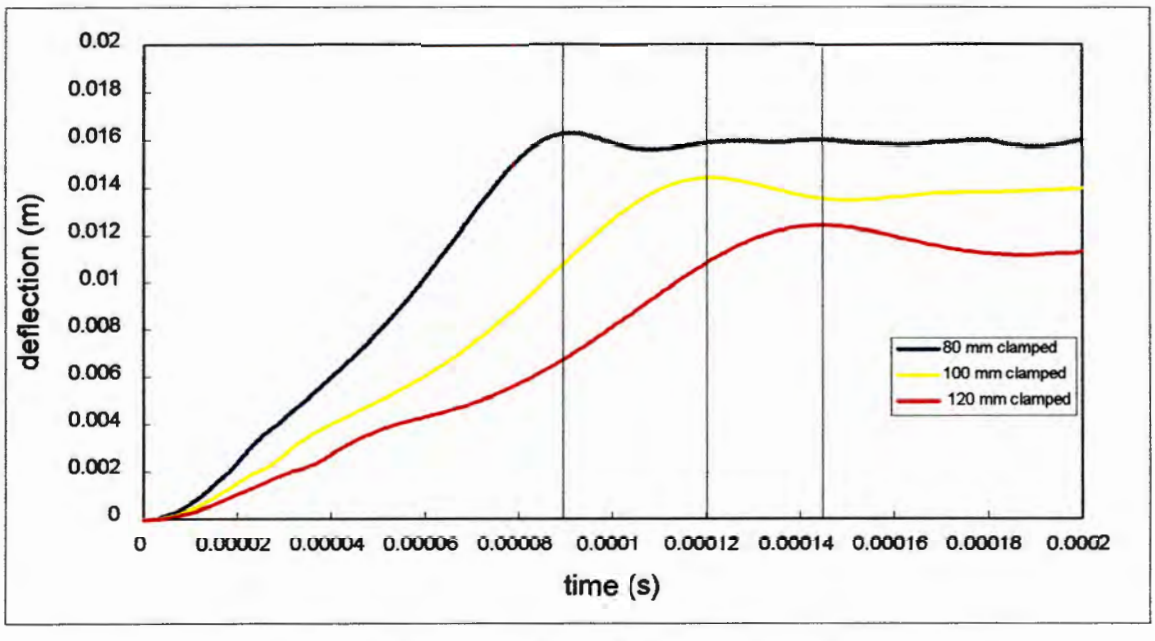

Figure {4.3} Response paths of the plate centre for clamped plates of diameters 80mm, 100mm and 120mm.

4.1.3 Mid-point deflections

The value of permanent deflection at the centre of the plate is the most commonly used criterion for comparison of response in the Mode I region, plotted against the value of applied impulse. In order to compare plates of differing thickness, diameter and yield stress, the deflection to thickness ratio is plotted against the damage number ϕ, which is a dimensionless impulse (given by equation 2.4). Such results for the range of impulses 4, 8, 12, 16 and 20Ns were obtained for all the plate diameters and boundary conditions under consideration. Figures {4.4} and {4.5} show the numerical predictions plotted against experimental data for 100mm plates with a sharp edge clamped boundary condition and a fully built-in boundary condition with no fillet radii.

The ABAQUS predictions for mid-point deflection are seen to follow the same linearly increasing trend with dimensionless impulse as the experiments. In general the deflections are slightly under-predicted, but this is limited to less than the thickness of the plate itself. Similar results are obtained for the clamped plates of different overall diameter and with edge radii included, and graphs for comparison with all the experimental data are found in Appendix 1.

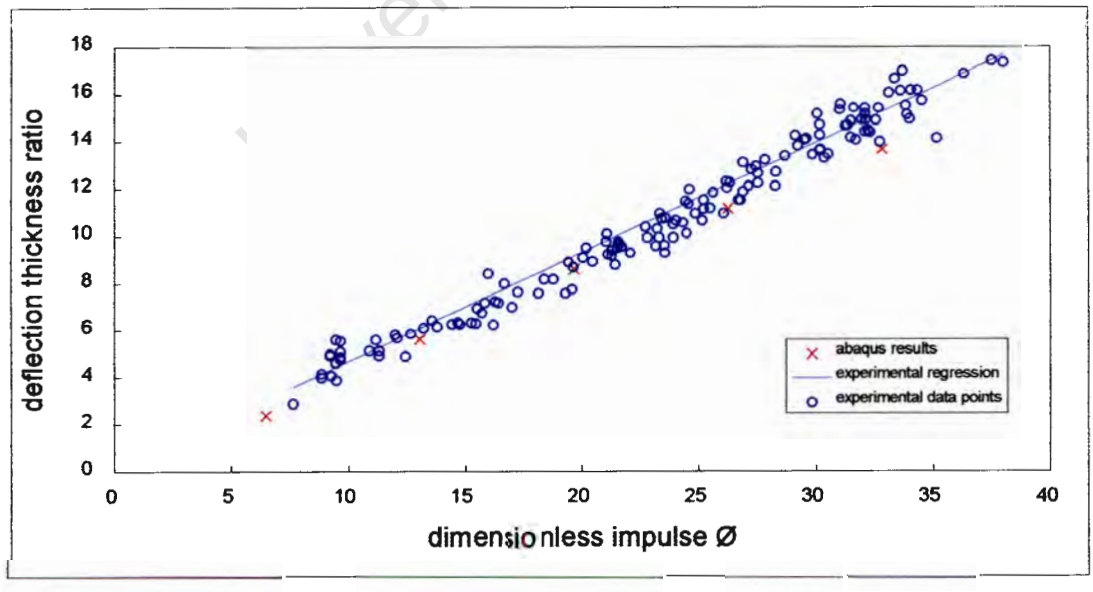

Figure {4.4} Experimental results and numerical predictions for 100mm clamped plates with a sharp clamp edge.

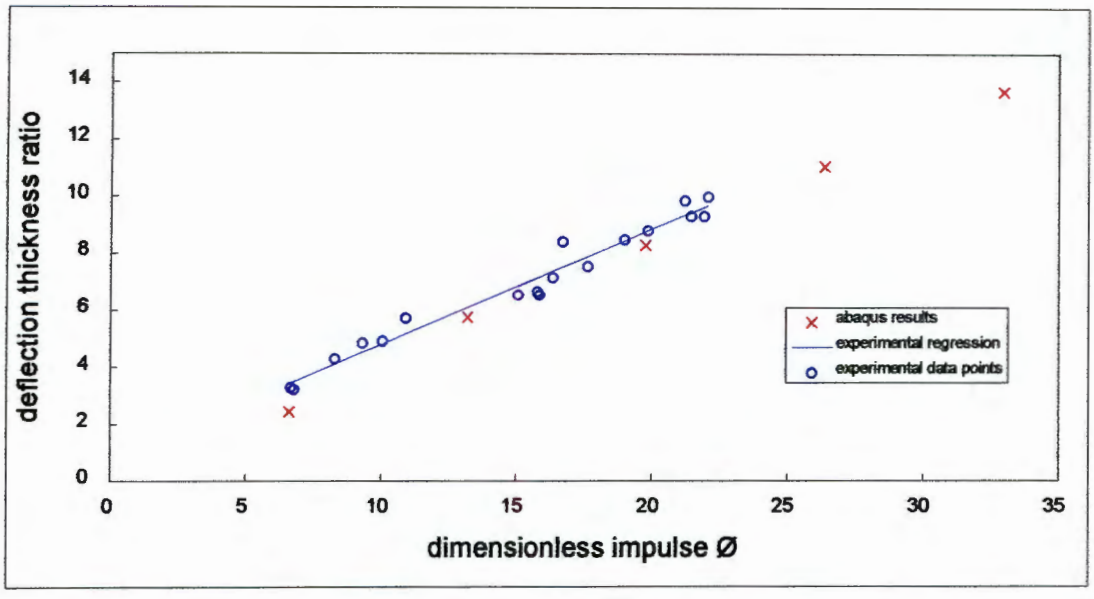

Figure {4.5} Experimental results and numerical predictions for 100mm fully built-in plates with a sharp corner at the boundary.

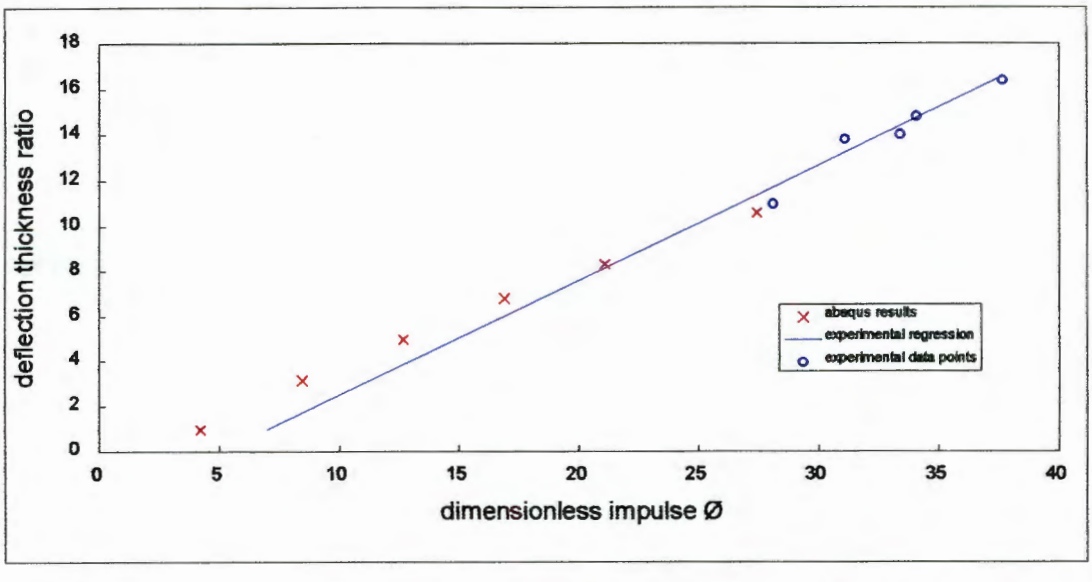

Figure {4.6} Experimental results and numerical predictions for 100mm fully built-in plates with thickness = 2.0mm and a 2.0mm fillet radius at the boundary.

In the case of fully built-in plates with fillet radii, the experimental trends are obscured in some cases due to data being available only for a narrow range of applied impulse. However where the experimental trend is interpolated, good correlation can be deduced. The example of 2.0mm plates with a 2.0mm fillet radius is presented in figure {4.6}, while the other cases appear in Appendix 1.

Comparison is also made with some of the analytic and numerical predictions discussed previously. Figure {4.7} shows the predicted trends for both clamped and fully built-in 100mm plates alongside analytic predictions due to Lippman [21], Perrone and Bhadra [22], Symonds andWierzbicki [23] and Jones [25], and the numerical predictions of Farrow [32]. Correlation is seen to be very good, in particular with the numerical predictions of Farrow. The solutions of Jones, and Symonds and Wierzbicki do not take into account strain hardening, and this may explain their somewhat high predictions.

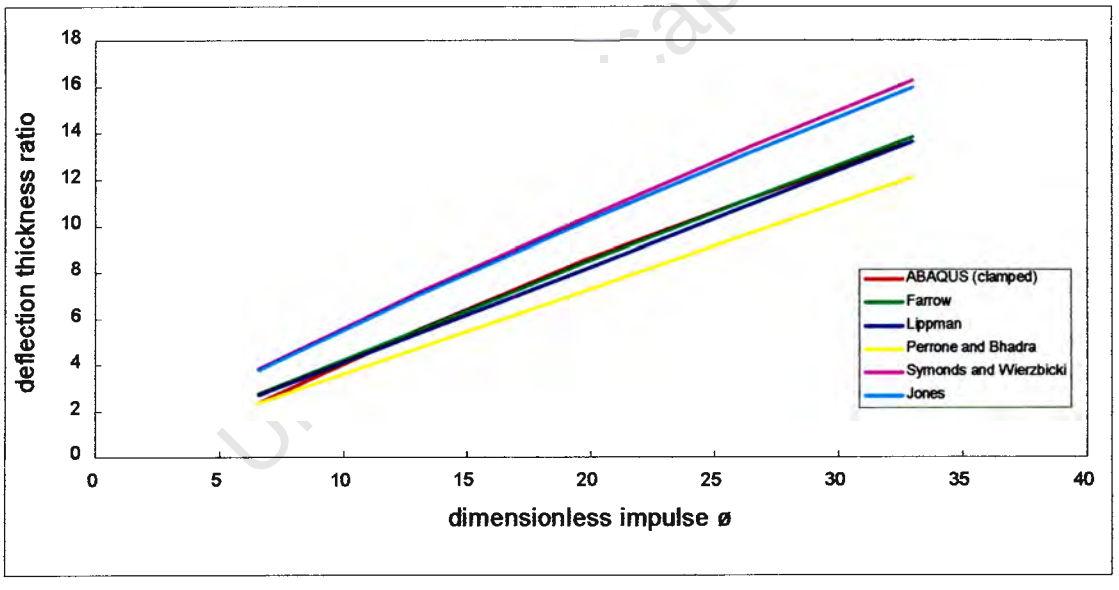

Figure {4.7} Deflection-thickness ratio vs. dimensionless impulse ø, comparing the current numerical model to various analytic predictions.

The effect of the inclusion of an edge radius on the clamped boundary condition, is demonstrated in figure {4.8}. Deflections are slightly increased as the boundary condition is relaxed, which is consistent with the experimental observations of Marshall [16], but no distinction can be made as the edge radius is increased from 1.6mm to 3.2mm.

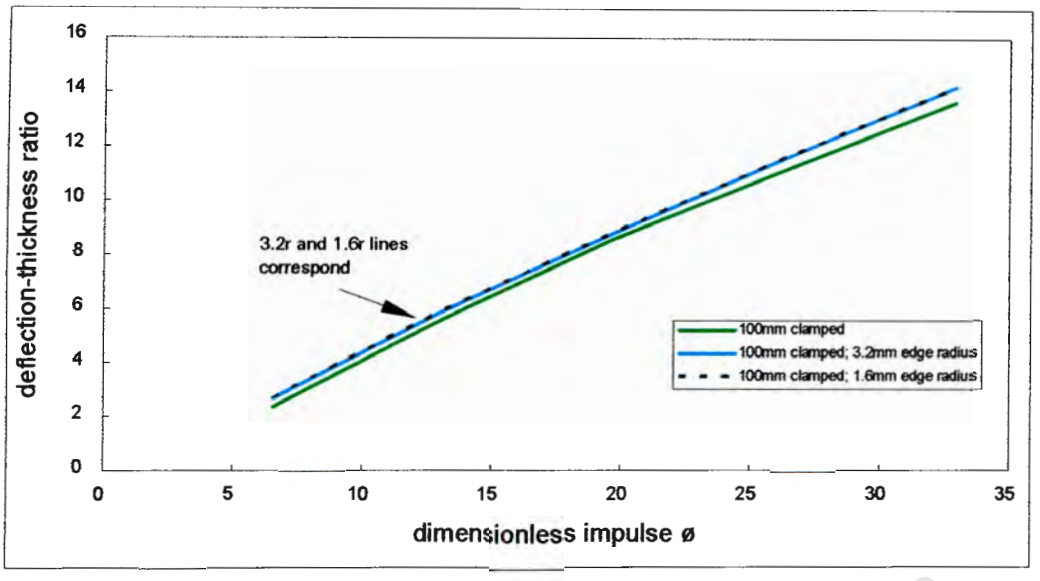

Figure {4.8} Graph showing the influence of edge radius on the Mode I response of clamped plates.

The effect of inclusion of a fillet radius on mid-point deflection in the case of built-in plates, is somewhat obscured by the fact that plates of different thicknesses are involved. However it can be seen in figure {4.9} that variations in deflection to thickness ratio are very slight for the cases investigated, and assuming that the effect of the fillet radius is not large, the validity of the use of dimensionless measures for both deflection and impulse is noted, in that the trends for plates of thicknesses of 1.6mm, 1.9mm, 2.0mm and 3.0mm are collapsed into a band narrower than one plate thickness. This is again demonstrated where clamped plates of various diameters are involved, as shown in figure {4.10}. Plate stiffness is observed to increase slightly as diameter decreases, but once again the dimensionless data falls in a narrow band.

Finally in order to compare the overall influence of boundary condition, figure {4.11} shows deflection-thickness ratio against dimensionless impulse for one of each of the four categories of boundary condition under scrutiny. It is seen that variation in deflection across the range of impulses is of the order of one plate thickness or less. Figure {4.12} represent the deflection-thickness data for all the boundary conditions discussed.

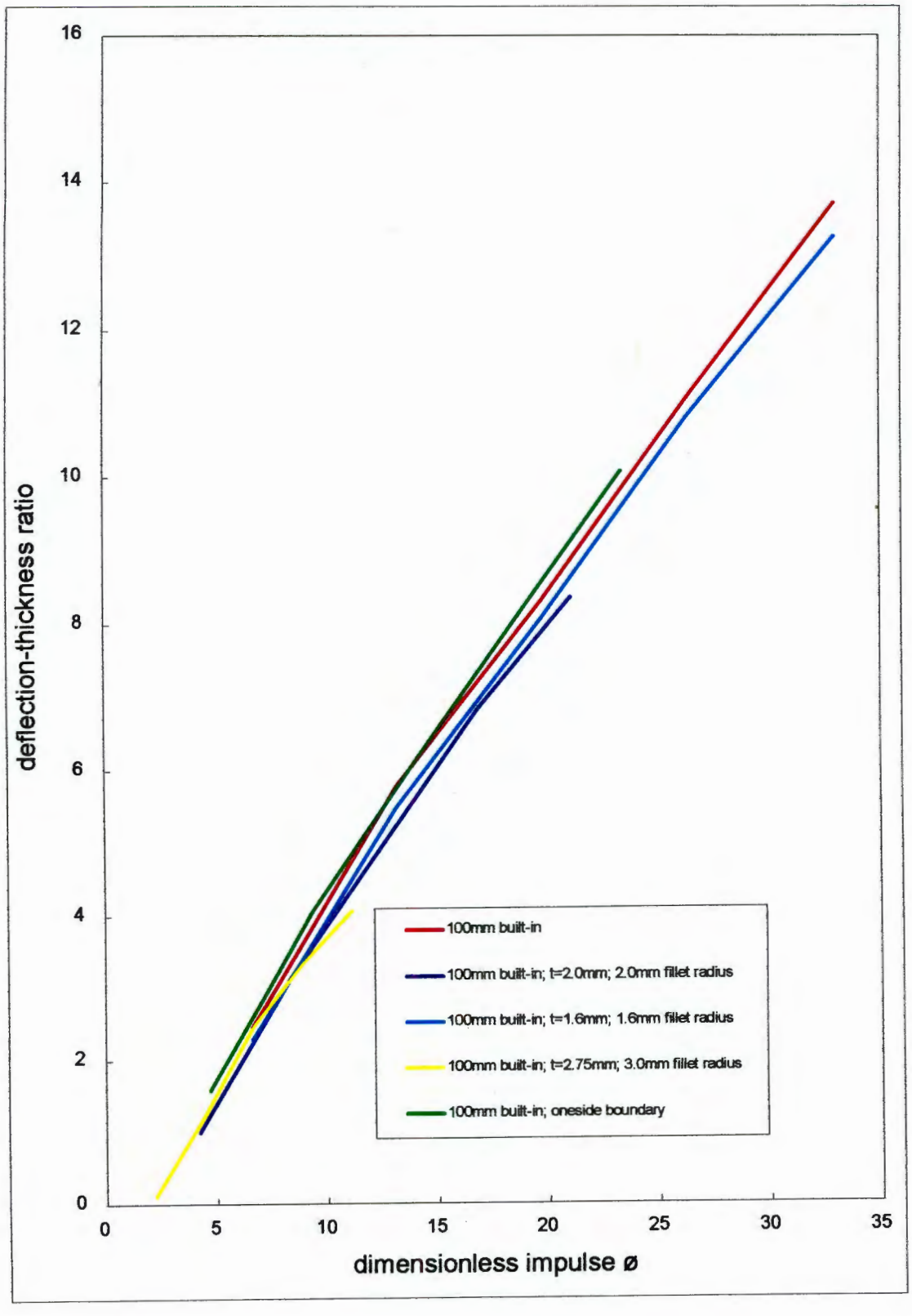

Figure {4.9} Graph showing the influence of plate thickness and fillet radius on the Mode I response of fully built-in plates.

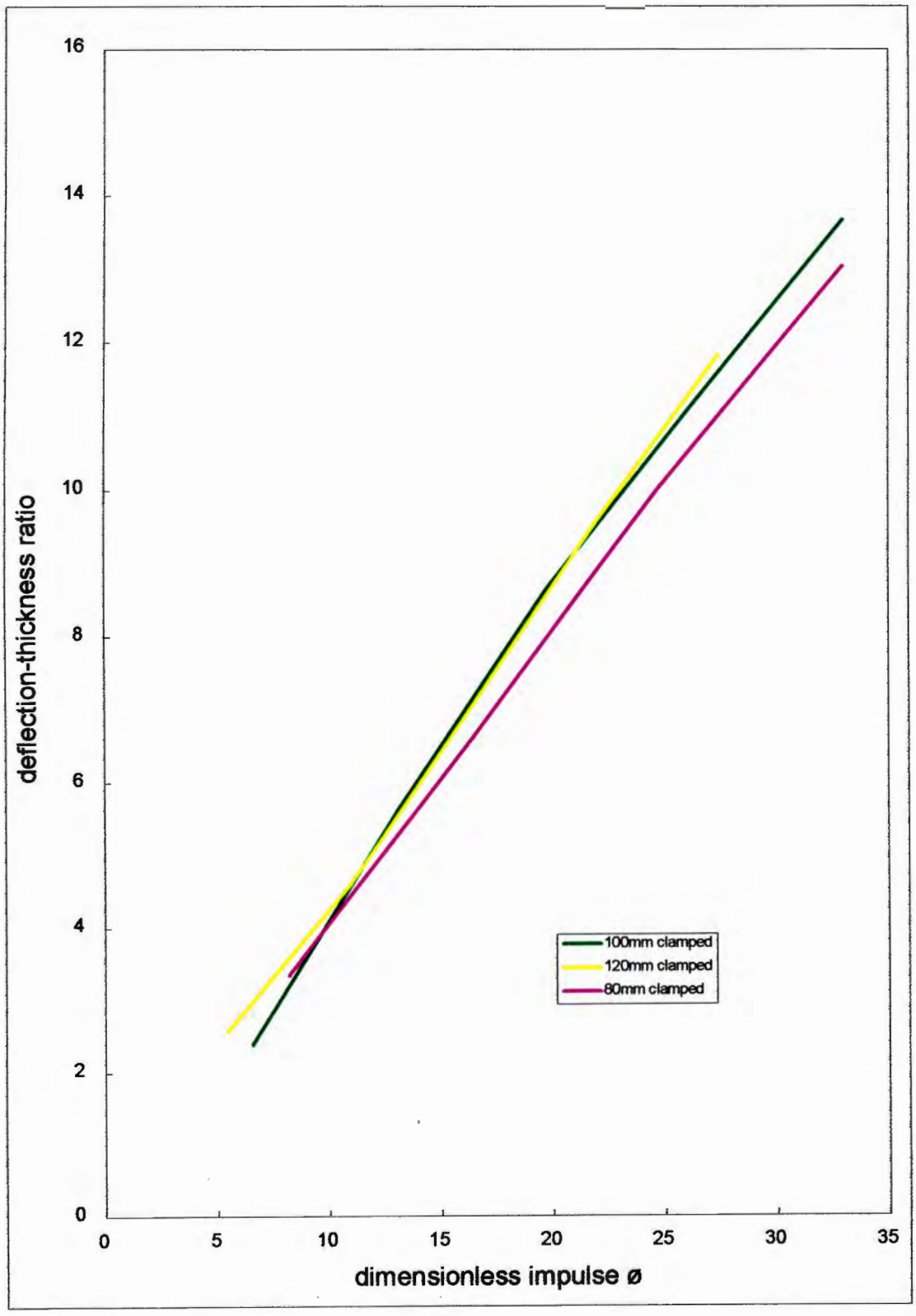

Figure {4.10} Graph showing the influence of plate diameter on the Mode I response of clamped plates.

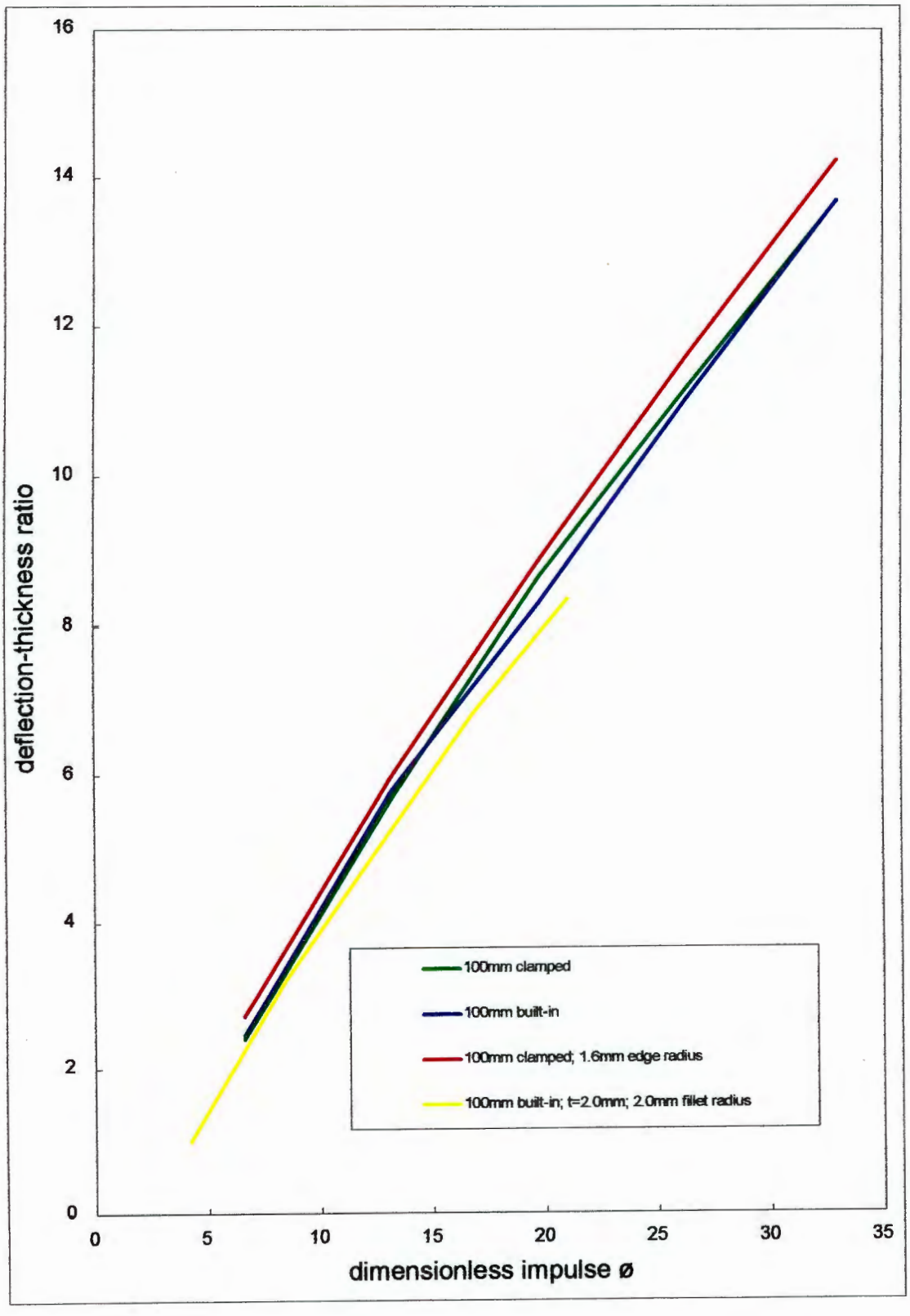

Figure {4.11} Graph showing the effect of boundary fixation method on the Mode I response of plates.

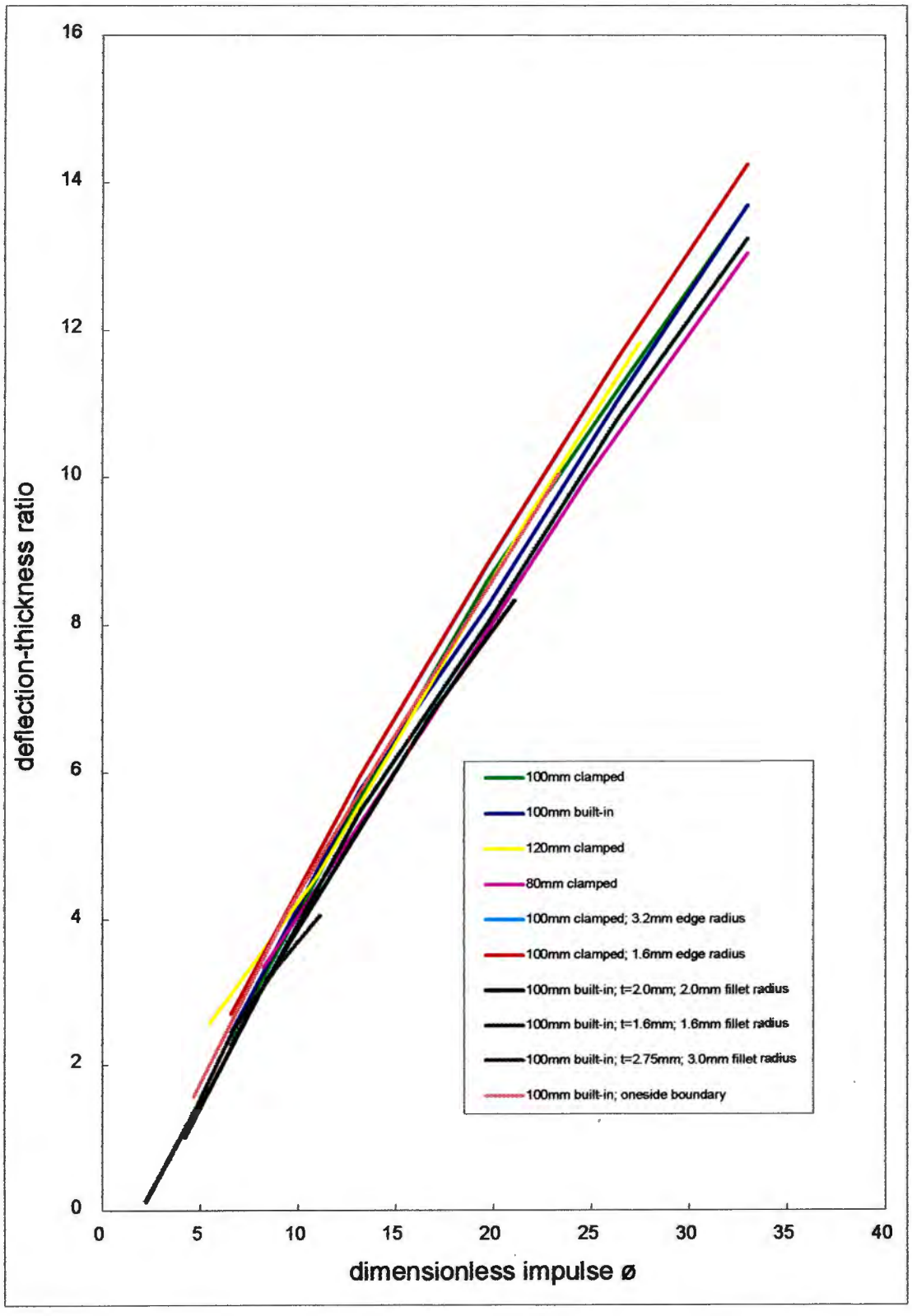

Figure {4.12} Deflection-thickness ratio against dimensionless impulse ø for all the plate configurations modelled in the investigation.

4.1.4 Deformed plate profiles

Overall deflected shapes resulting from the current analysis correlate reasonably well with those experimentally observed, as shown in figure {4.13}. The experimental profile was observed by Teeling-Smith [14] to be in the form of a cosine, but the current predictions, and those of Farrow [32] using shell elements, are somewhat flatter in the mid-section of the plate. Figure {4.13} also indicates that for the different parameters investigated, final deflected profile is not highly dependent on element type, boundary fixation method, or load model. Similar profiles are obtained for both the clamped and built-in boundary conditions and these are similar to the profile predicted by Farrow using shell elements, and a fully built-in boundary. The use of a uniform initial velocity load leads to similar plate shapes as a short duration pressure pulse for a range of Mode I impulses, as illustrated in figure {4.14}.

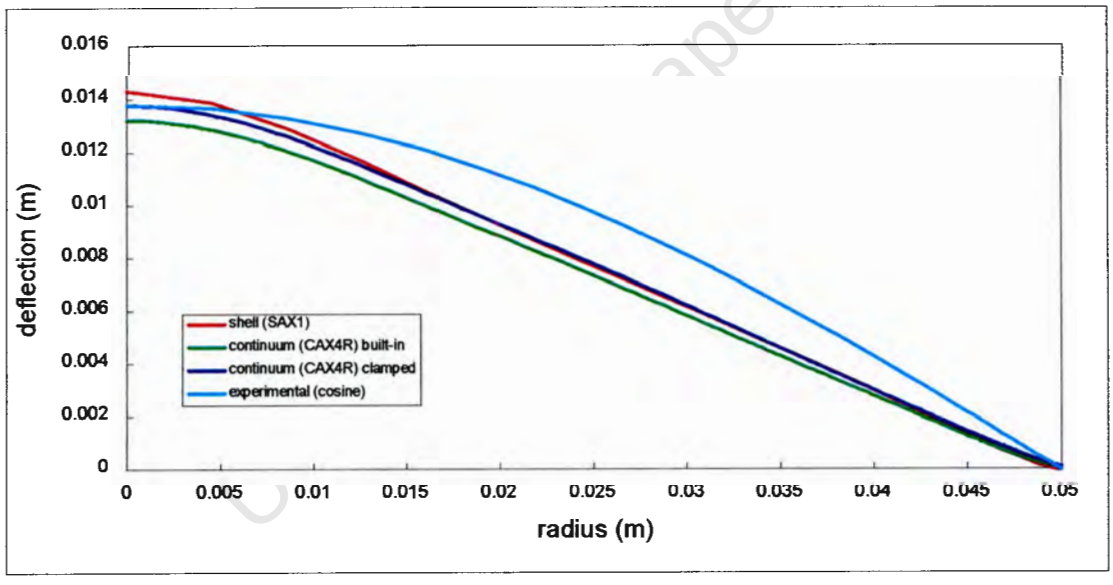

Figure {4.13} Deflected profiles for clamped and fully built-in plates at I = 12 Ns, using axisymmetric shell elements and quadrilateral continuum elements.

The effect on overall deflected shape of the parameters associated with the clamping model are illustrated in figure {4.15}. Analyses were performed for a 100mm clamped plate at a high value of impulse of 20Ns that would lead to an increased tendency for material draw through to occur. Clamping conditions in the finite element model were made increasingly severe and it can be seen that where clamp coefficient of friction μ was increased from 0.2 to 0.7 and simultaneoulsy clamping

pressure from approximately 600MPa to 1250MPa, there is little change in the Mode I response in terms of mid-point deflection or deformed profile. However the effect of clamping on strains is significant especially at the boundary itself, and thus Mode II tearing based on a maximum strain criterion can be expected to be influenced.

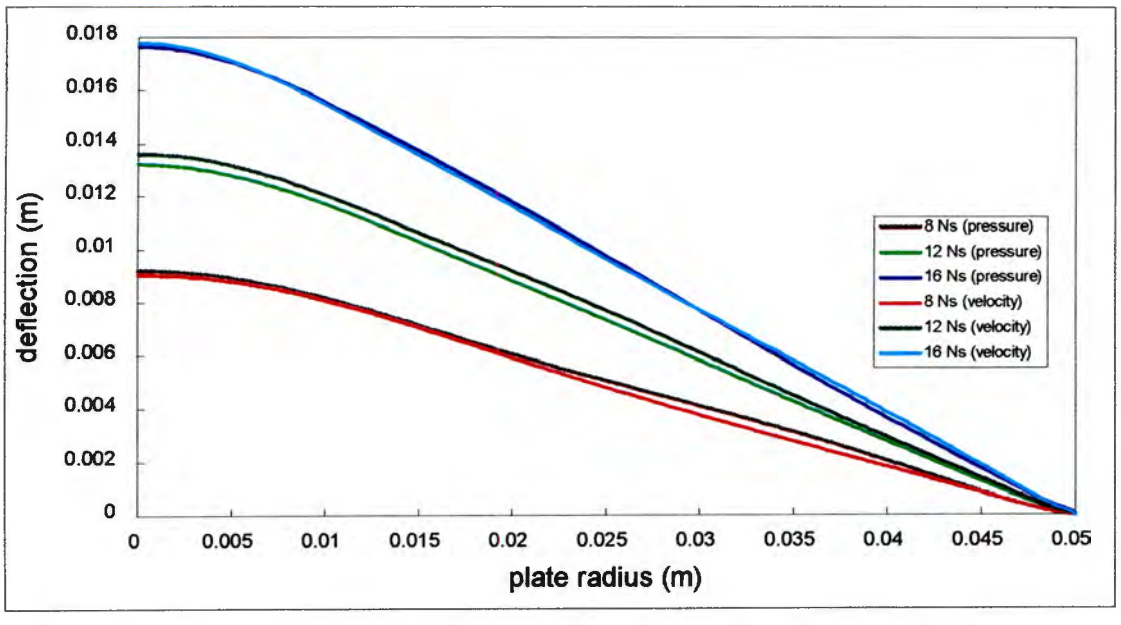

Figure {4.14} Deflected profiles for a 100mm built-in plate; using a pressure time history loading method; using an initial velocity profile.

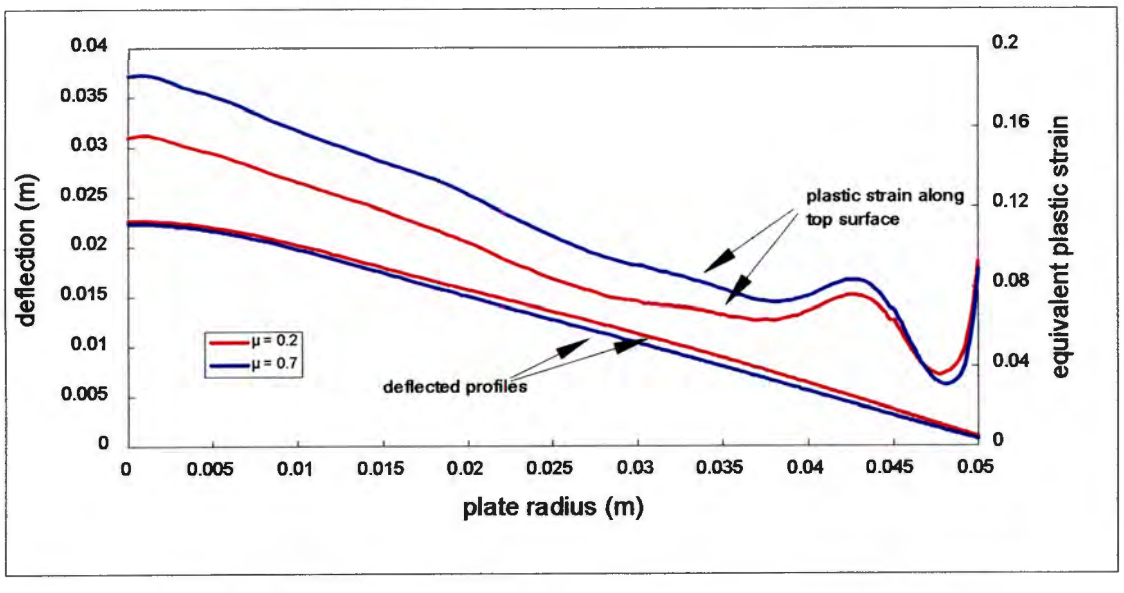

Figure {4.15} The effect of coefficient of friction μ at the clamped boundary on deformed plate profile and plastic strain distribution.

The deflected profiles for all the plate configurations are recorded in Appendix 2 for reference. An example of the effect of boundary condition on deflected shape is given in figure {4.16}. The form of the deflected profile does not appear to be influenced significantly by the method of boundary fixation, as approximately similar shapes result for both clamped and fully built-in plates, as well as with the inclusion of an edge radius.

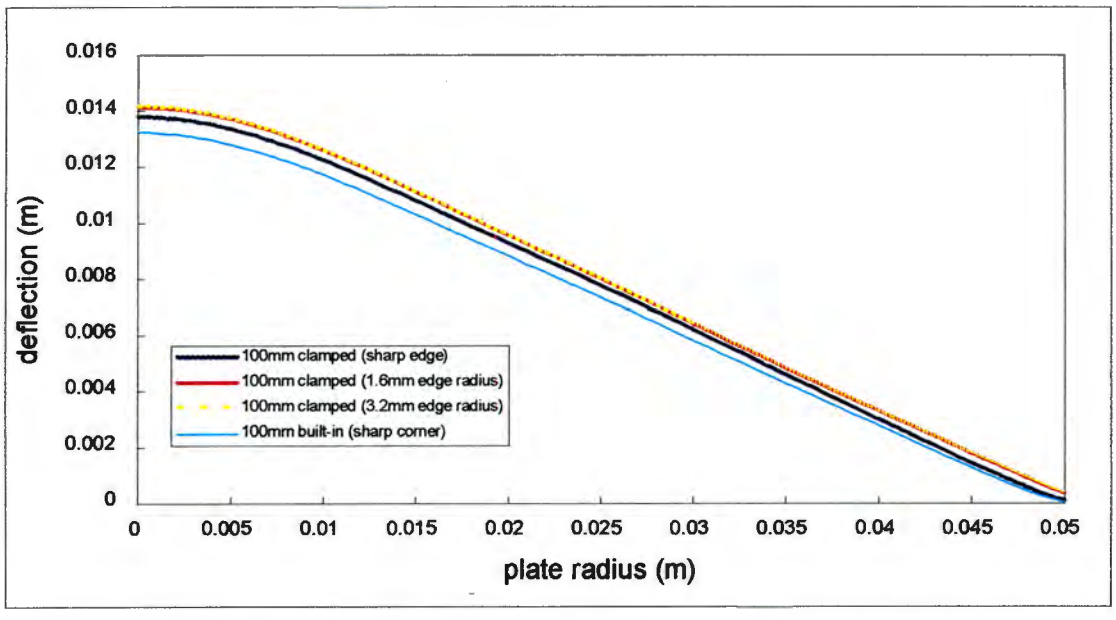

Figure {4.16} The effect of edge radius on the deflected profiles of 100mm clamped plates.

Thomas [18] observed that while overall deflected profiles were similar for clamped and built-in plates, there were differences in profile very close to the boundary. Figure {4.16} does not indicate whether such a difference in profile is predicted by the current model. Detailed observations of the boundary, however, are made later in this chapter.

4.2 TRANSIENT RESPONSE

A large number of increments are required by ABAQUS/Explicit to solve the plate response for the meshes used, typically of the order of 10 000 to 15 000, and information is available after each of these increments for displacements and strains. This allows the transient response of the plate to be observed in considerable detail.

4.2.1 Transient plate profiles

It has been noted that in an experimental situation, the transient deformation response of a blast loaded plate is difficult to observe. Figure {4.17} shows such a time history of deformed plate profile for a 12Ns impulse acting on a 100mm fully built-in plate, obtained from the numerical analysis.

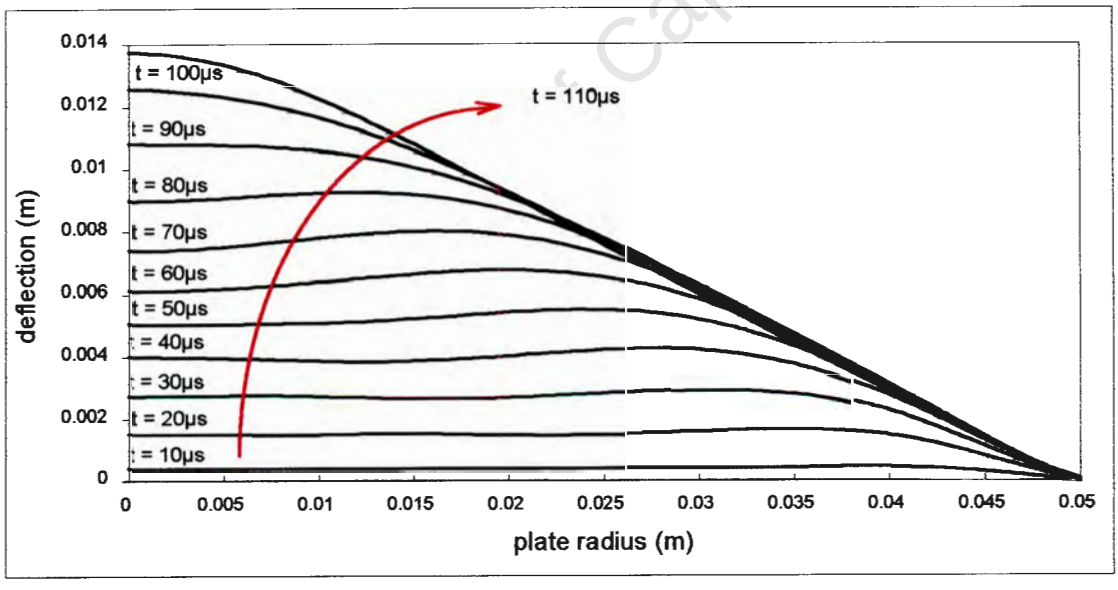

Figure {4.17} The transient profile response of a 100mm built-in plate at I = 12 Ns.

It is observed that near the beginning of the response, for times less than around 10μs, the entire plate (other than close to the fixed boundary) accelerates to move with approximately an uniform speed of around 125m/s, hence maintaining an almost flat profile. Although the speed of the plate is not exactly constant throughout due to the restriction placed by the boundary, and also not instantaneously reached due to the plate accelerating from its initial state of rest, the value of speed away from the boundary is very close to the 121m/s calculated for use with the initial velocity profile method described previously. This is consistent with the similar Mode I response reported in the previous section for both loading methods.

4.2.2 Deformation mechanism

The final resultant shape of the plate appears to be as the result of the propagation of a plastic hinge that forms near the plate boundary at the start of the response and travels toward the plate centre. When this plastic hinge reaches the plate centre the response of the plate is complete. This explains the increase of response time with plate diameter noted in the previous section, since the hinge has a greater distance to travel.

The propagation of this plastic hinge is better illustrated in figure {4.18}, which shows the growth of plastic strain on the bottom (loaded) surface of the plate. By 10μs, three distinct zones on the plate surface have reached yield. It is seen that by 30μs a peak value of plastic strain has been reached at the boundary, where a stationary plastic bending hinge forms. Another stationary plastic bending zone develops at the plate centre. The propagating plastic hinge is seen to form close to the plate boundary and travel toward the plate centre, so that the by the end of the response the entire plate surface had yielded, with peaks of plastic strain occurring at the boundary and centre, and a distinct minimum of plastic strain existing at about 3mm from the boundary. In figure {4.19} the propagating plastic hinge which corresponds to a zone of high bending stresses, is made visible by plotting areas of high Mises stress. The initiation and progress of the bending is clearly visible.

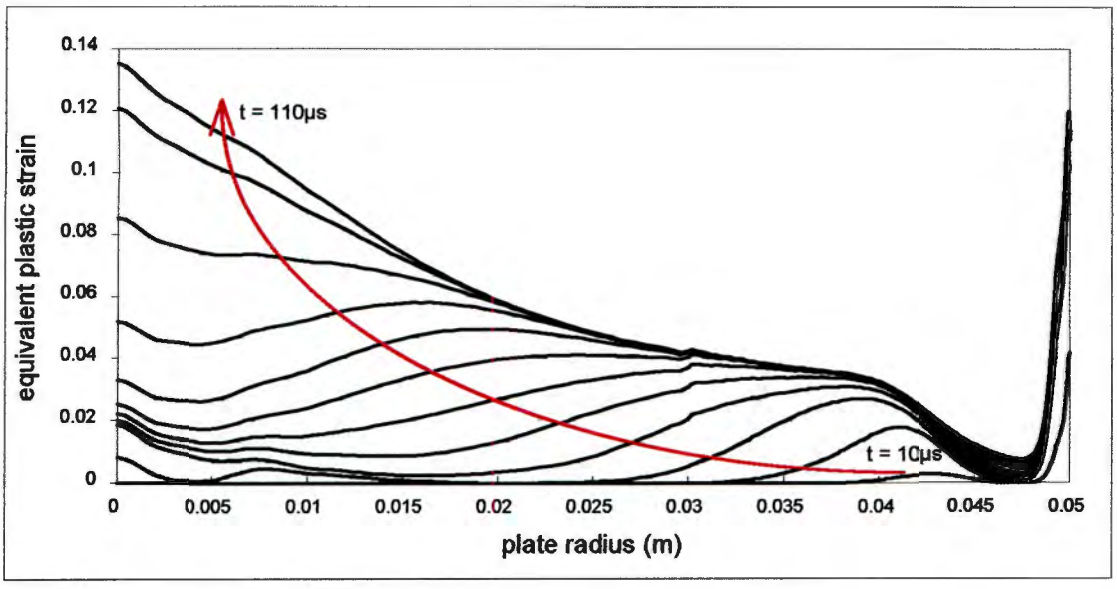

Figure {4.18} Plasticity growth due to the propagation of a bending hinge in a 100mm built-in plate at I = 12 Ns.

Figure {4.19} Visualisation of the propagation of the plastic bending hinge through Mises stress.

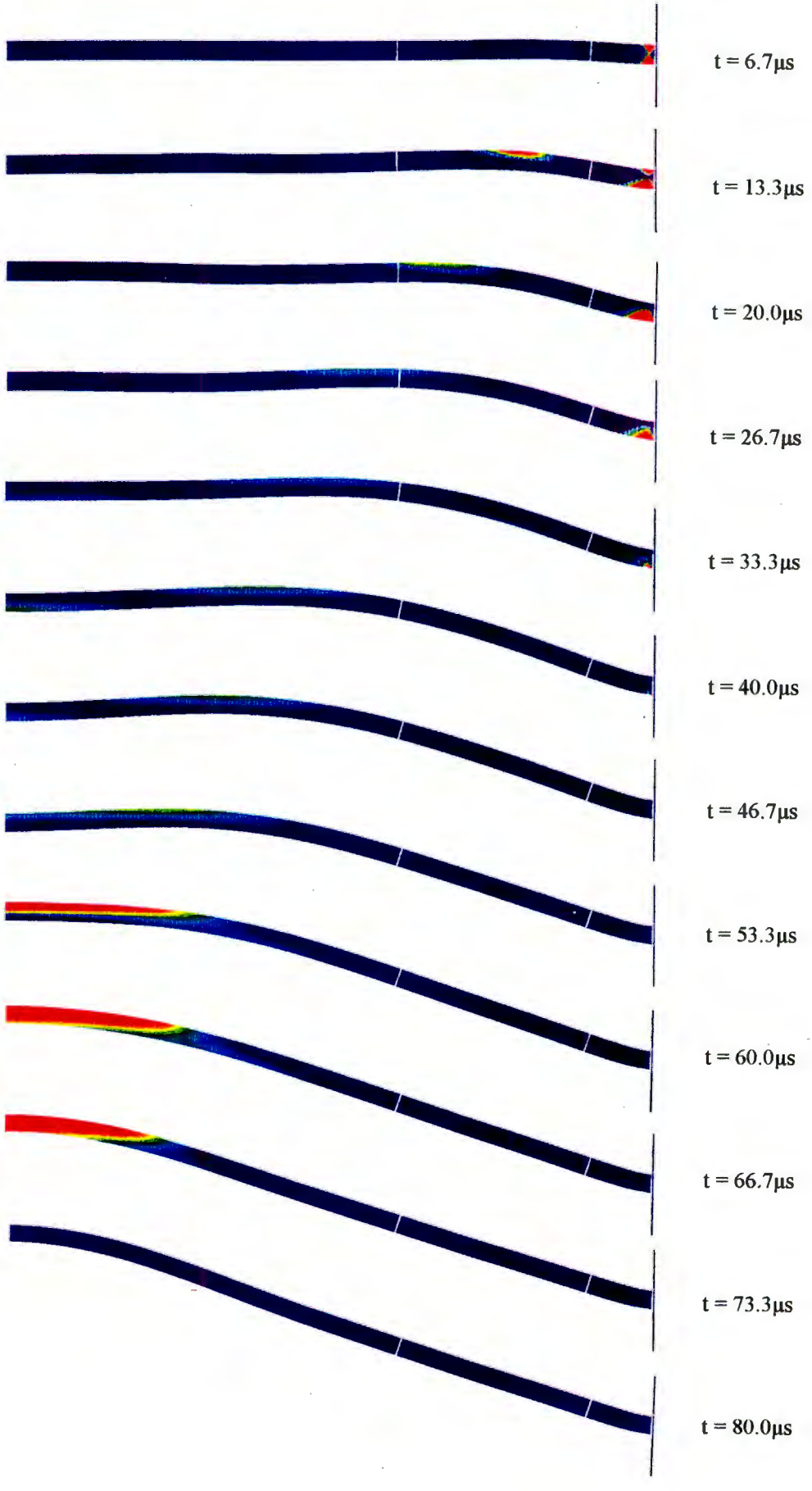

4.3 DETAILED BOUNDARY BEHAVIOUR

The use of several 2 dimensional elements through the plate thickness allows detailed observations of behaviour at the plate boundary and this section investigates the effect of boundary fixation method on localised behaviour, for the range of impulses covered in the previous sections.

4.3.1 Thinning and indentation

Figures {4.20} through {4.27} show detail of deflections near the plate edge for all the boundary fixation conditions studied. These plots are from analyses where the ABAQUS strain based failure model is not incorporated, and so there is no allowance made for the "strain softening" type of behaviour that occurs in true localisation, where a tensile specimen for example loses overall stiffness as a neck forms. As a result, only thinning due to localised stretching is predicted. Actual necking prior to rupture will be considered where the failure model is included in the analysis, later in this chapter.

In general there is some visual evidence of thinning for higher impulses in the case of clamped plates and this is not as readily apparent for the built-in plates. Thomas [18] observed this to be true from experimental evidence, and found that clamped plates had a greater tendency to display thinning at the boundary over a wider range of impulses, while built-in plates showed only limited thinning over a narrow range of impulse, followed by a tendency towards shear. For built-in plates with fillet radii, there is no visual evidence of thinning behaviour at all. Figure {4.28} shows a plot of the percentage thinning that occurs at the boundary with increasing impulse for plates of different diameter and boundary fixation. The percentage reported relates to the thinnest point of the plate and does not indicate the extent of thinning away from this point. Thus in the case of clamped plates the effect of indentation is very significant and greatly overshadows the effect of stretching, in producing a minimum thickness which is very localised.

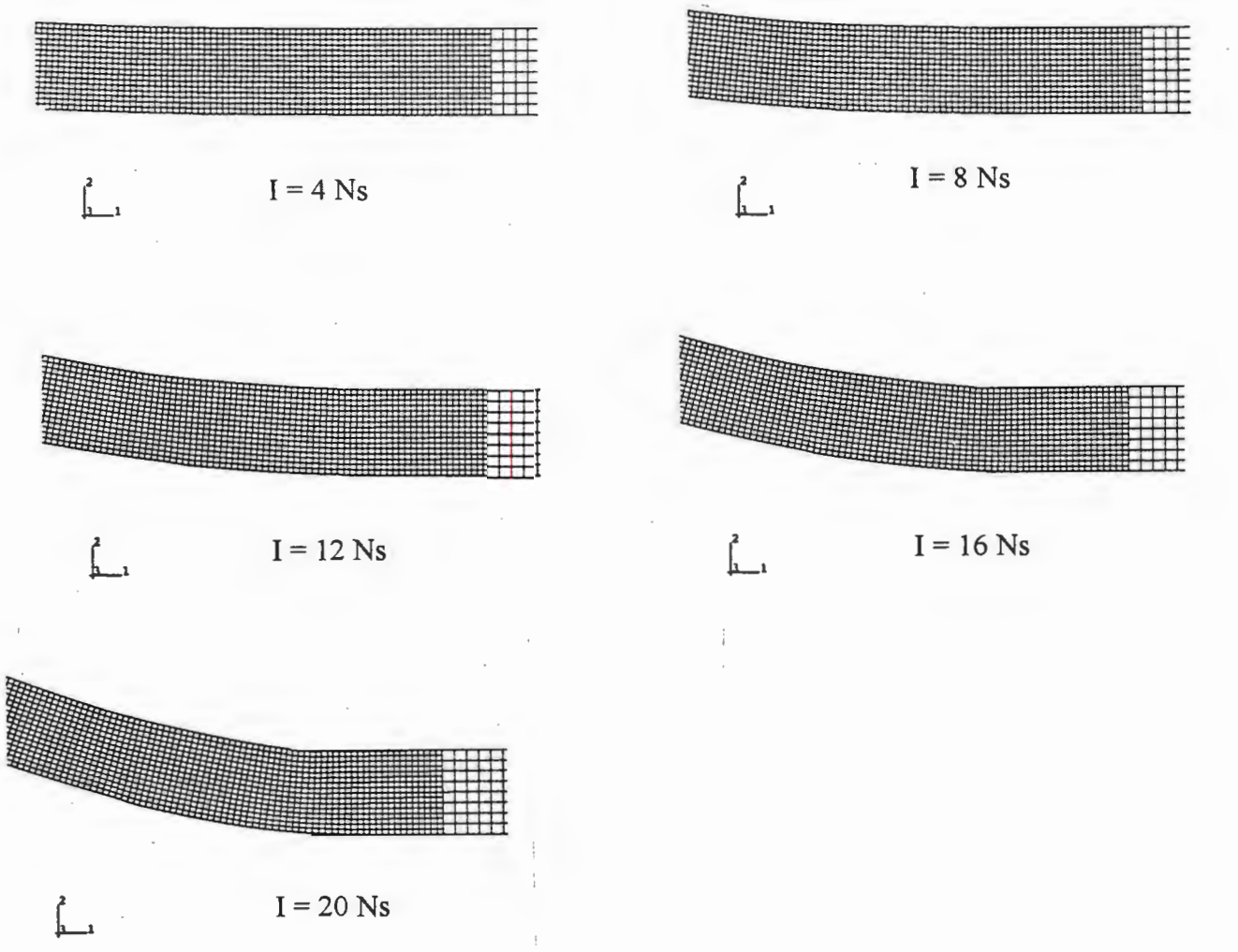

Figure {4.20} Boundary detail for 120mm clamped plate with sharp clamp edge.

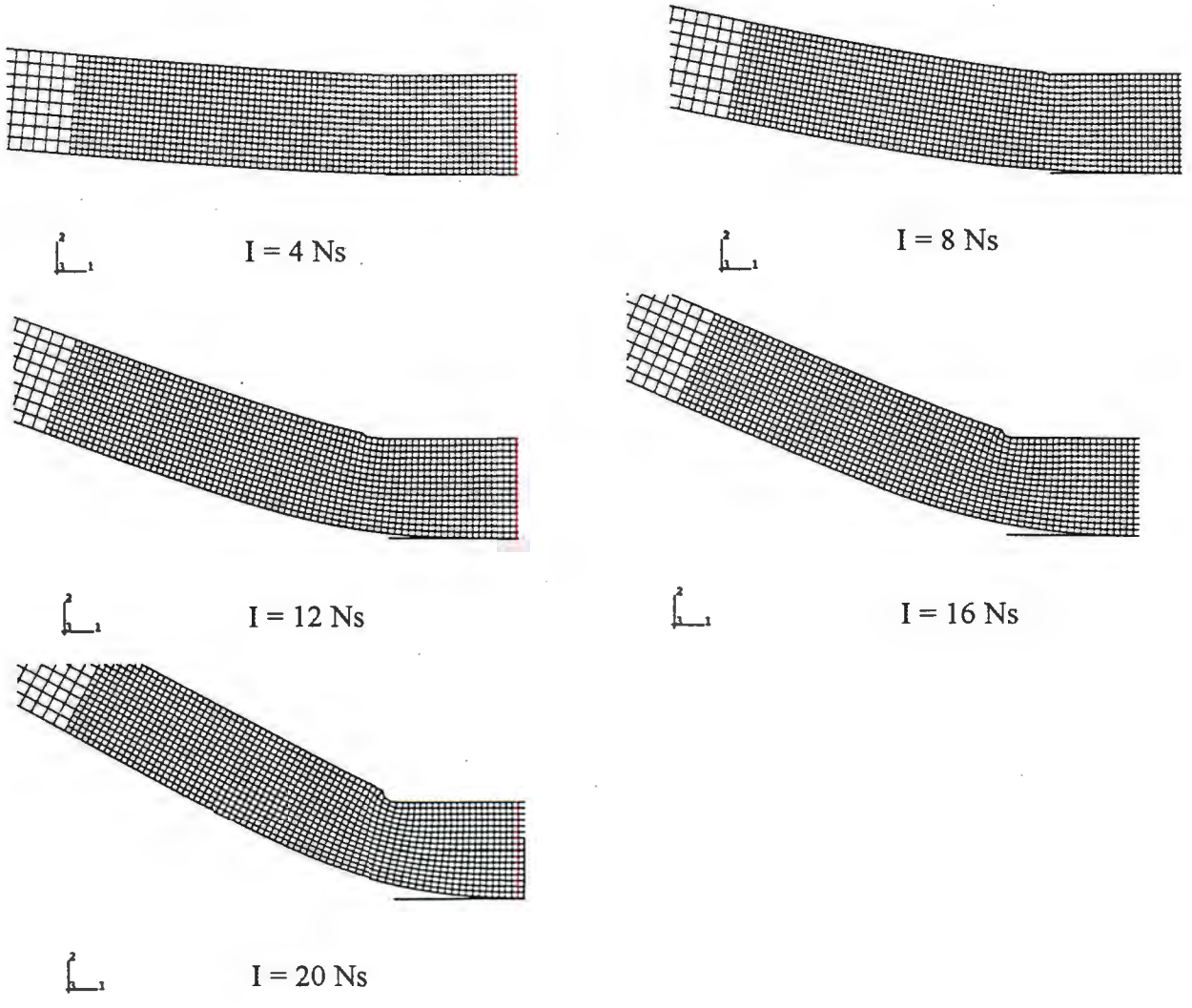

Figure {4.21} Boundary detail for 100mm clamped plate with sharp clamp edge

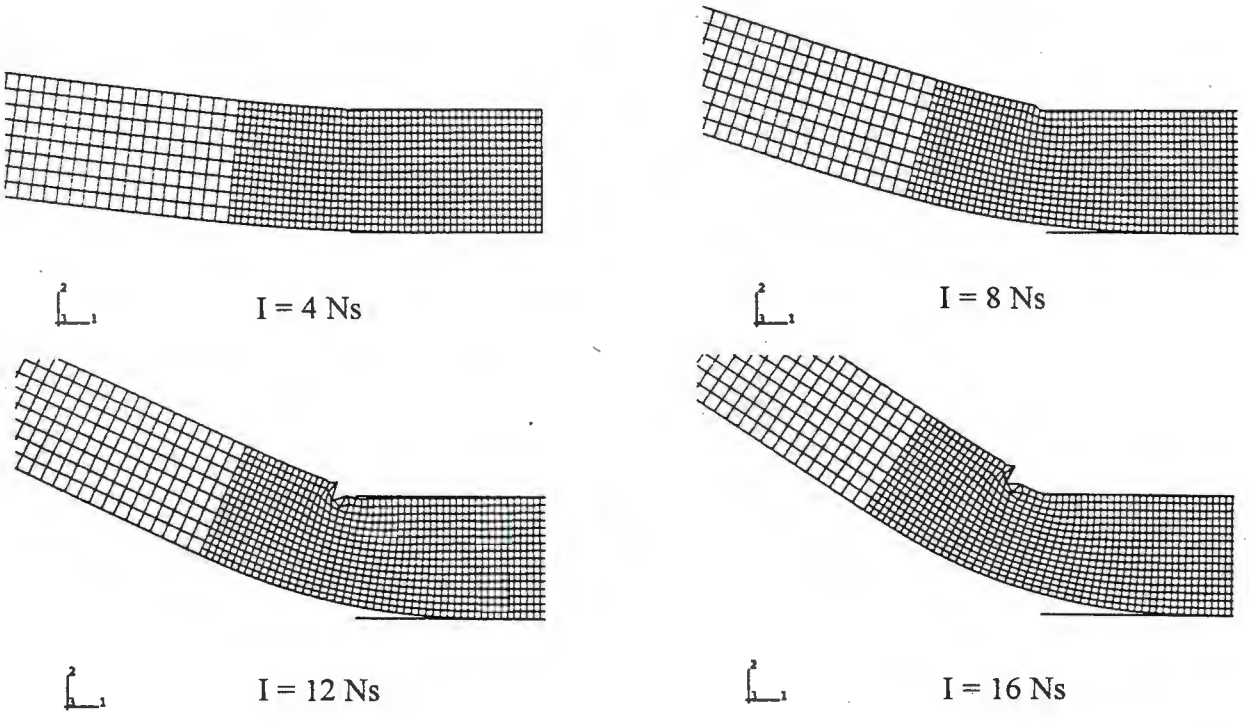

Figure {4.22} Boundary detail for 80mm clamped plate with sharp clamp edge.

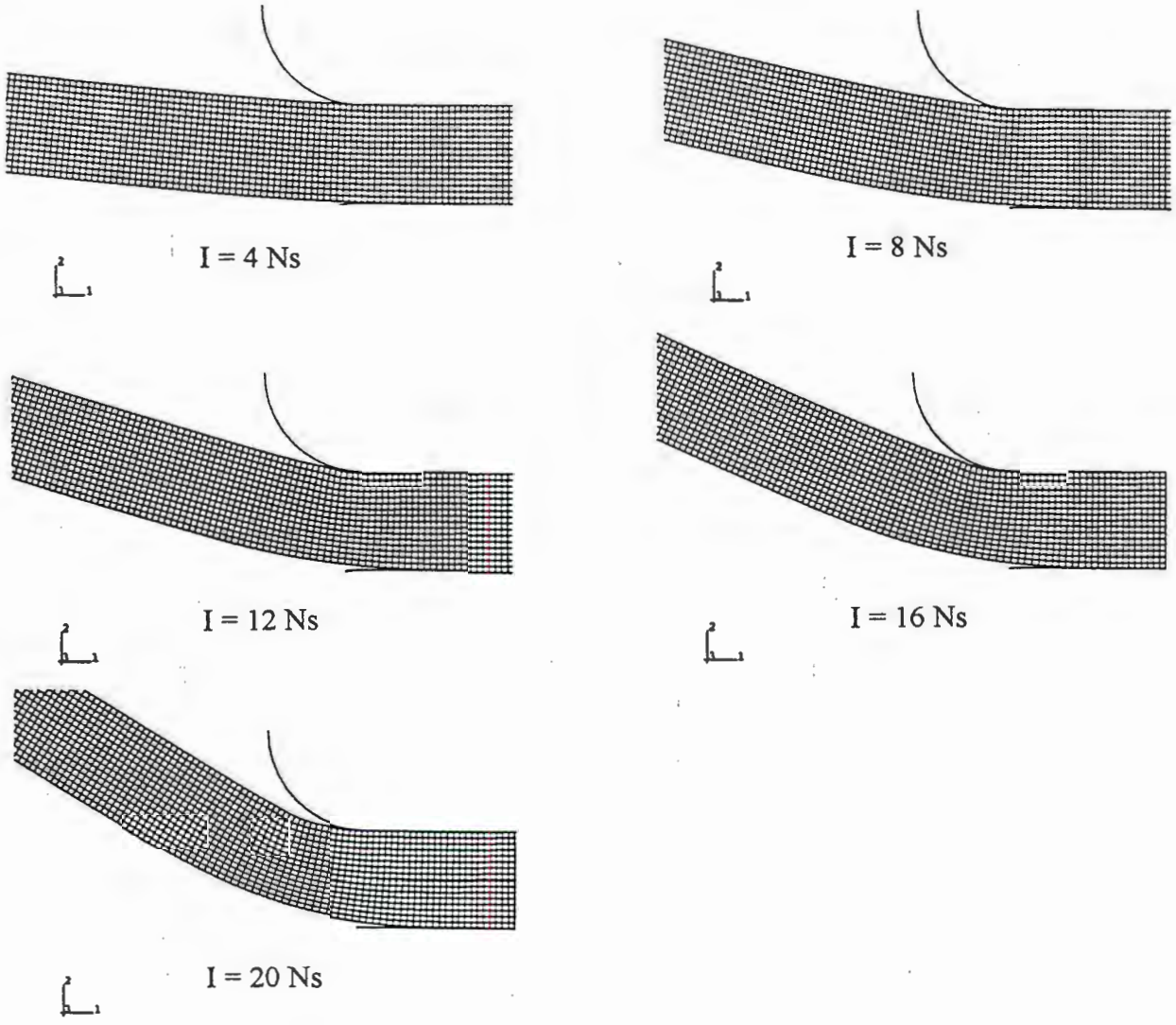

Figure {4.23} Boundary detail for 100mm clamped plates with 1.6mm clamp edge radius.

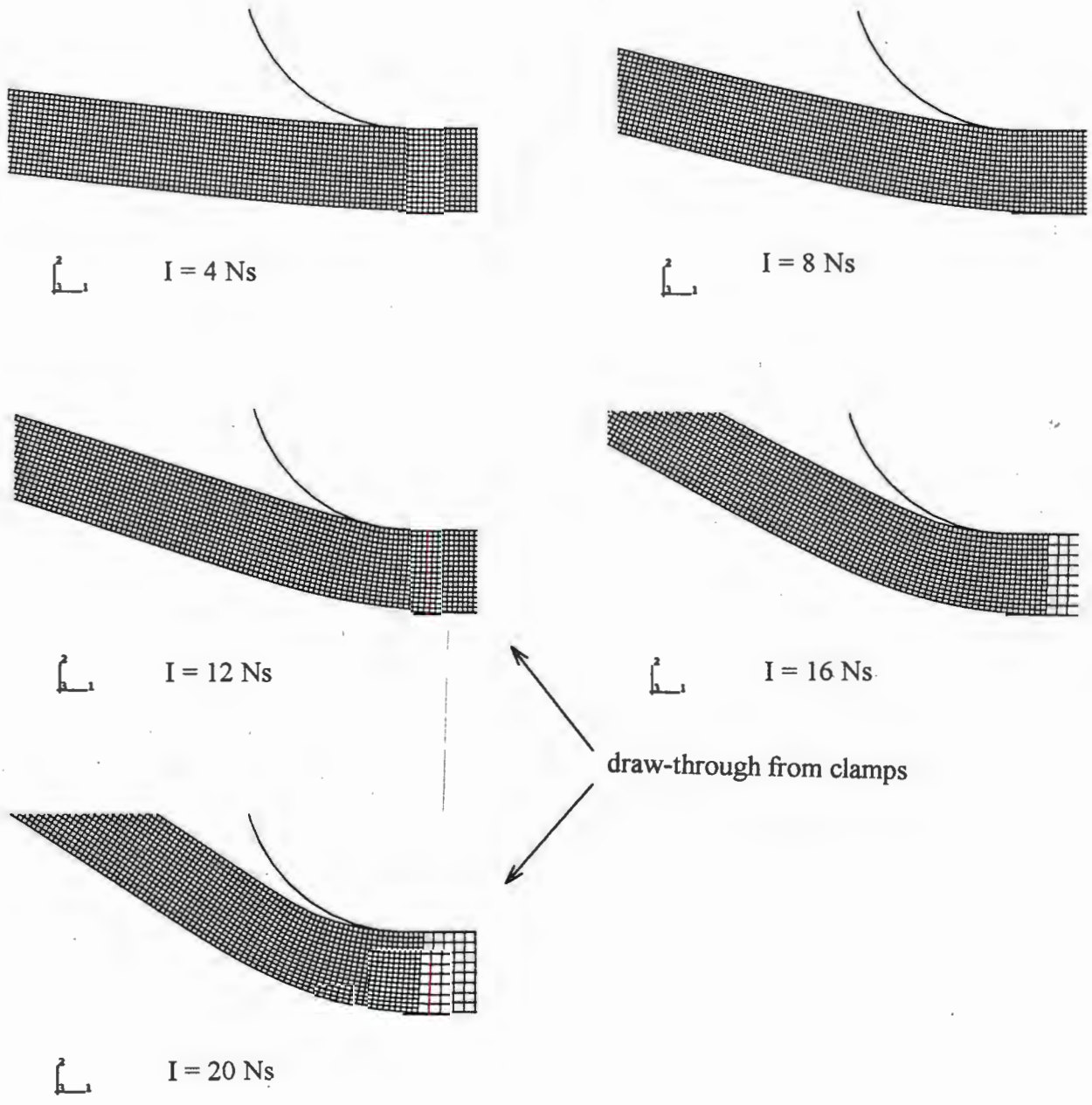

Figure {4.24} Boundary detail for 100mm clamped plate with 3.2mm clamp edge radius.

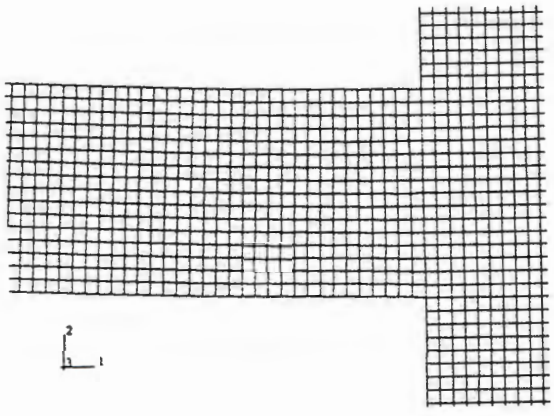

I = 4 Ns

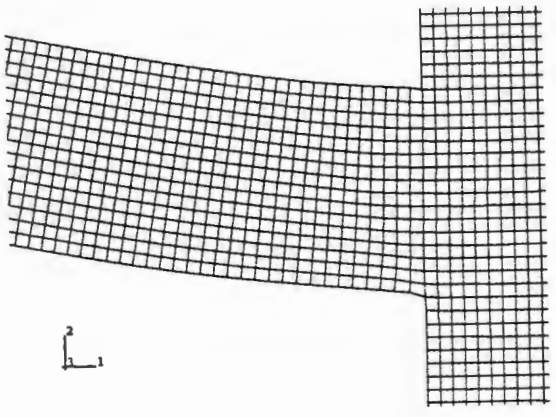

I = 8 Ns

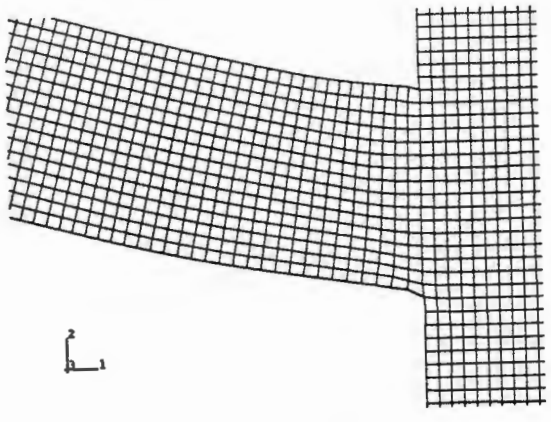

I = 12 Ns

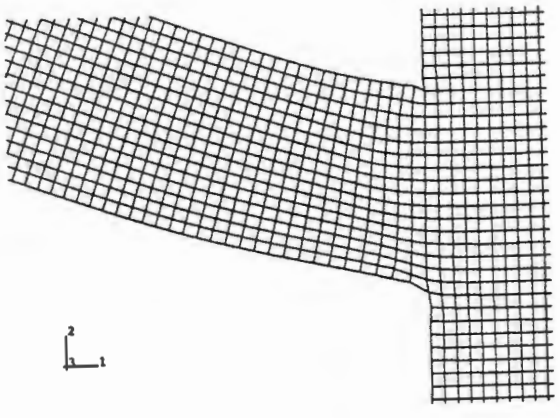

I = 16 Ns

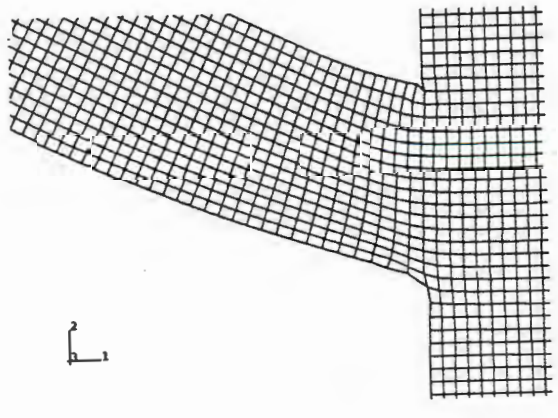

I = 20 Ns

Figure {4.25} Boundary detail for 100mm built-in plate with sharp corner.

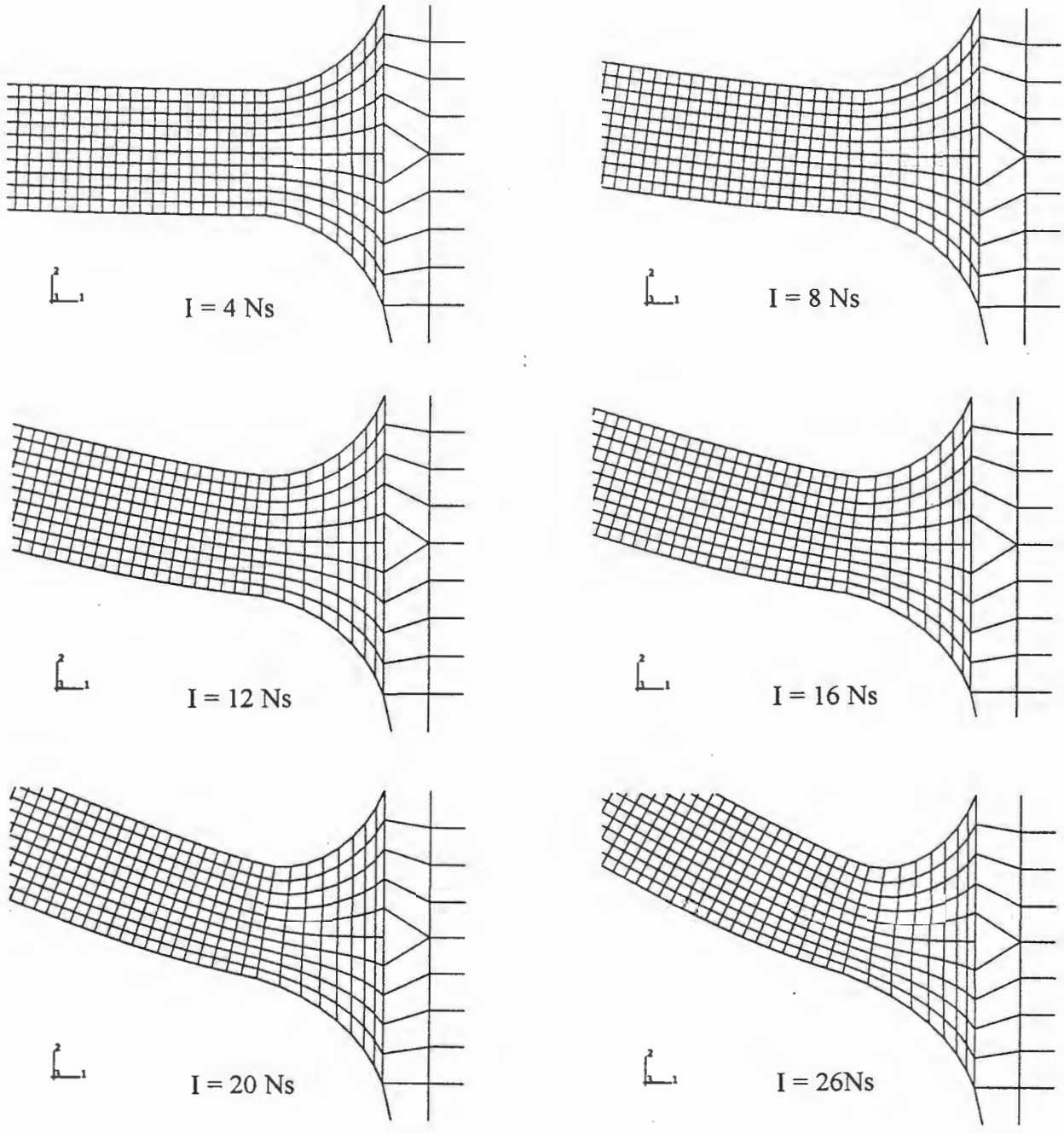

Figure {4.26} Boundary detail for 100mm built-in plate with 2.0mm fillet radius

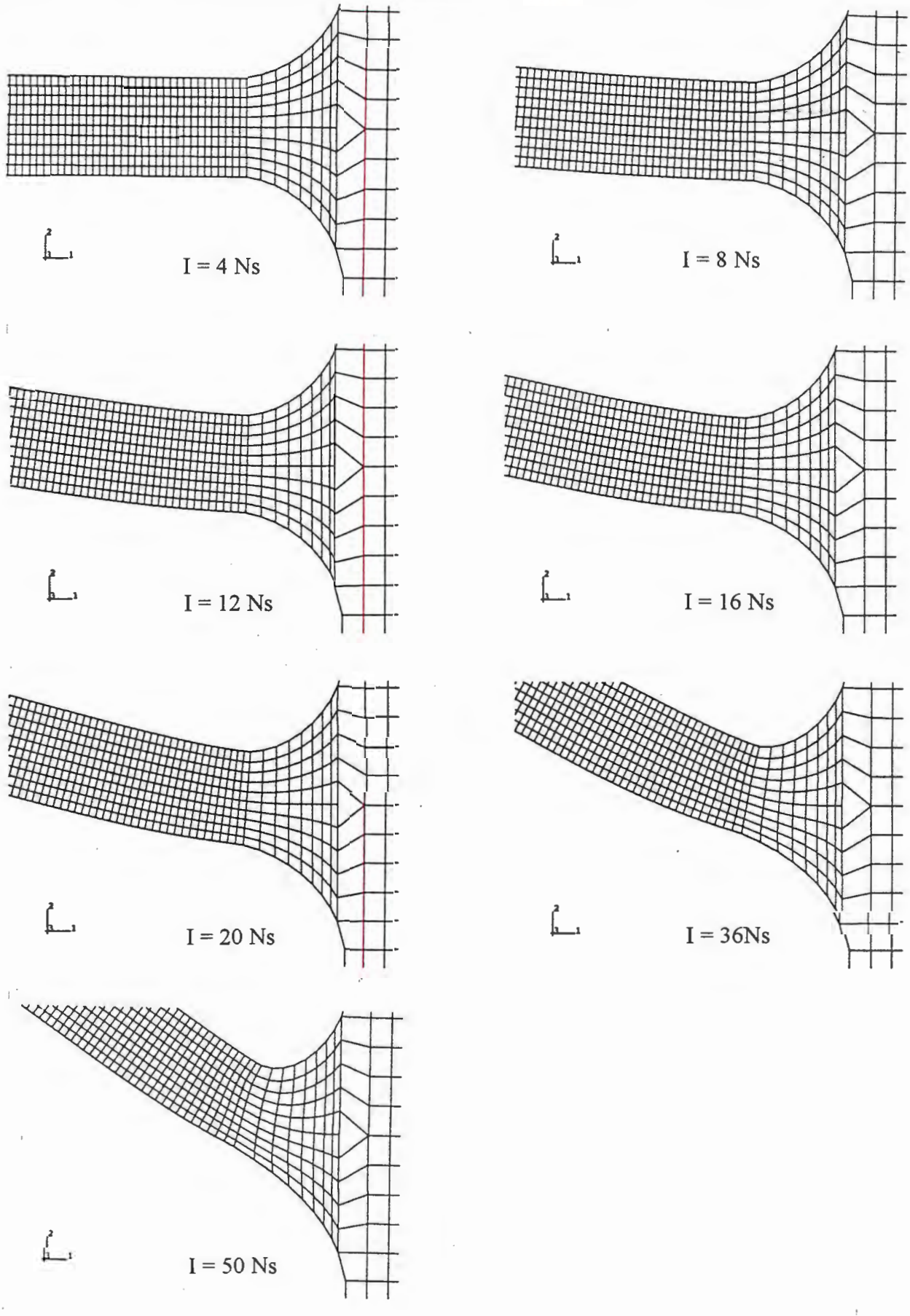

Figure {4.27} Boundary detail for 100mm built-in plate with 3.0mm fillet radius.

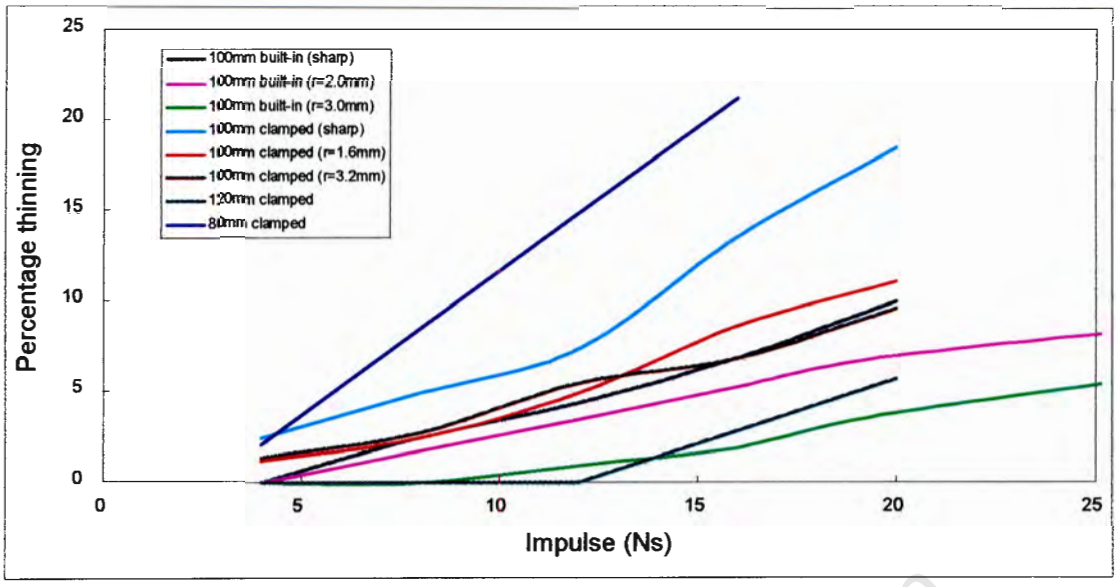

Figure {4.28} Graph showing the degree of thinning predicted near the plate boundary for the various boundary conditions, and with increasing impulse.

Figure {4.28} indicates more clearly the increased tendency towards boundary thinning for clamped plates, particularly where a sharp clamp edge is involved. However the variation in the thinning behaviour for the various boundary conditions is essentially limited to the region very close to the boundary. Figure {4.29} shows the *approximate* thickness of both a built-in and a clamped 100mm plate for an impulse of 16Ns. This is calculated from the difference in vertical deflection between the top and bottom surfaces of the plate, and does not consider horizontal displacements. From this figure it is obvious that the degree of stretching in both plates is almost equal, and that the only significant variation in thickness is at the boundary. It is also interesting to notice that most thinning occurs at the plate centre, even though failure by tearing occurs at the boundary. This trend was also predicted by Farrow [32] using shell elements, and observed experimentally by Thomas [18] for built-in plates. Later in this chapter experimental microstructural evidence will be presented that supports these predictions.

The occurrence of draw through of clamped plates from within the clamped region is clearly demonstrated in particular by figure {4.24}.

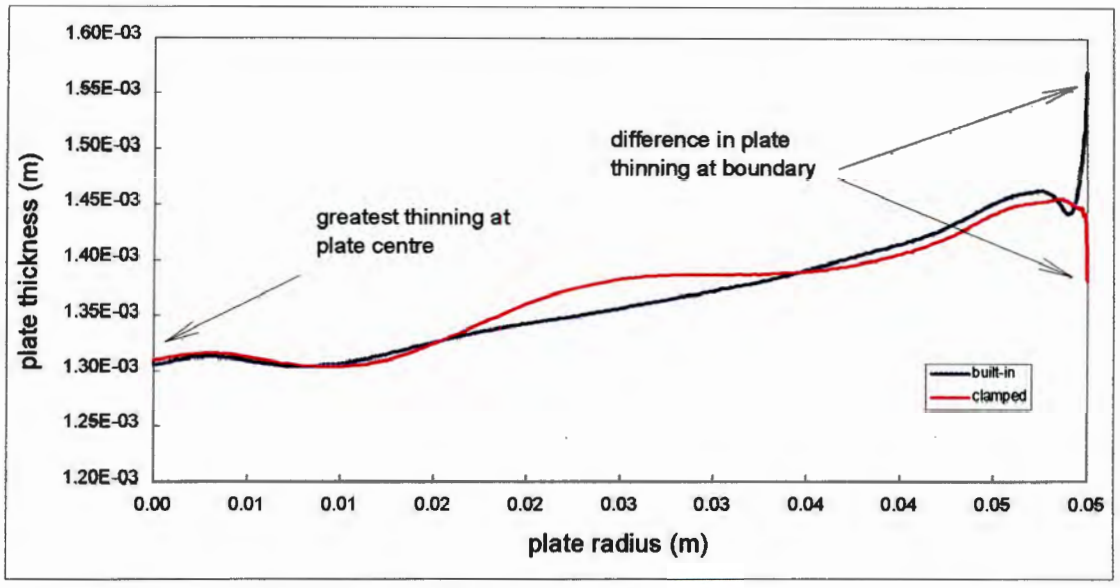

Figure {4.29} - Approximate plate thickness along the radius of both clamped and fully built-in 100mm plates for I = 16 Ns.

Discontinuities in the form of sharp corners or edges exist in the finite element meshes representing both clamped and built-in boundary conditions, in the cases where edge or fillet radii are not included. In both cases this can lead to large distortions of the elements closest to the discontinuity. For 100mm clamped plates this is seen to quite closely follow actual behaviour, which becomes apparent when referring to the pictures in Appendix 4. There is a tendency in the experiments for the clamps to indent the plate surface and provide an initiation point for necking at the point of contact. This is true also of the finite element analysis. However the accuracy of this indentation prediction is limited by the size of the elements at the contact point and this is best demonstrated by reference to figure {4.22} where one element has clearly undergone excessive distortion and the modelling of indentation can no longer be taken as accurate.

In the case of built-in plates, the corner modelled as sharp in the finite element mesh, is in reality not exactly a right angled corner, due to limitations of machining accuracy. Whilst distortion of the elements in this sharp corner do not appear to be too excessive, it is likely that the strain predicted is somewhat higher than would be predicted if the corner were modelled as slightly rounded.

4.3.2 Strain distribution

Figure {4.30} shows the maximum value of plastic strain at the plate boundary for increasing impulse, for all the boundary conditions. It can be seen that there is a trend separating plates with clamped and built-in boundary conditions, where in general the built-in plates undergo more severe plastic straining than the clamped plates, with the exception of the 80mm clamped plates.

It should be noted that these maxima are those occurring on the bottom (loaded side)of the plate where tearing is likely to initiate, and the highly localised plastic strain resulting from excessive element distortion due to clamp indentation is not considered. In order to more accurately visualise the dependence of strain distribution on boundary condition, figures {4.31} and {4.32} show contour plots of equivalent plastic strain at each boundary, for an impulse of 12Ns.

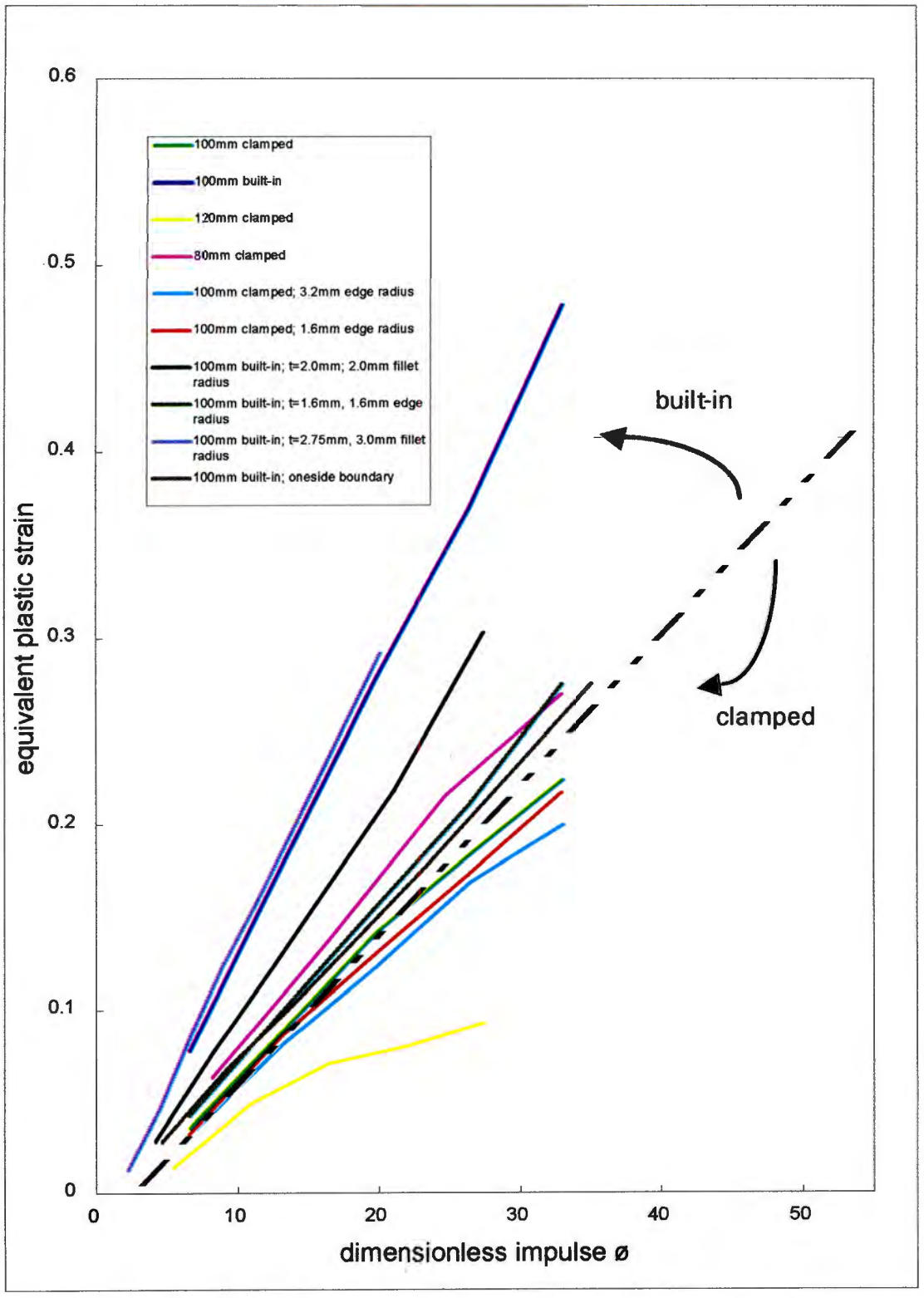

Figure {4.30} Graph of the maximum equivalent plastic strain predicted near the plate boundary for the various boundary conditions, and with increasing impulse.

Figure {4.31} Contour plots of equivalent plastic strain distribution at the boundary of (a) 100mm clamped plate with no edge radius, (b) 100mm clamped plate with a 1.6mm edge radius and (c) 100mm clamped plate with a 3.2mm edge radius.

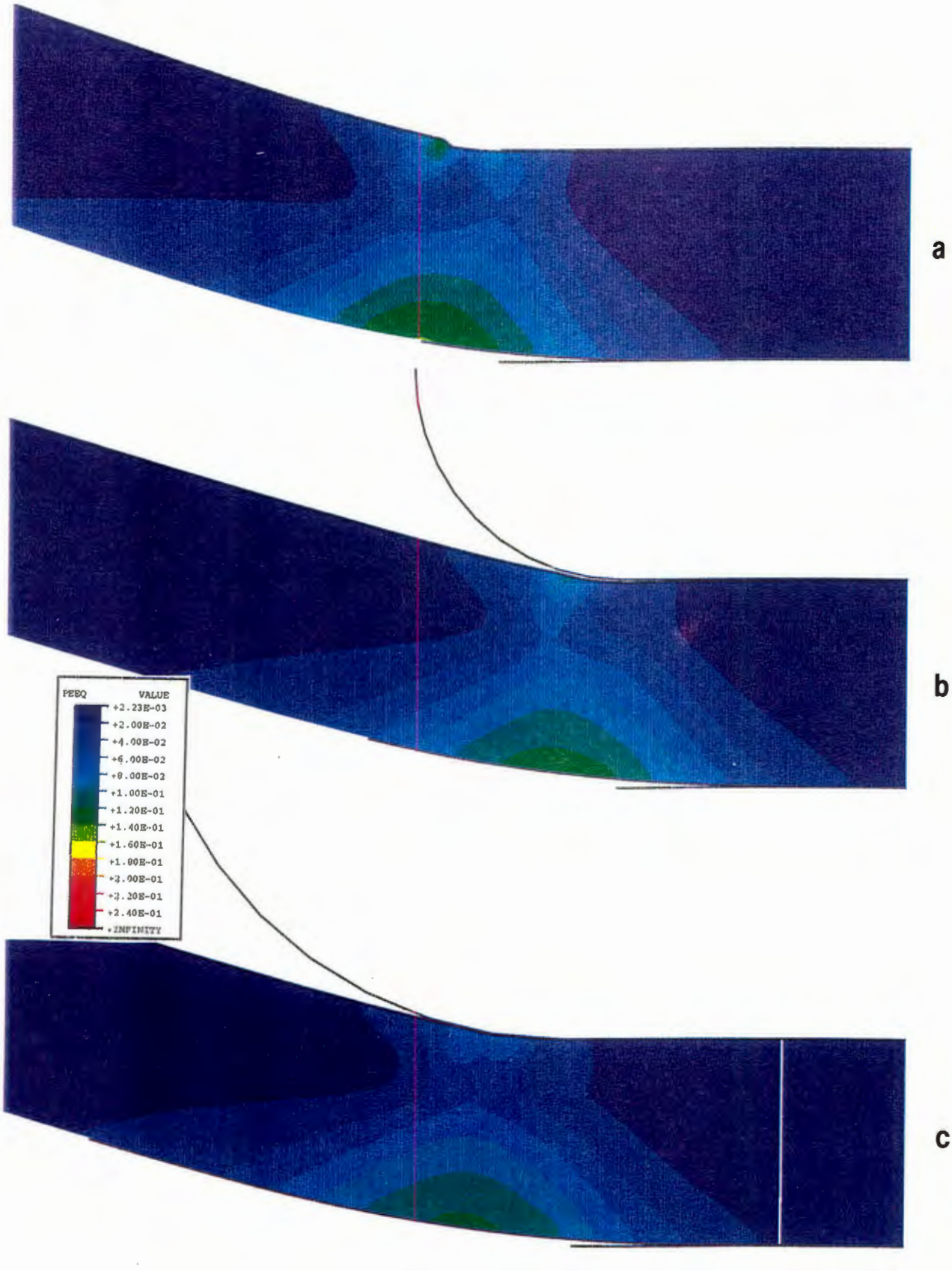

Figure {4.32} Contour plots of equivalent plastic strain distribution at the boundary of (a) 100mm fully built-in plate with sharp corners and (b) 100mm fully built-in plate with a 2.0mm fillet radius.

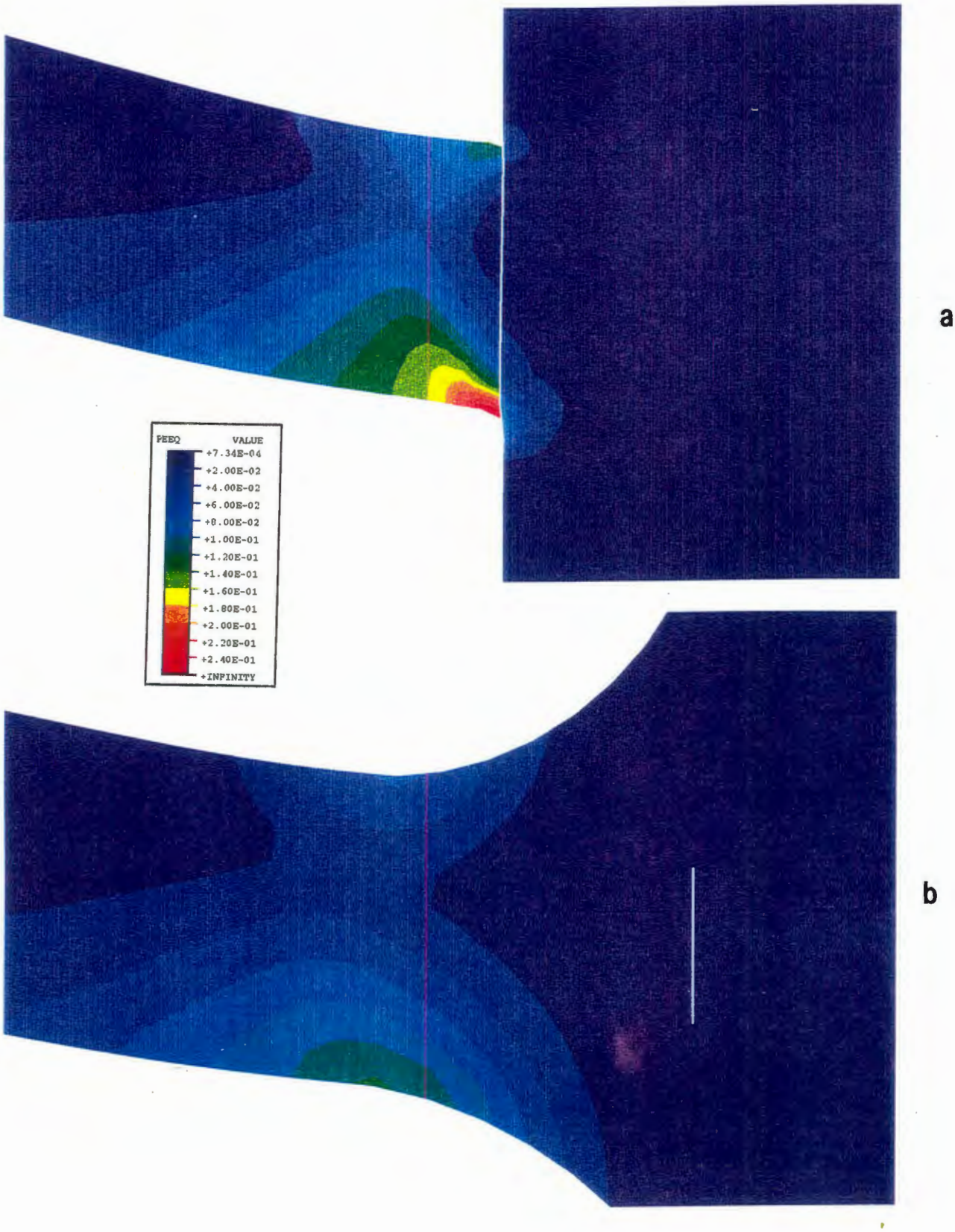

Figures {4.31} and {4.32} clearly demonstrate once again the plastic hinge that exists at the plate boundary for all the boundary conditions. The contour plots legends are all relative to the same scale and so allow direct comparisons. The concentration of plasticity at the sharp corner of the fully built-in plate is clearly visible, as is the localised plasticity associated with clamp indentation for the sharp edged clamped plate.

Figure {4.33} below shows the equivalent plastic strain distribution for an entire clamped 100mm plate, at I = 12 Ns and I = 20 Ns. There are clear areas of increased plastic straining corresponding to both the plastic bending hinge at the plate boundary, and the area of maximum stretching and subsequent thinning at the centre, that was shown to occur in figure {4.29}. An interesting comparison of these observations may be made with experimental microstructural evidence gathered for clamped plates by Sanders [37].

Sanders obtained micrographs for a series of blast loaded clamped plates using a scanning electron microscope at positions along the plate radius. Analysis of these micrographs allowed the relative elongation of the metallic grain structure to be quantified, defined as the ratio of grain length to grain breadth. When this data is normalised relative to an area of the plate that has not undergone significant stretching, the results give an indication of the degree of permanent plastic straining that has occurred in the direction of the plate radius and in the plane of the plate. An example of these results is given in figure {4.34} for 100mm plates, at impulses ranging from 12.65 Ns to 21.1 Ns. It is clear that peaks of tensile plastic strain exist at the boundary and centre and that for the lower impulse, strains are higher at the plate centre, while at the higher impulse, straining appears greater at the boundary. This is seen to agree very well with the contour plots.

Reference to figure {4.18} will remind the reader that the peak strain at the boundary is reached early in the response when compared to that at the centre. This probably aids in explaining why failure occurs at the boundary (early in the response), even though final values of plastic strain at the plate centre may be higher.

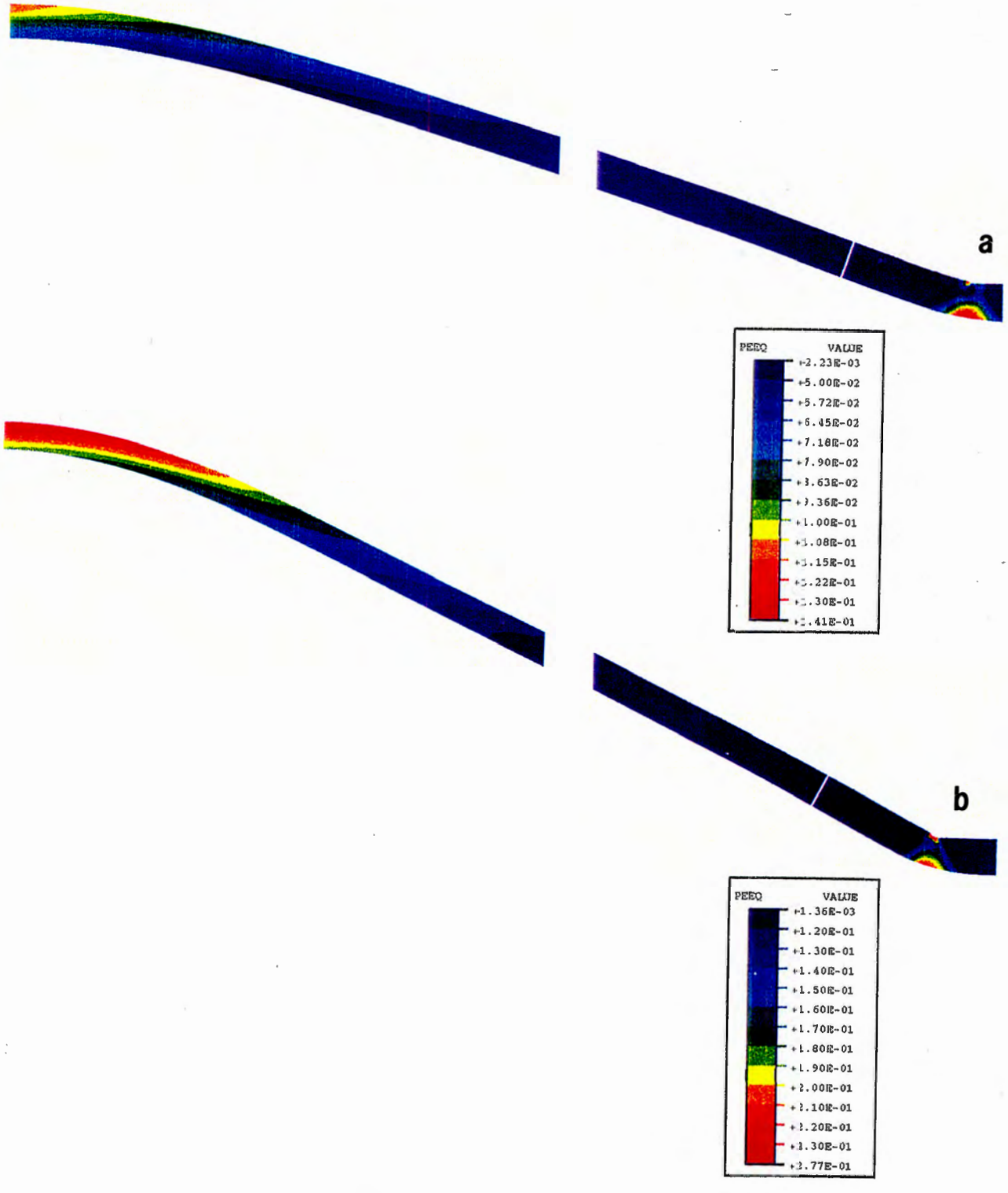

Figure {4.33} Contour plots of equivalent plastic strain for 100mm clamped plates at (a) I = 12 Ns and (b) I = 20 Ns.

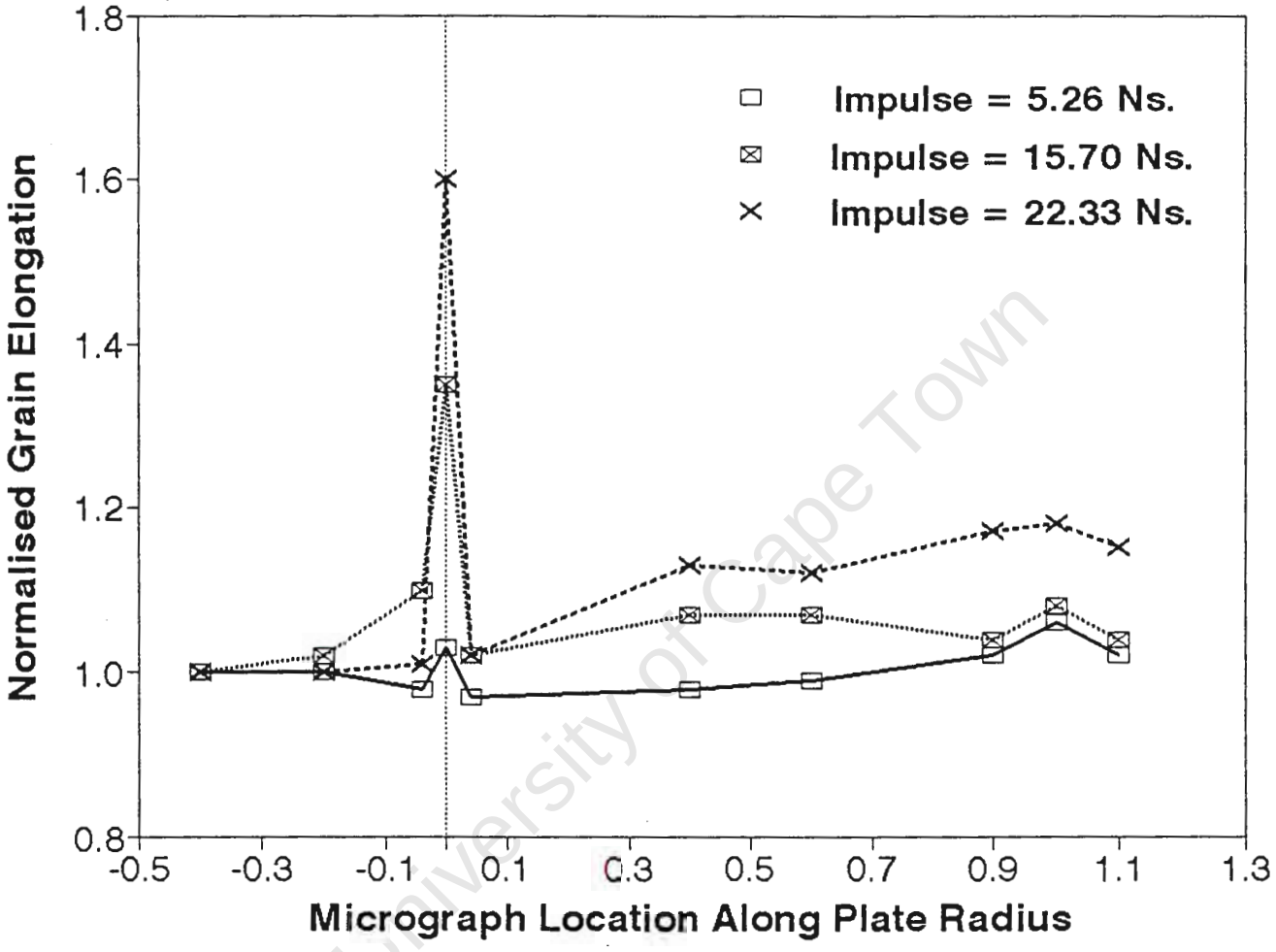

Figure {4.34} Micrograph showing normalised metal grain elongation along the radius of 100mm clamped plates for three values of applied impulse.

4.4 MODE II FAILURE

4.4.1 Introduction

Experimental evidence has shown three distinct modes of failure to occur in blast loaded steel plates. Mode I failure involves the generation of large permanent deformations without any evidence of material failure, and has been demonstrated in the previous sections. The onset of Mode II failure is defined by the first occurrence of tearing of the material of the plate and describes all the tearing behaviour that occurs thereafter until the onset of Mode III failure. In Mode III the energy of the blast is sufficient to cause shearing failure around the entire circumference of the plate before any significant displacement has occurred in the remainder of the plate, whereby an almost flat disk results. These failure modes were illustrated in figure {1-1}.

This section will document the implementation of a maximum strain based model of material rupture in an attempt to predict the onset of Mode II failure. Tearing at the boundary has been shown to be sensitive in particular to the method of fixation and this will be investigated.

4.4.2 Material parameters

The formulation of the rupture model is discussed in the analysis chapter, and is seen to be based on two material properties, namely offset and rupture equivalent plastic strain, as was illustrated in figure {3.2}. While measurements of engineering strain relative to the entire length of a tensile specimen are easily obtained and widely reported in the experimental plate studies [14,16], the values required by ABAQUS are those of true stress at a material point, and in particular at the point where failure occurs. Such measurements proved to be scarce in the literature for quasi-static tests, and non-existent at the high rates of strain encountered here. Gupta and Karunes [38] provide quasi-static values for offset and rupture plastic strain for annealed mild steels based on extensive tensile testing. These are reported as $\varepsilon_o = 0.19$ and $\varepsilon_f = 0.38$ and have been used for all

analyses reported here. However other reported values [39] for various steels show considerable variation with ε_0 ranging from 0.1 to 0.5.

Some dependence of ductility and localisation on strain rate has been reported [33] but no reliable values for the two required failure parameters could be found at high rates of strain.

ABAQUS/Explicit does not at present support the use of the ductile tearing model in conjunction with the Cowper-Symonds relationship for strain rate effects. This necessitated the substitution of an approximation by Jones [25] for the effect of strain rate at a point on the associated flow stress. This is based on a scalar multiplier n given by

$$n \cong 1+\left\{\frac{V_0^2}{3DR}\left(\frac{\rho}{3\sigma_0}\right)^{1/2}\right\}^{1/q} \quad . \quad . \quad . \quad . \quad . \quad 4.1$$

The form of n is illustrated in figure {4.35}, for plates of different diameter and thickness.

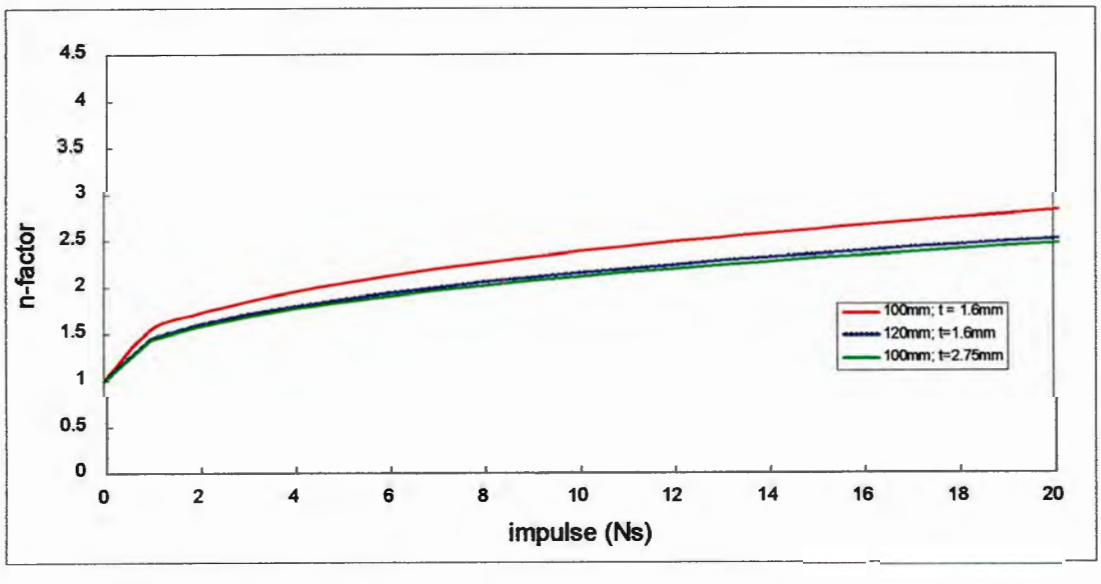

Figure {4.35} The form of the Jones n-factor for increasing applied impulse.

The factor n acts as a scalar multiplier that modifies the static yield and hardening behaviour of the material and is based on the average strain rate in the plate material throughout the response. Since the plate exhibits very much higher strains in regions such as near the boundary and centre, this averaging is a significant approximation, underestimating the effect of strain rate in these critical regions and overestimating it in regions of lower overall straining. As well as such a spatial approximation, the use of n is also a temporal approximation, since strain rate at a point is not expected to be constant throughout the response.

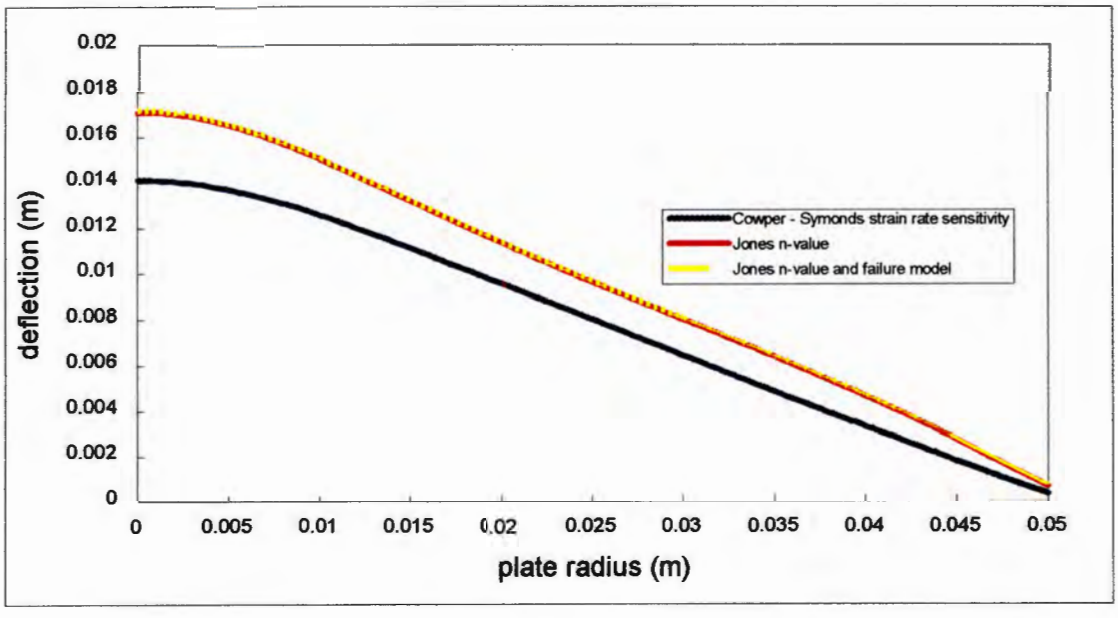

Figure {4.36} The effect of the Jones n-factor and the ABAQUS ductile tearing model on Mode I response.

The effect of this approximation on overall response is illustrated in figure {4.36}. This shows Mode I deformed profiles for a 100mm built-in plate at an impulse of 8 Ns where no points in the finite element mesh have reached the rupture strain $\bar{\varepsilon}_f^p$, and hence no elements have failed, but where near the boundary, values of strain have exceeded the offset plastic strain $\bar{\varepsilon}_0^p$ and thus some loss of stiffness has occurred. Profiles are plotted for three distinct model cases; firstly using the Cowper-Symonds law for strain rate sensitivity as used in the previous Mode I predictions; secondly with the Jones n-value

approximation for strain rate sensitivity but with no failure model; thirdly incorporating both the n-value approximation and the ductile tearing model. It can be seen that the effect of the n-value approximation on its own is to decrease the overall plate stiffness. Furthermore a somewhat different deformed plate profile results due to the spatial averaging of strain rate effects. The effect of the failure model on Mode I response is seen to be negligible.

It was noted previously that shell structures in general exhibit a biaxial distribution of stress and strain. In order to justify the use of the current model for failure which is based on uniaxial failure in tension, it is noted that due to the constraints imposed by the boundary, the state of stress in an impulsively loaded plate varies from biaxial at the plate centre, to approximately uniaxial at the boundary, where tearing has been observed to occur. Figure {4.37} shows a plot of radial and hoop strain for a typical plate analysis, where it can be seen that the hoop strain is indeed zero at the boundary, and a uniaxial state of strain thus exists. The use of a uniaxial criterion for tearing is thus felt to be not as severe an approximation as was reported by Duffey [33].

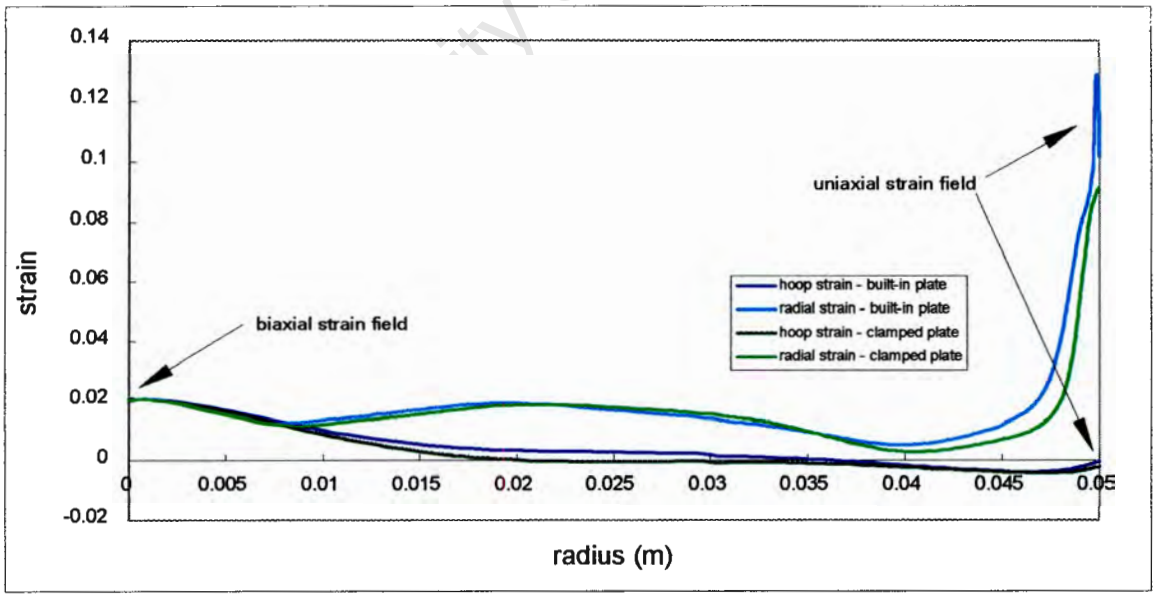

Figure {4.37} Strain distribution on the bottom surface of 100mm plates, for I = 8 Ns.

4.4.3 Onset of tearing

A further approximation introduced by the current model is that of axisymmetry of tearing at the plate boundary. This assumption is enforced due to the axisymmetric nature of the finite element mesh. In practice the onset of Mode II failure is characterised by partial tearing around a fraction of the plate circumference. Such behaviour cannot be modelled using axisymmetric elements.

The identification of tearing in the ABAQUS model is iterative, with analyses being undertaken for increasing values of impulse until upper and lower bounds on tearing are established. This was undertaken for four boundary conditions; clamped, built-in, clamped with 1.6mm edge radius, and built-in with 2.0mm fillet radius. Results for the onset of tearing for all four cases are plotted in figure {4.38} alongside the values reported in experimental studies [12, 14, 16, 17, 19].

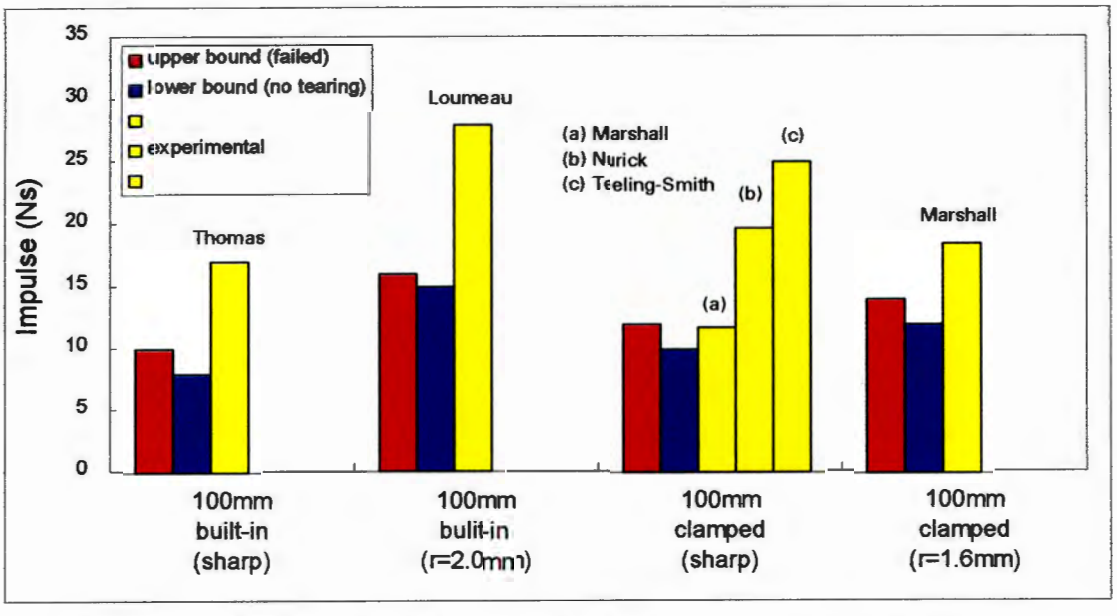

Figure {4.38} Predicted threshold impulses for Mode II tearing compared to experimental observations.

It is immediately obvious that for most cases the ABAQUS predictions for the onset of tearing are very low as compared to most of the experiments, occurring at about 60% of

the actual threshold impulses required to cause tearing in each case. For clamped plates the correlation to the data from Marshall appears somewhat better, but there is a wide range of observations for Mode II threshold impulse in this case, as seen by the data of Teeling-Smith, where tearing was observed to occur at an impulse nearly double that of Marshall.

In the case of all built-in plates, the current predictions are consistently low. For the model having sharp corners at the boundary, it seems possible that this is related to mesh design. The corner is modelled as perfectly sharp and this results in stress concentration and distortion at the corner element that may be unrealistically high, since the corner as machined on an actual test specimen is unlikely to be this sharp, due to limitations of the machining technique. Once this element fails, an even more acute stress concentration is formed, and hence the failure will propagate freely. However this is not the case in the mesh where a fillet radius is included, because there is no initial stress concentration, and so other limitations of the failure model must be cited. It is far more likely that the tearing parameters of Gupta and Karunes [38] are inappropriate for use in the tearing model. It was mentioned earlier that the values used do not take into account the effect of strain rate. However a more complete discussion of the poor prediction of Mode II failure attempted at the end of the chapter.

4.4.4 Tearing mechanisms

Whereas the values reported for the onset of tearing show poor correlation with experiment, observations show that actual localised tearing behaviour is reasonably approximated. For example in all instances tearing occurs at or very near to the boundary of the plate and this is as observed in experiments.

The onset of tearing occurs in the range of 33μs to 47μs for all the plates, and the variation in this time is dependent on the boundary condition. The built-in plates with no fillet radius have the shortest time to failure of 33μs and the clamped plates with no edge

radius also show failure at around 35μs. Where the boundary conditions are relaxed in both cases, the time to failure is increased to 47μs and 40μs respectively.

Figure {4.39} shows the transient response of the fully built-in plate at an impulse of 10Ns representing the predicted threshold of Mode II. The separation of the plate at the boundary is apparent at around 30μs, when the plate profile is still relatively flat, whereafter the plate continues to move in a free flight motion. It is seen from figure {4.39} that the plate continues to deform after failure has occurred, resulting in a similar rounded profile as that occurring for Mode I.

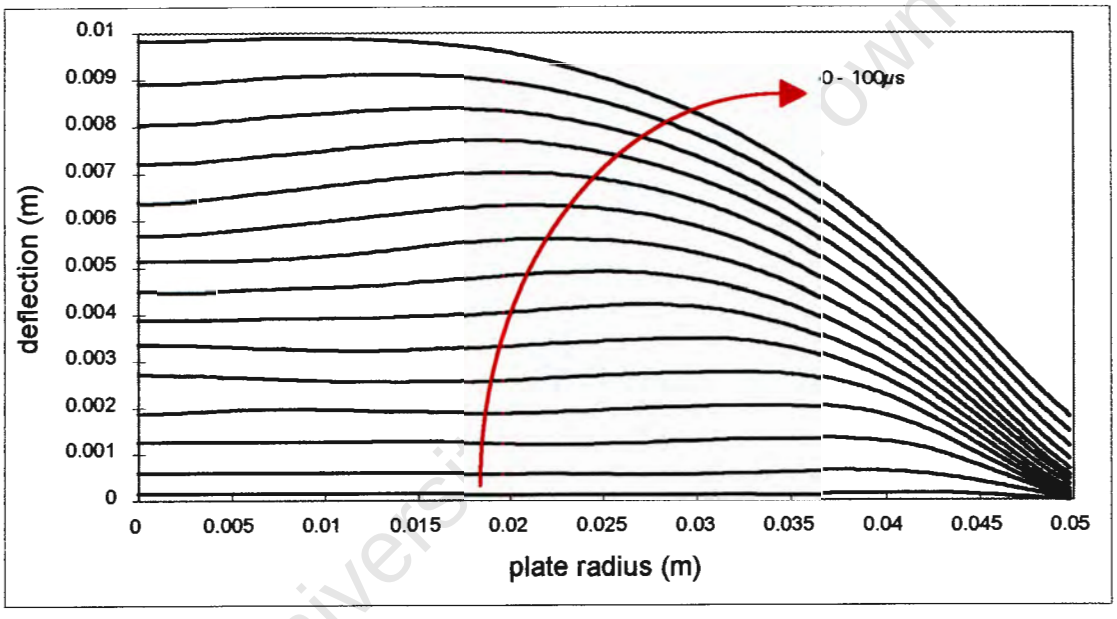

Figure {4.39} The transient response of a 100mm built-in plate above the threshold for Mode II failure

Figures {4.40} through {4.43} show the actual occurrence of tearing in the finite element mesh, for each boundary condition. It is interesting to note that the clamped plates exhibit an initial occurrence of failed elements at the upper surface where indentation with the clamps occurs. This results in a V shaped failure as indicated, whereas for built-in plates, failure initiates on the bottom surface and results in a 45 degree line of failure, also marked.

Marshall [16] observed that for clamped plates, obvious necking took place at the boundary before and at the onset of actual tearing, whereas Thomas [18] found that no necking was visible for fully built-in plates. Reference to the figures {4.40} through {4.43} below shows clear evidence of necking in all the failed plates including the fully built-in plates and this has been indicated on the figures.

In the case of the clamped plate with a sharp clamp edge, failure of elements occurs at the top surface of the plate before necking begins. It is observed that this acts as an initiation for a neck to form *during* the failure, most clear when t = 40μs. The extent of necking however is not as marked as in experiments, an example of which is provided in Appendix 4.

The same kind of behaviour seems true of all the plates at failure, with necking really only occurring *during* failure, when the cross section of the plate has been reduced by the failure of elements (such as in the sharp corner in the case of the fully built-in plate). Thus the type of necking and strain localisation that has been observed to occur in experiment is not that well predicted by the "strain softening" of the current failure model, nor by the Von Mises viscoplastic material alone, as reported in the previous section.

It was shown in figure {4-15} that altering the coefficient of friction and clamping pressure for clamped plates has the effect of changing the strain distribution. Figure {4.44} is the result of an analysis using the ABAQUS failure model where coefficient of friction at the clamps was increased from $\mu = 0.2$ to $\mu = 0.7$, and clamping pressure from 600 MPa to around 1200 MPa. The impulse chosen was that shown to be close to the previous threshold for tearing, but resulting in only a Mode I response. It can be seen that for the increased clamping condition, failure now occurs at this lower impulse.

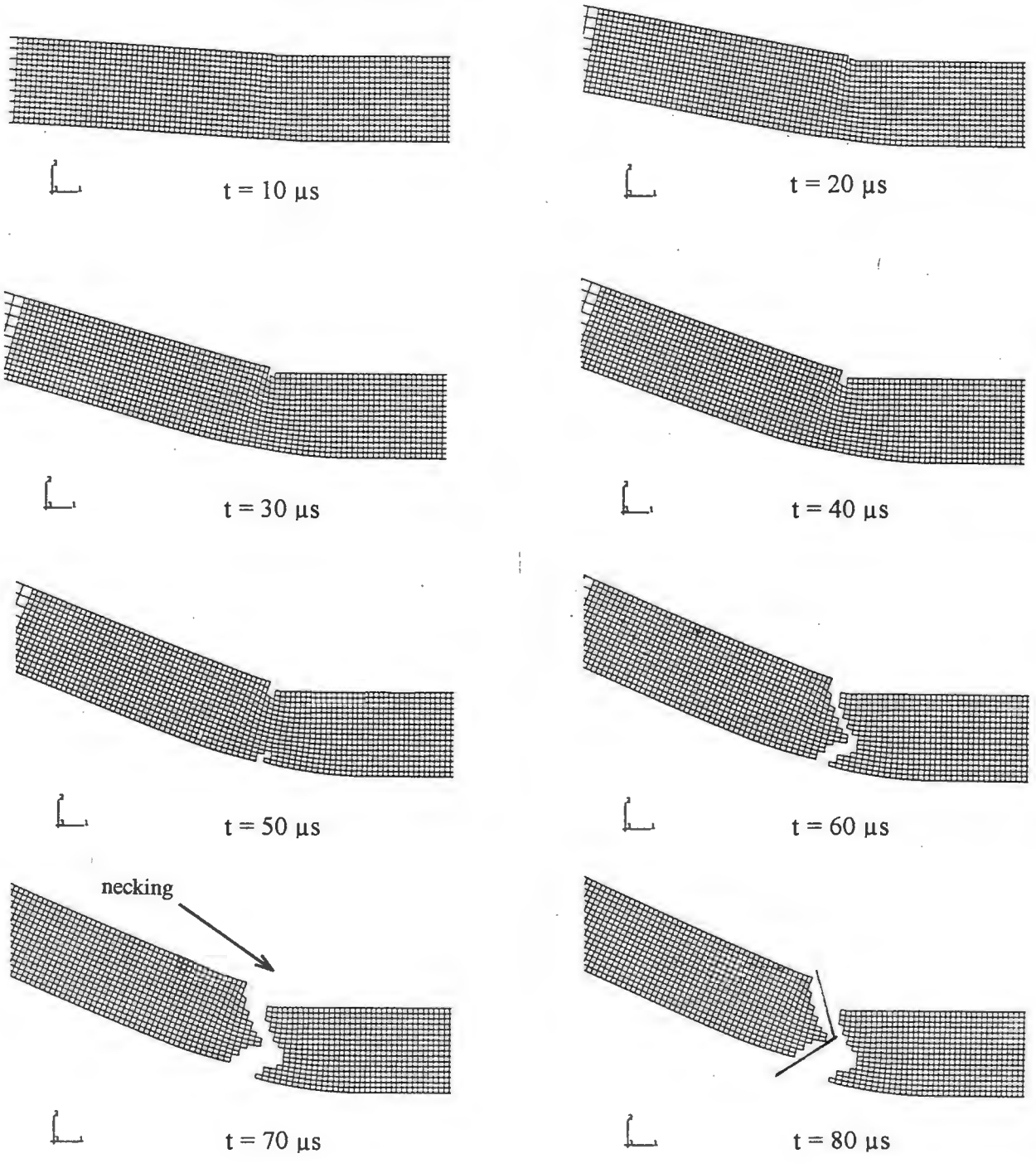

Figure {4.40} Predicted transient tearing behaviour of 100mm clamped plates with a sharp edge boundary condition and I = 12 Ns.

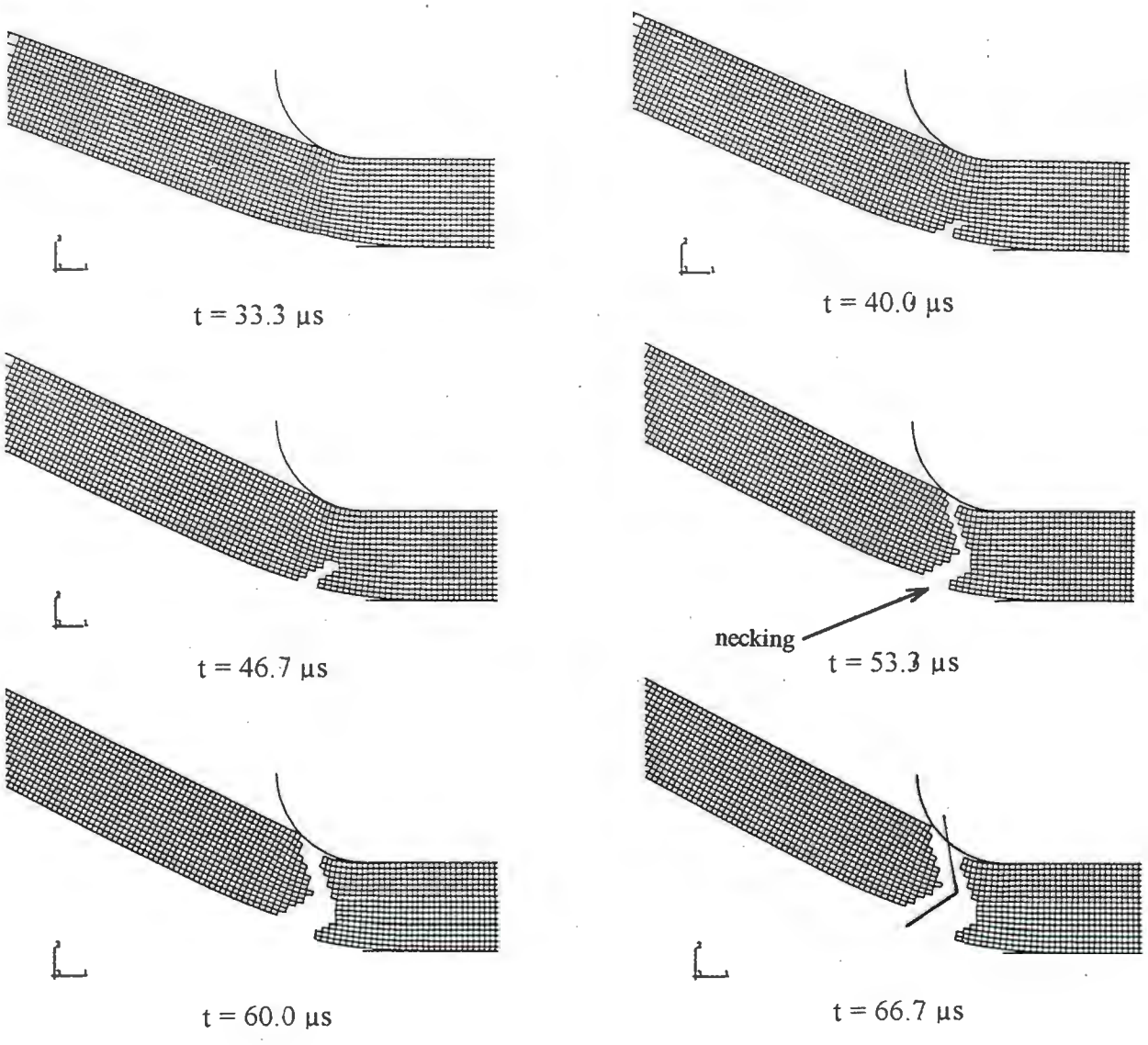

Figure {4.41} Predicted transient tearing behaviour of 100mm clamped plates with a 1.6mm edge radius at the boundary, and I = 12 Ns.

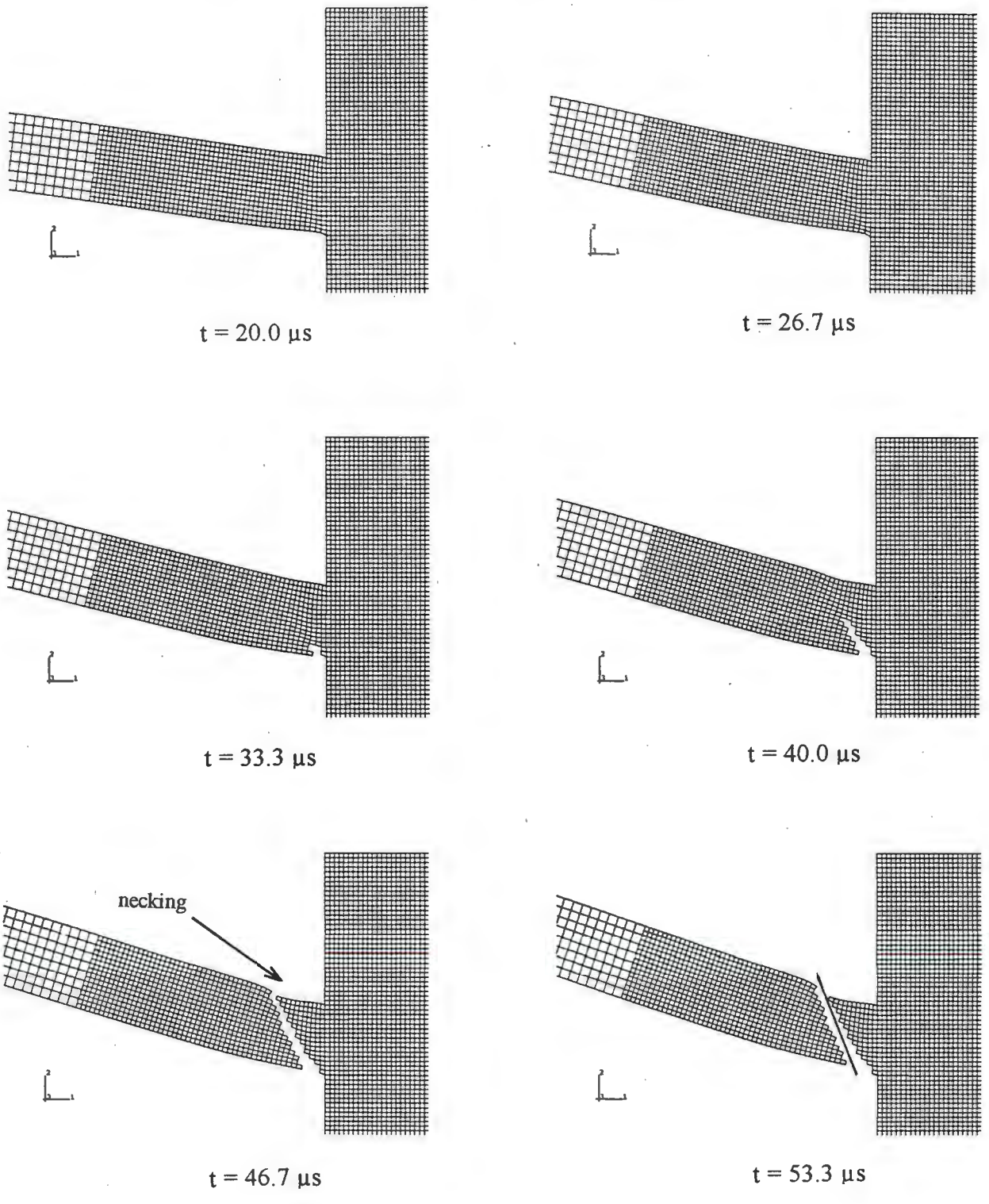

Figure {4.42} Predicted transient tearing behaviour of 100mm fully built-in plates with a sharp corner at the boundary, and I = 10 Ns.

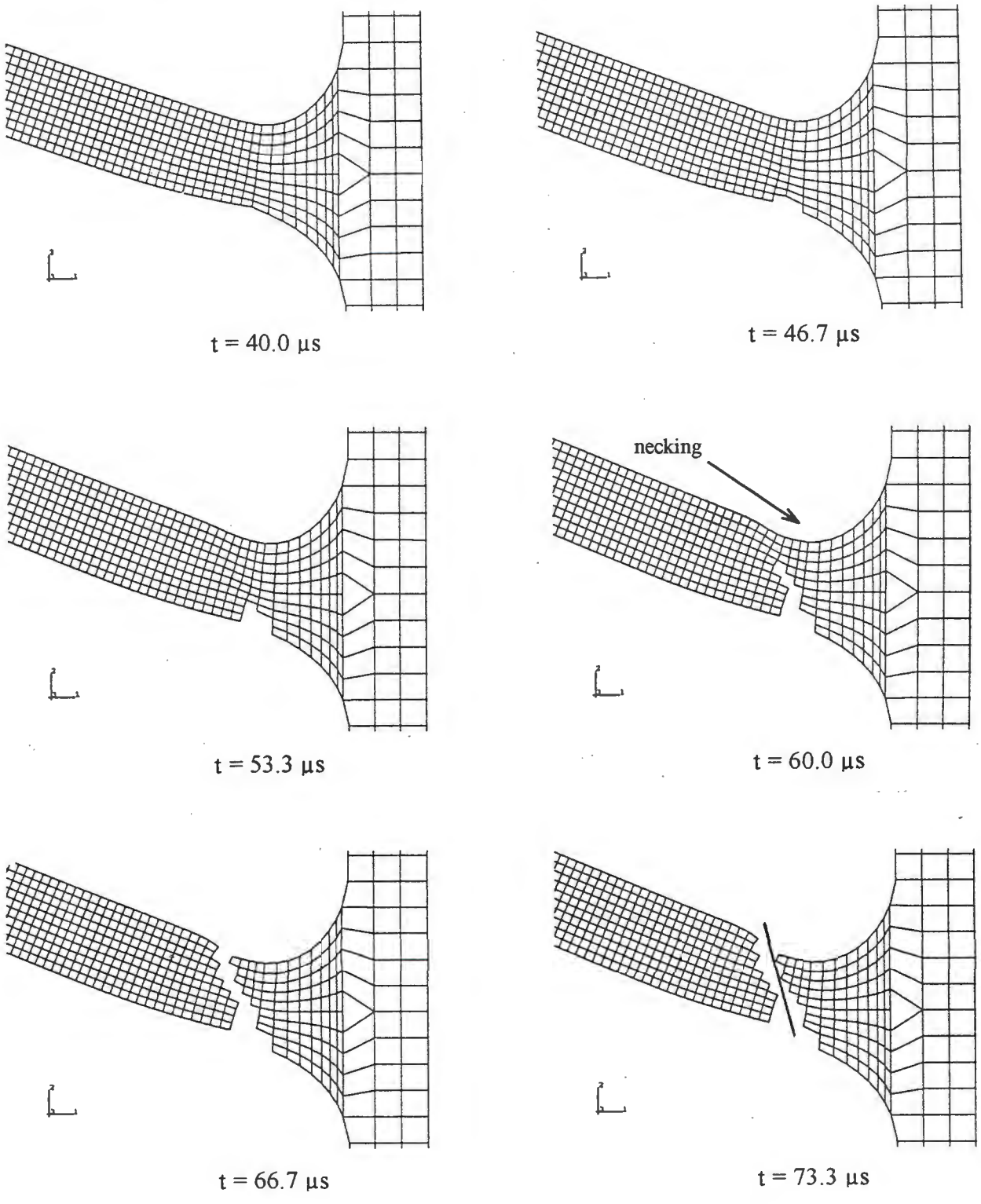

Figure {4.43} Predicted transient tearing behaviour of 100mm fully built-in plates with a 2.0mm fillet radius at the boundary, and I = 16 Ns (t=2.0mm).

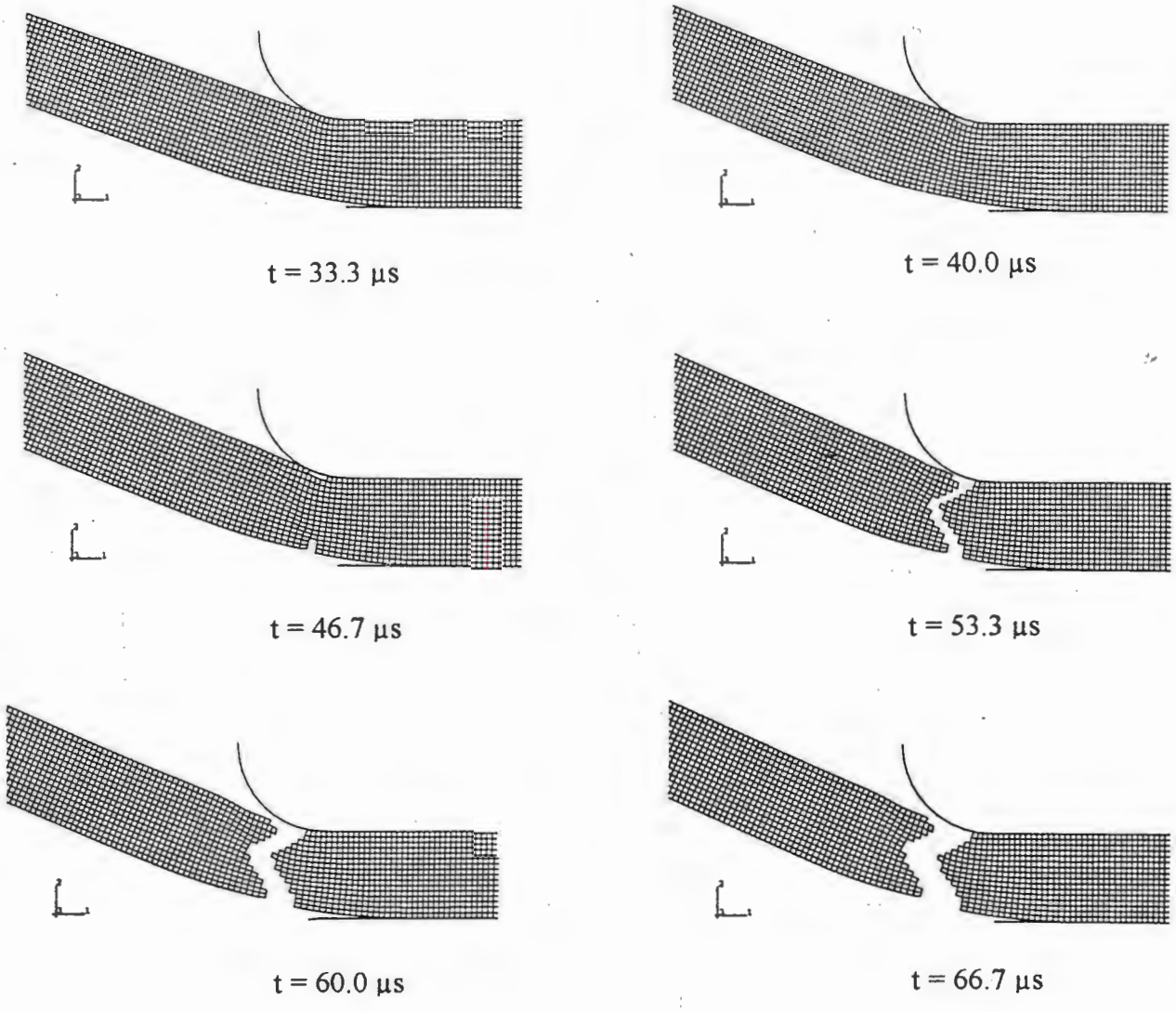

Figure {4.44} Predicted transient tearing behaviour of 100mm clamped plates with a sharp edge boundary condition and I = 10 Ns, and with increased clamping friction and pressure.

4.4.5 Discussion of Mode II predictions

In order to fully evaluate the validity of using the ABAQUS strain based rupture model to predict Mode II failure in plates, a far more exhaustive investigation is required. The current work has however identified possible areas that require further investigation.

- Mesh design appears to have an influence on tearing behaviour in the finite element model, in particular where stress concentration due to sharp corners and edges occurs. The speed of propagation of failure through the thickness of the plate may also be influenced by mesh design, and no attention has been given to quantifying the duration of the tearing event experimentally.

- In analyses where the failure model is not included, clamp indentation is seen to at least approximate real behaviour. Experimentally it would seem that this indentation helps to initiate necking and hence ductile tearing, whereas in the finite element model actual element level failure is seen to occur where the plate contacts the top clamp, and so indentation no longer occurs in a realistic manner.

- The suitability of the material parameters available in the literature for strains at localisation and rupture is a key issue in the successful implementation of such a model. There is considerable doubt that the values employed here adequately represent the actual material behaviour. This is due to the difficulty in measuring such quantities, and the complete lack of data at high strain rates. The use of different values would completely change the predicted Mode II thresholds, and this may explain the consistent underestimation of the onset of tearing in this work.

- While the inability of the ABAQUS code at present to combine Cowper-Symonds strain rate sensitivity with the rupture model is an acknowledged bug that has been avoided in this investigation by the use of the Jones n-factor, there is the possibility

that further errors do exist in the functioning of the failure model, that are more subtle and hence are undetected.

- The use of the Jones n-factor to approximate the effects of strain rate must itself introduce errors that are difficult to quantify. The fact that the use of this factor results in somewhat different deformed plate profiles implies that the subsequent strain distribution is also altered, and this will have an effect on tearing behaviour.

- There is some difficulty in making comparisons with experimental work particularly in the case of clamped plates, since such a wide range of Mode II thresholds have been reported. It is considered likely that this is the influence of factors such as clamping pressure which are not well documented. The current work has demonstrated that the onset of failure is indeed sensitive to these parameters.

The performance of the failure model as reported here is thus a complex interaction of these factors, as well as relying on the assumption that Mode II failure is in fact based on ductile tearing as implied by the model. Without adequately addressing each of the factors listed, and probably others, it is not possible to conclude with certainty the reason for the poor correlation of the predictions made in this section.

5. SUMMARY AND CONCLUSIONS

The results of a numerical investigation into the response of thin circular plates have been presented. The finite element model used in the investigation was formulated using the ABAQUS/Explicit code and made use of a standard axisymmetric continuum element for the meshing of the plates, and of intrinsic options for the modelling of elastic-plastic material behaviour, load application, boundary fixation and material rupture. Meshes were generated to model a range of plate diameters, thicknesses and types of boundary condition. Analyses were conducted for a range of impulses expected to cause Mode I and Mode II type response. This chapter summarises and discusses the main observations that have arisen from the study and conclusions are thus drawn.

5.1 Finite element model

- The explicit solution scheme in ABAQUS has proved to be successful in the analysis of blast loaded plates, which involves highly non-linear material and geometric behaviour. The conditional stability of the scheme leads to increased solution times as the finite element mesh is refined. In the case of this study, where large numbers of small elements have been used to model detailed boundary behaviour, the cost of solution has been high. Prediction of global response is adequately achieved with a coarse mesh of shell elements, and the cost of solution is far lower.

- The Von Mises yield criteria selected for the viscoplastic behaviour of the mild steel plates appears to model actual material behaviour well, in conjunction with the Cowper-Symonds strain rate sensitivity relationship. The approximate n-factor derived by Jones does not provide as good a description of strain rate sensitivity, based on the average strain rate encountered during the response. Overall stiffness is thus underestimated, resulting in overpredicted mid-plate deflections, and inaccurate deformed plate profiles.

- The use of a pressure-time history to model the impulsive blast load leads to good correlation with experimental results. Very similar result were obtained in the Mode I region using a simple uniform velocity profile. This implies that provided kinetic energy is imparted to the plate rapidly near the start of the response, so that the entire plate accelerates to move with an approximately uniform speed, the global response can be expected to be insensitive to the exact duration of the load, and dependent only on the magnitude of the energy imparted.

- While not intended specifically for the analysis of shell structures, the CAX4R axisymmetric continuum element has been successful in the modelling of blast loaded plates. For global criteria such as mid-plate deflection, deformed plate profile, and overall response time, the meshes used throughout this study yield insignificantly different results to the SAX1 and S4R shell elements also provided by ABAQUS. The CAX4R element has the advantage of allowing realistic modelling of different boundary conditions, and provides detailed observation of deformation and straining in the entire plate. Phenomena such as the propagation of zones of bending, and plate thinning and necking, are also predicted by this element. The disadvantage of the element is in the size and complexity of the mesh, and in the increased cost of solution that results.

5.2 Mode I prediction

Mode I response has been well predicted for a range of plates, with diameter ranging from 80mm to 120mm, thickness from 1.6mm to 2.75mm, and with a range of clamped and fully built-in boundary conditions. Comparisons with experimental data for mid plate deflections indicate very good correlation for the full range of impulses tested, and the predictions are as good or better than most theoretical solutions discussed. Deformed profiles are also reasonably predicted, but appear somewhat flat in the mid-section.

While no upper or lower limit on useful predictions has been established for plate thickness and diameter, it is felt that the finite element model in its current form is

capable of predicting Mode I response for a wide range of plate configurations. Specific conclusions concerning Mode I response include :

- Mode I response is not highly dependent on boundary fixation method, for the range of cases described in this report, although small variations are noted. Similar deflections and profiles result for both clamped and fully built-in plates of equivalent dimensions, and the effect of edge and fillet radii applied to each of these boundary conditions is also found to be negligible for Mode I response.

- Global plate stiffness is found to increase with increasing thickness and with increasing diameter. However the validity of the dimensionless forms of deflection-thickness ratio and dimensionless impulse ø are confirmed, as mid-point deflection predictions for plates of differing geometry are collapsed into a narrow band, when dimensionless axes are employed.

- Response times are of the order of 110μs for 100mm plates, 90μs for 80mm plates, and 150μs for 120mm plates. This is in good agreement with the limited experimental observations and the predictions of other numerical analyses.

- The transient response of the plate has been shown to involve the formation of two distinct bending hinges. A stationary plastic hinge forms at the boundary early in the response, where large rotations occur. A second hinge forms close to the boundary and travels toward the plate centre. Its arrival at the centre corresponds to the end of the Mode I response.

5.3 Detailed behaviour

The meshes used in the investigation allow detailed observations to be made of localised behaviour.

- Some degree of thinning is observed to occur throughout the entire plate, and the extent of this is greatest at the plate centre. This is consistent with microstructural evidence, and plots of plastic strain. Thinning behaviour away from the boundary is found to be largely independent of boundary condition.

- Thinning at the boundary is found to be dependent on the nature of the boundary condition. The built-in boundary is more highly constrained and so there is less thinning, particularly where a fillet radius is included. Rotations are allowed by the clamped boundary and so thinning due to stretching occurs to a greater extent. This is exaggerated by the effect of clamp indentation, which appears to provide an initiation point for necking, although the strain hardening material on its own does not provide for true localisation. The inclusion of an edge radius on the clamp prevents this indentation from occurring.

5.4 Mode II prediction

An investigation has also been reported into the use of an ABAQUS failure model in an attempt to predict Mode II tearing. The failure model is based on a criterion of maximum equivalent plastic strain, and works in conjunction with the Von Mises viscoplastic material model. The investigation was hampered by a bug in the finite element code, that did not allow the concurrent use of the Cowper-Symonds power law for strain rate sensitivity. An *approximate* factor derived by Jones was substituted and this allowed preliminary results to be obtained. While tearing behaviour is observed, correlation with experimental evidence for the onset of this tearing is in general not good. The onset of tearing is severely underpredicted in most cases, and in particular for built-in plates. For clamped plates correlation with the some results is good, but with others is poor. However it is felt that the model has failed to accurately predict tearing in blast loaded plates. This is not attributable to any one factor, but rather an interaction of several possible causes:

- Tearing behaviour has been shown to be dependent on boundary condition, and it is concluded that the accuracy with which these boundary conditions are modelled thus becomes very important. For example the onset of tearing in clamped plates is retarded by the relaxing of clamping pressure and friction. However no experimental data exists to apply to the clamping model. Also plate indentation from the rigid clamps, and possibly unrealistically sharp corners in the fully built-in model, may both lead to the premature onset of tearing.

- Reliable parameters for material failure are needed before other aspects of the model can be properly scrutinised, and these appear to be scarce. While the values employed here are felt to be the most reliable available, they relate to one specific set of tests and do not account for the possible variations in material properties. Also the effects of strain rate are not considered. This is thought to be the most likely cause of inaccuracy in the predictions at present.

- Evidence has been presented that the strain field near the boundary of both clamped and built-in plates in approximately uniaxial. Thus the use of uniaxial failure values is not though to be unreasonable.

- Even without strain rate sensitivity included in the model, it is possible that there is still an error in the actual functioning of the failure model.

Despite the limitations in predicting the onset of failure, certain experimental observations have been well supported, such as the location of the tearing, and the time to failure. Also the failure model allows true localisation to occur in the form of necking before failure, and evidence has been presented of this necking type failure for all plates. However the degree of necking predicted is less than that experimentally observed, and this may again be attributable to unrealistic parameters being used in the failure option.

6. RECOMMENDATIONS

The investigation has highlighted the importance of boundary conditions in the occurrence of tearing of impulsively loaded membranes. In real world applications where boundary conditions are not idealised and may be difficult to specify, the designer should be aware of the importance of boundary detail in promoting or retarding tearing. The avoidance of stress concentrating corners and edges is thus imperative where blast loads are to be successfully contained. The use of fillet and edge radii to "soften" boundary discontinuities should be encouraged in design codes.

The model presented here may be used with confidence to predict Mode I response for a wide range of plate geometry. However it should not be used in its present form for the prediction of Mode II tearing. Before useful predictions can be obtained, it is recommended that the following areas be further investigated:

1. Reliable parameters for use in the failure model must be obtained and the effect of strain rate on these parameters should be established. This may involve extensive experimental work.
2. A further attempt should be made with the current model once the ABAQUS code has been properly debugged. This will allow use of the Cowper-Symonds strain rate sensitivity relationship.
3. Even more accurate modelling of boundary conditions may be attempted, where for example realistic clamping parameters are specified, corners are not modelled as perfectly sharp, and clamps as not perfectly rigid.

Finally it has been observed that the response of blast loaded circular plates is often not axisymmetric. An interesting area for research would involve a 3-dimensional model of a circular plate, that would allow an asymmetric response to be predicted. The only limitations to such studies is the cost of solution in terms of CPU time, and as processing accelerates in the future, more complete models will be realised.

REFERENCES

1. S. B. MENKES and H. J. OPAT, Tearing and shear failures in explosively loaded clamped beams, *Exp. Mech.*, **13**, 480-486 (1973).
2. R. G. TEELING-SMITH, *An investigation into the deformation and tearing of thin circular plates subjected to impulsive loads*, M.Sc., University of Cape Town (1989).
3. G. I. TAYLOR, The distortion under pressure of a diaphragm which is clamped along its edge and stressed beyond its elastic limit, *Underwater Explosion Research,* **3,** *The Damage Process,* 107-121. Office of Naval Research (1950).
4. A. J. HOFFMAN, *The plastic response of circular plates to air blast,* M.Sc, University of Delaware, (1955).
5. J .S. HUMPHREYS, Plastic deformation of impulsively loaded straight clamped beams, *J. Appl. Mech.* **32,** 7-10 (1965)
6. G. N. NURICK, H. T. PEARCE and J. B. MARTIN, *The deformation of thin plates subjected to impulsive loading.* In Inelastic behaviour of plates and shells, ed. L. BEILACQUA, (Berlin: Springer-Verlag, 1986)
7. G. N. NURICK, H. T. PEARCE and J. B. MARTIN, Prediction of transverse deflections and in-plane strains in impulsively loaded thin plates. *Int. J. of Mech. Sci.* **29**, 435-442 (1987).
8. G. N. NURICK and J. B. MARTIN, Deformation of thin plates subjected to impulsive loading-A review: Part II - Experimental studies. *Int. J. Impact Engng.* **8,** 159-186 (1989).
9. T. WIERZBICKI and A. L. FLORENCE, A theoretical and experimental investigation of impulsively loaded clamped circular viscoplastic plates, *Int. J. Solids Struct.* **6,** 553-568 (1970).
10. T. A. DUFFEY and S. W. KEY, Experimental-theoretical correlation of impulsively loaded clamped circular plates. Sandia Laboratories Research Report No. SC-RR-68-210 (1968)
11. S. R. BODNER and P. S. SYMONDS, Experiments on viscoplastic response of circular plates to impulsive loading, *J. Mech. Phys. Solids* **27**, 91-113 (1979)

12. G. N. NURICK, *Large deformations of thin plate subjected to impulse loading,* Ph.D., University of Cape Town (1987).

13. G. N. NURICK, The prediction of the deformation response of a structure subjected to an explosive load using a light interference technique. *Proceedings of the SEM Spring Conference on Experimental Mechanics*, 105-114 (1986).

14. R. G. TEELING-SMITH and G. N. NURICK, The deformation and tearing of thin circular plates subjected to impulsive loads. *Int. J. Impact Engng.* **11,** 77-91 (1991).

15. G. N. NURICK and R. G. TEELING-SMITH, *Predicting the onset of necking and hence rupture of thin plates loaded impulsively - An experimental view*, In Structures Under Shock and Impact II, ed. P. S. BULSON. (London: Thomas Telford, 1992).

16. N. S. MARSHALL, *An investigation of the boundary conditions of impulsively loaded plates,* B.Sc, University of Cape Town (1992).

17. B. M. THOMAS, *The effect of boundary conditions on the failure of thin plates subjected to impulsive loading*, M.Sc., University of Cape Town (1995).

18. B. M. THOMAS, G. N. NURICK, The effect of boundary conditions on thin plates subjected to impulsive loads, *Proceedings of Plasticity '95: The fifth international symposium on plasticity and its current applications, Osaka* (1995).

19. J. F. LOUMEAU, *An investigation into the effects of thickness and boundary conditions of integral circular plates subjected to impulsive loading,* B.Sc, University of Cape Town (1995).

20. G. N. NURICK and J. B. MARTIN, Deformation of thin plates subjected to impulsive loading-A review: Part I - Theoretical Considerations. *Int. J. Impact Engng.* **8,** 159-186 (1989).

21. H. LIPPMAN, Kinetics of the axisymmetric rigid-plastic membrane supplied to initial impact. *Int. J. Mech. Sci.* **16**, 297-303, 945-947, (1974).

22. N. PERRONE and P. BHADRA, A simplified method to account for plastic rate sensitivity with large deformations, *J. App. Mech*, **46**, 811-816 (1979).

23. P. S. SYMONDS and T. WIERZBICKI, Membrane mode solutions for impulsively loaded circular plates. *J. App. Mech.* **46,** 58-64 (1979).

24. HIBBITT, KARLSSON & SORENSEN, INC, *ABAQUS theory manual.* (1996).

25. N. JONES, *Structural impact.* (Cambridge University Press, 1989).

26. W. G. SHEN and N. JONES, Dynamic response and failure of fully clamped circular plates under impulsive loading. *Int. J. Impact. Engng.* **13**(2), 259-278 (1993).

27. Q. M. LI and N. JONES, Blast loading of fully clamped circular plates with transverse shear effects. *Int. J. Solids Structures.* **31**(14), 1861-1876, (1994).

28. M. D. OLSON, G. N. NURICK and J. R. FAGNAN, Deformation and rupture of blast loaded square plates-predictions and experiments. *Int. J. Impact Engng.* **2,** 279-291 (1993).

29. G. N. NURICK, M. D. OLSON, J. R. FAGNAN and A. LEVIN, Deformation and tearing of blast-loaded stiffened square plates. *Int. J. Impact. Engng.* **16**(2), 273-291, (1995)

30. M. D. OLSON, J. R. FAGNAN and G. N. NURICK, Analysis of the deformation and tearing of blast loaded circular plates. (Submitted Nov. 1994) *Int. J. Impact Engng.*

31. G. H. FARROW, *The response of impulsively loaded sandwich plates,* M.Sc, University of Cape Town, (1995).

32. G. H. FARROW, G. N. NURICK, and G. P. MITCHELL, Modelling of impulsively loaded circular plates using the ABAQUS finite element code, *Proceedings of the 13th Symposium on Finite Element Methods in South Africa,* (1995).

33. T. A. DUFFEY, *Dynamic Rupture of Shells,* In Structural Failure, eds. T, Wierzbicki and N. Jones, (New York: Wiley, 1989)

34. D. J. BAMMANN, M. L. CHIESA, M. F. HORSTEMEYER, and L. I. WEINGARTEN, *Failure in ductile materials using finite element methods,* In Structural Crashworthiness and Failure, eds. N. Jones and T. Wierzbicki, (Elsevier Applied Science, 1993).

35. HIBBITT, KARLSSON & SORENSEN, INC, *ABAQUS user manual.* (1996).

36. Y. ESTRIN, Rate effects and the role of thermomechanical coupling in shear localisation. *Proceedings of the 1st International Conference on Mechanics of Time Dependent Materials*. 299-303 (1995).

37. T. A. J. SANDERS, *A microstructural investigation of impulsively loaded plates,* B. Sc, University of Cape Town, (1994).

38. N. K. GUPTA, and B. KARUNES, Dynamic analysis of necking phenomena, *Int. J. Mech. Sci.* **21**, 387-397, (1979).

39. J. LEMAITRE, *Formulation and identification of damage kinetic constitutive equations,* In Continuum Damage Mechanics, theory and applications, eds. D Krajcinovic and J Lemaitre, (New York: Springer-Verlag, 1987)

BIBLIOGRAPHY

1. T. WIERZBICKI and N. JONES, eds. *Structural Failure,* (New York: Wiley, 1989).
2. N. JONES and T. WIERZBICKI, eds. *Structural Crashworthiness,* (Kent: Butterworths, 1983).
3. N. JONES and T. WIERZBICKI, eds. *Structural Crashworthiness and Failure,* (London: Elsevier, 1993).
4. G. N. NURICK and G. C. SHAVE, The deformation and tearing of thin square plates subjected to impulsive loads - an experimental study, *Int. J. Impact Engng.* **18**(1), 99-116, (1996).
5. W. Q. SHEN and N. JONES, A failure criterion for beams under impulsive loading, *Int. J. Impact Engng,* **12**(1), 101-121, (1992).
6. W. Q. SHEN, Interaction yield hypersurfaces for the plastic behaviour of beams - II. Combining bending, tension, shear and torsion, *Int. J. Mech. Sci.* **37**(3), 239-247, (1993).
7. Q. M. LI and N. JONES, Blast loading of fully clamped beams with transverse shear effects, *Mech. Struct. & Mach.* **23**(1), 59-86, (1995).
8. P. S. WESTINE and W. E. BAKER, *Energy solutions for predicting deformation in blast loaded structures*, Proc. 16th Explosive Safety Seminar, Hollywood Beach, Florida, USA, 849-879.
9. R. E. BIMHA, G. N. NURICK and G. P. MITCHELL, Modelling the deformation of blast-loaded stiffened square plates, *Proceedings of the 1st South African Conference on Applied Mechanics,* (1996).
10. G. N. NURICK, M. E. GELMAN and N. S. MARSHALL, Tearing of blast loaded plates with clamped boundary conditions, *Submitted to Int. J. Impact. Engng.* (1996).

APPENDIX 1: EXPERIMENTAL RESULTS

In Chapter 4 results were presented for three configurations of plate showing the correlation of the numerical predictions to experimental data for deflection-thickness ratio with dimensionless impulse. The remainder of experimental results are plotted in the charts that follow, along with the current numerical predictions.

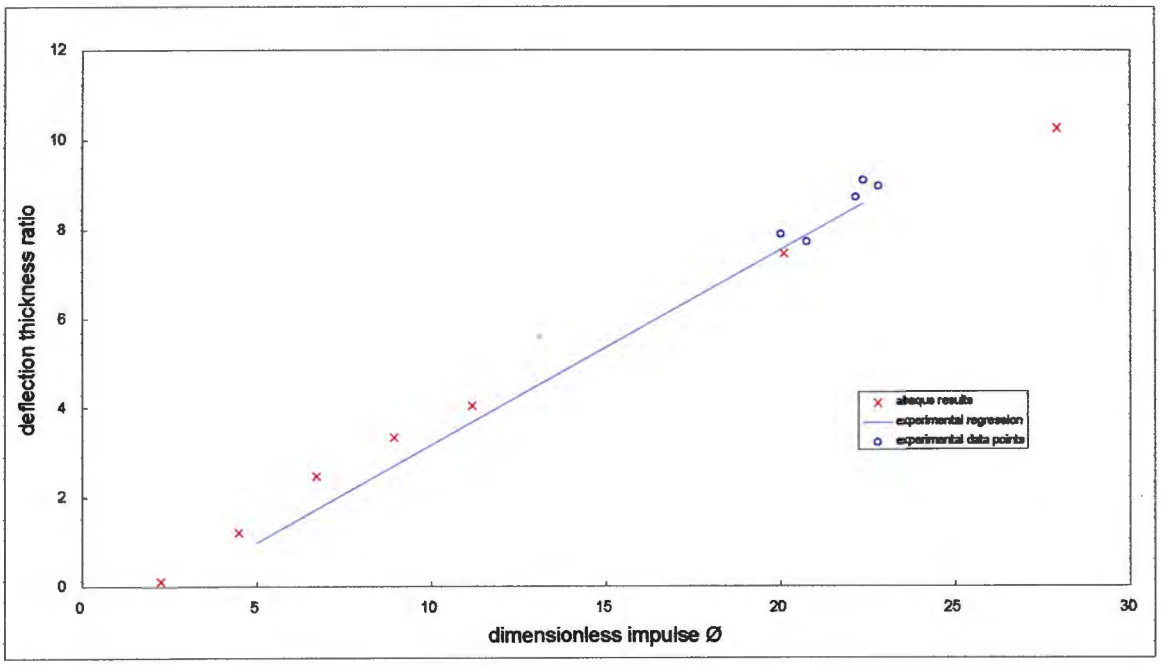

Figure {A1.1} Experimental results and numerical predictions for 100mm fully built-in plates with thickness = 2.75mm and fillet radius = 3.0mm

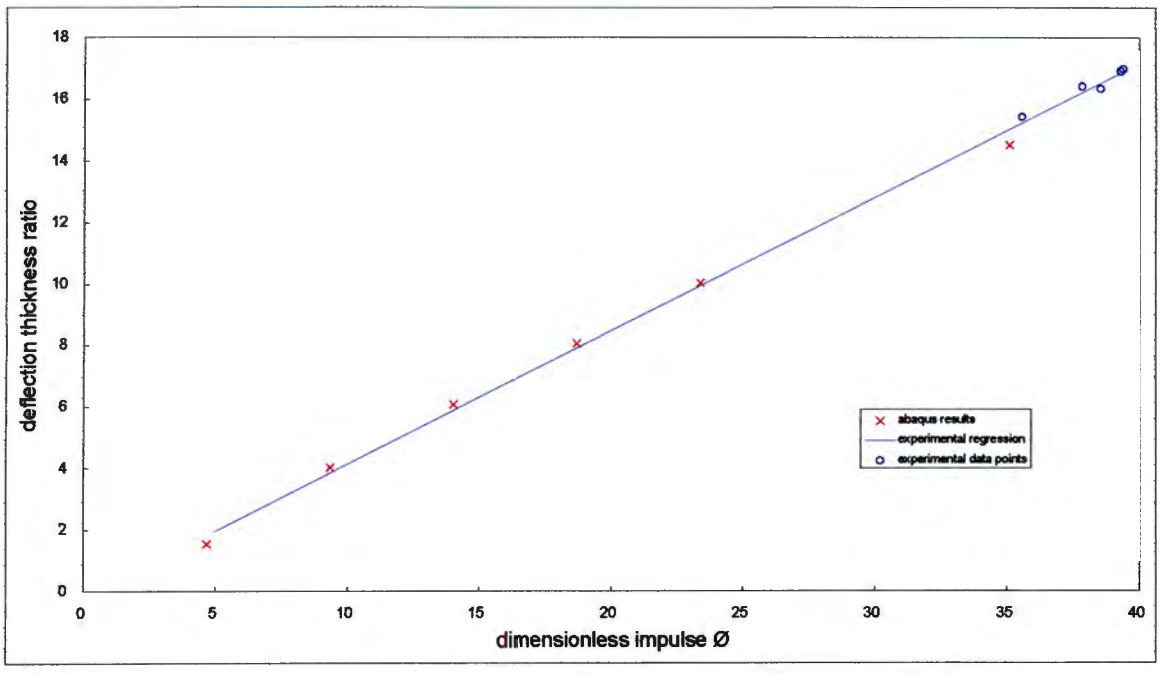

Figure {A1.2} Experimental results and numerical predictions for 100mm fully built-in plates with thickness = 1.9mm and a fillet radius on one side = 2.0mm.

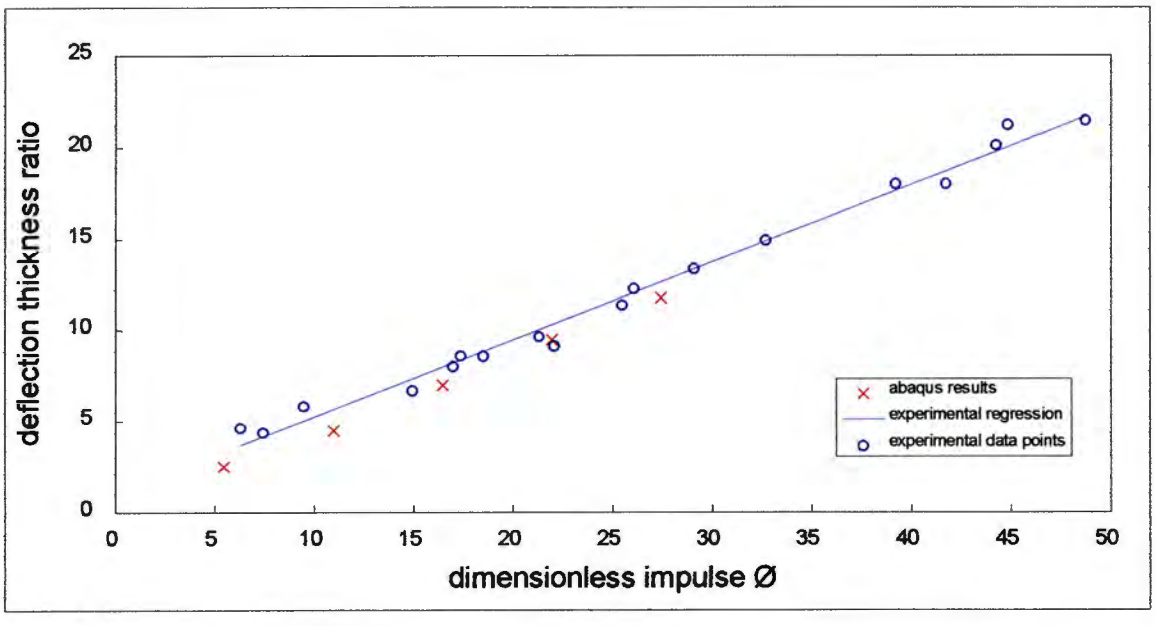

Figure {A1.3} Experimental results and numerical predictions for 120mm clamped plates, with no edge radius on the clamp, and thickness = 1.6mm.

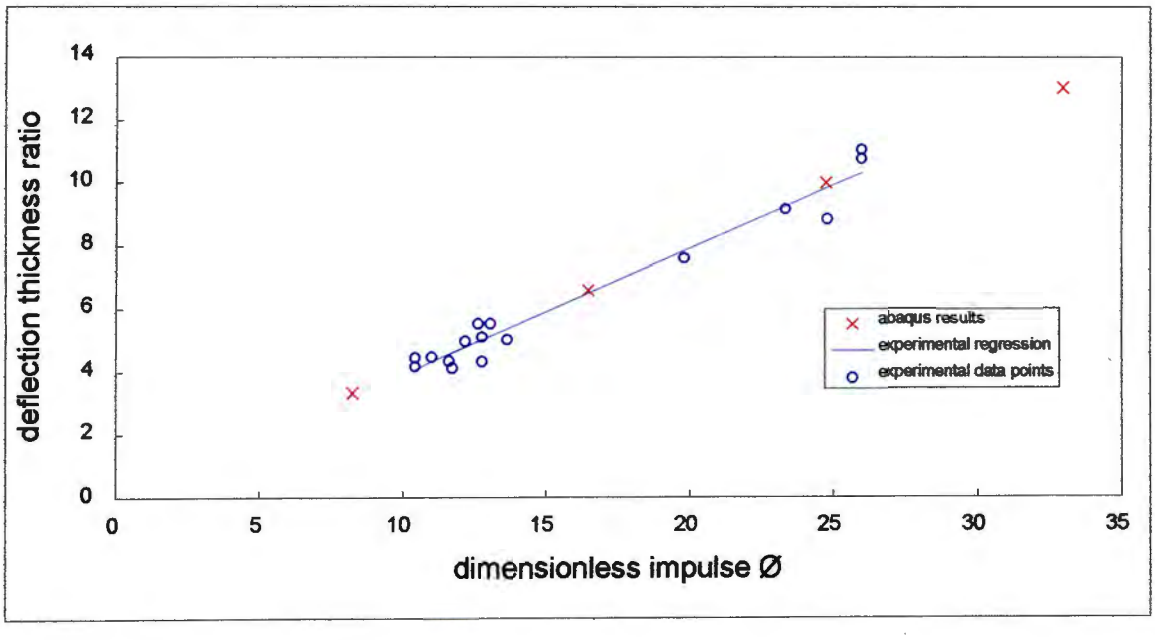

Figure {A1.4} Experimental results and numerical predictions for 80mm clamped plates with no edge radius on the clamp, and thickness = 1.6mm.

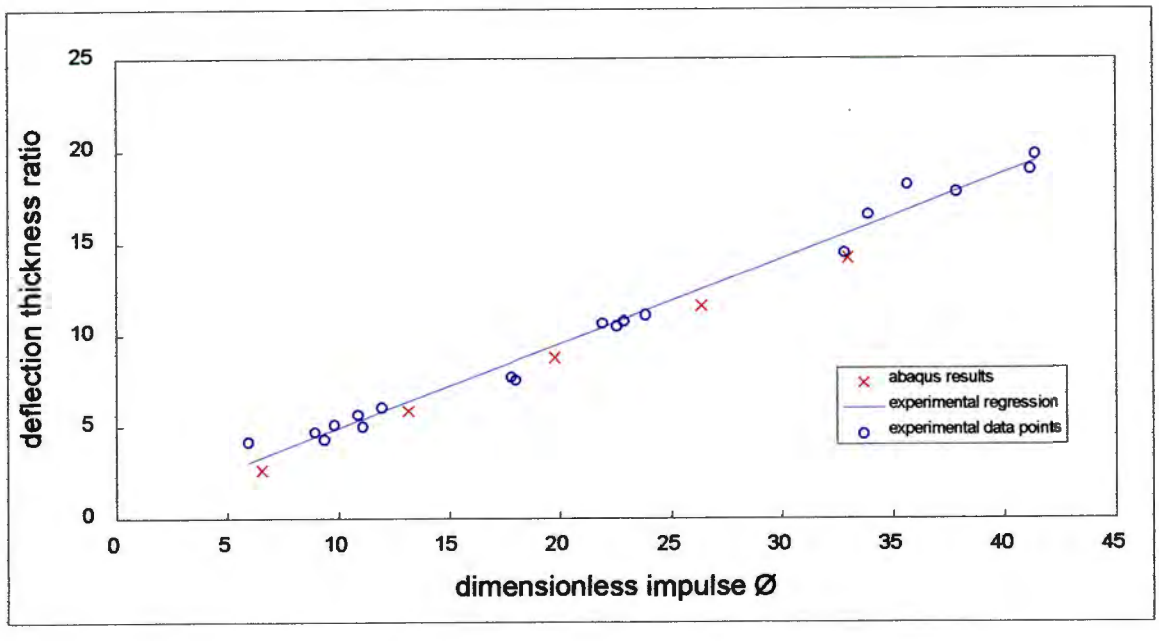

Figure {A1.5} Experimental results and numerical predictions for 100mm clamped plates with an edge radius = 1.6mm, and thickness = 1.6mm.

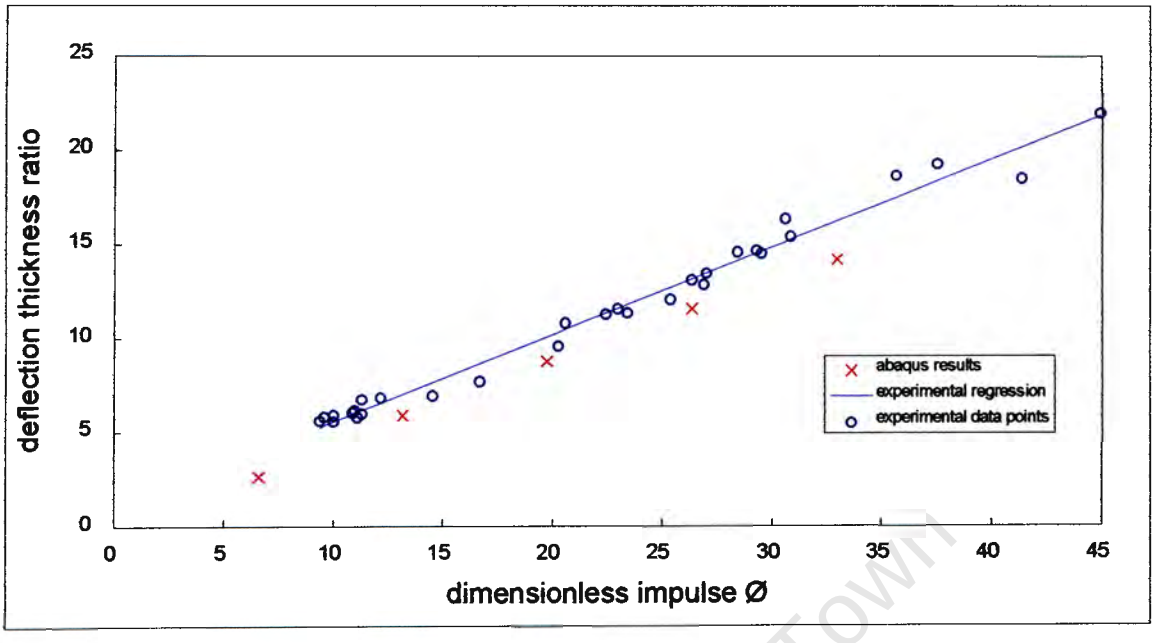

Figure {A1.6} - Experimental results and numerical predictions for 100mm clamped plates with an edge radius = 3.2mm and thickness = 1.6mm.

APPENDIX 2: PREDICTED PROFILES

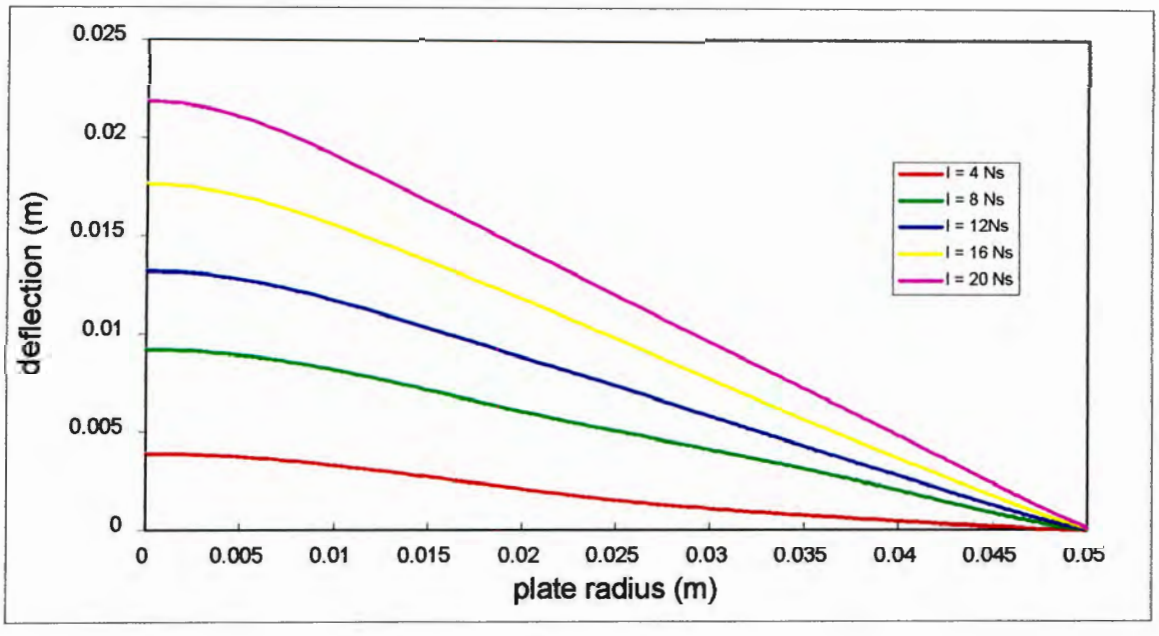

Figure {A2.1} Predicted plate profiles for 100mm fully built-in plates with no fillet radius, and thickness = 1.6mm.

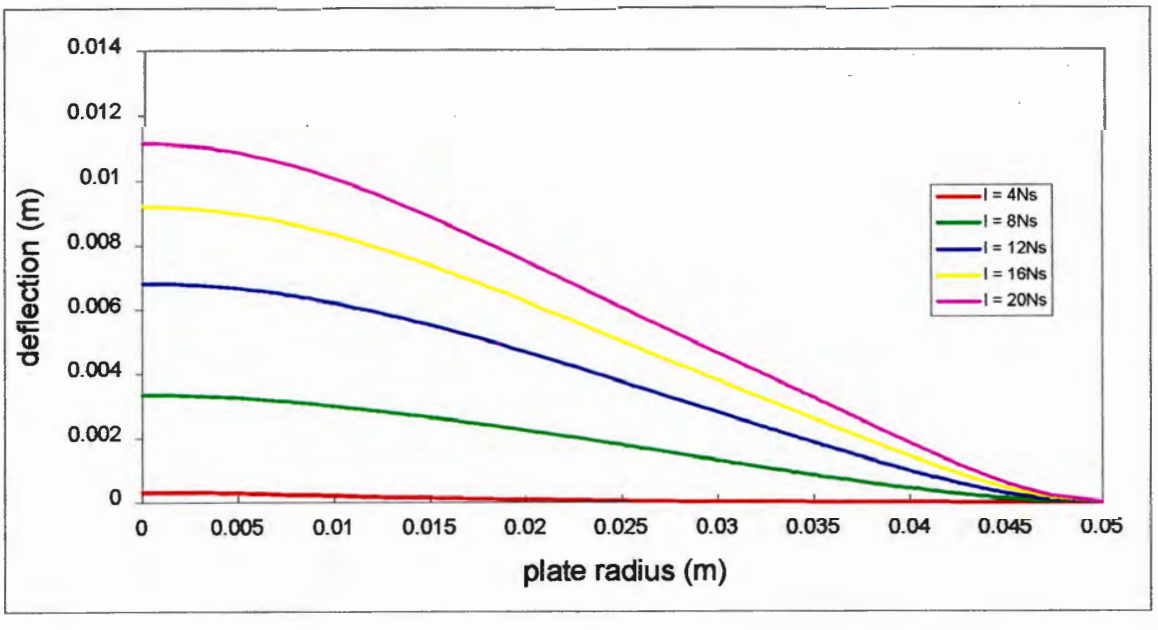

Figure {A2.2} Predicted plate profiles for 100mm fully built-in plates with fillet radius = 3.0mm and thickness = 2.75mm.

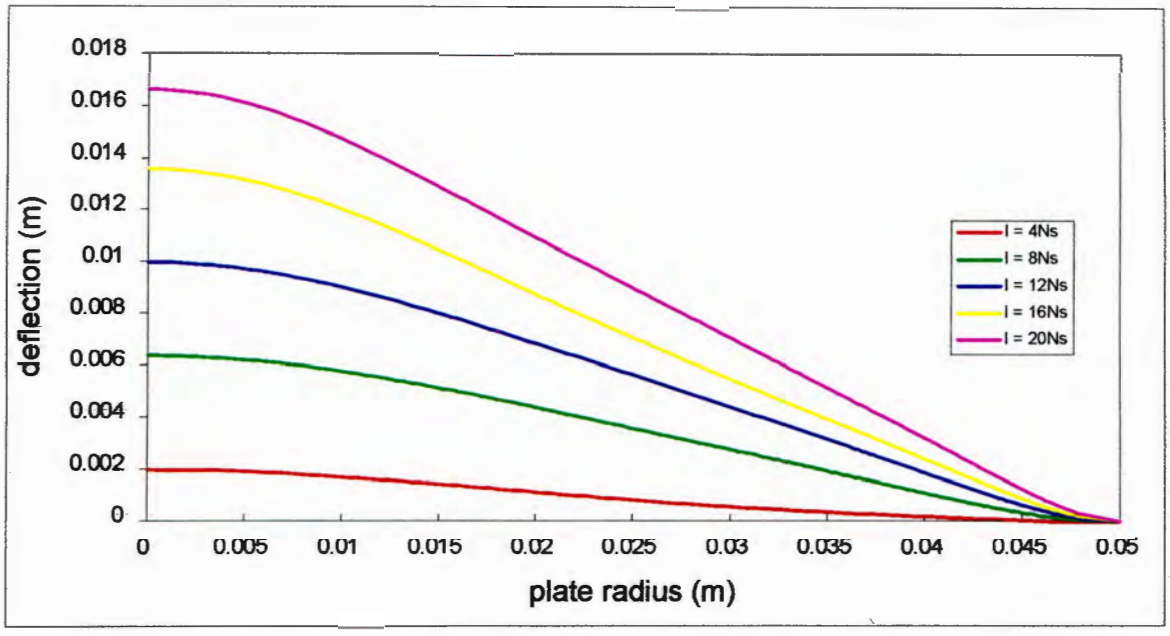

Figure {A2.3} Predicted plate profiles for 100mm fully built-in plates with fillet radius = 2.0mm and thickness = 2.0mm.

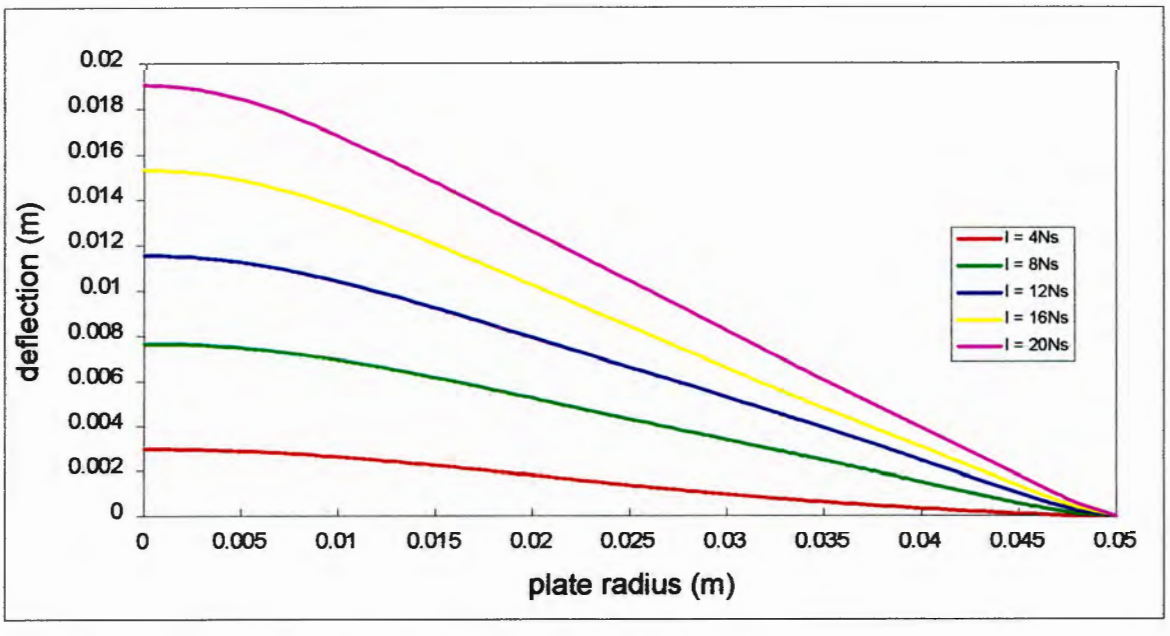

Figure {A2.4} Predicted plate profiles for 100mm fully built-in plates with a fillet radius on one side = 2.0mm, and thickness = 1.9mm.

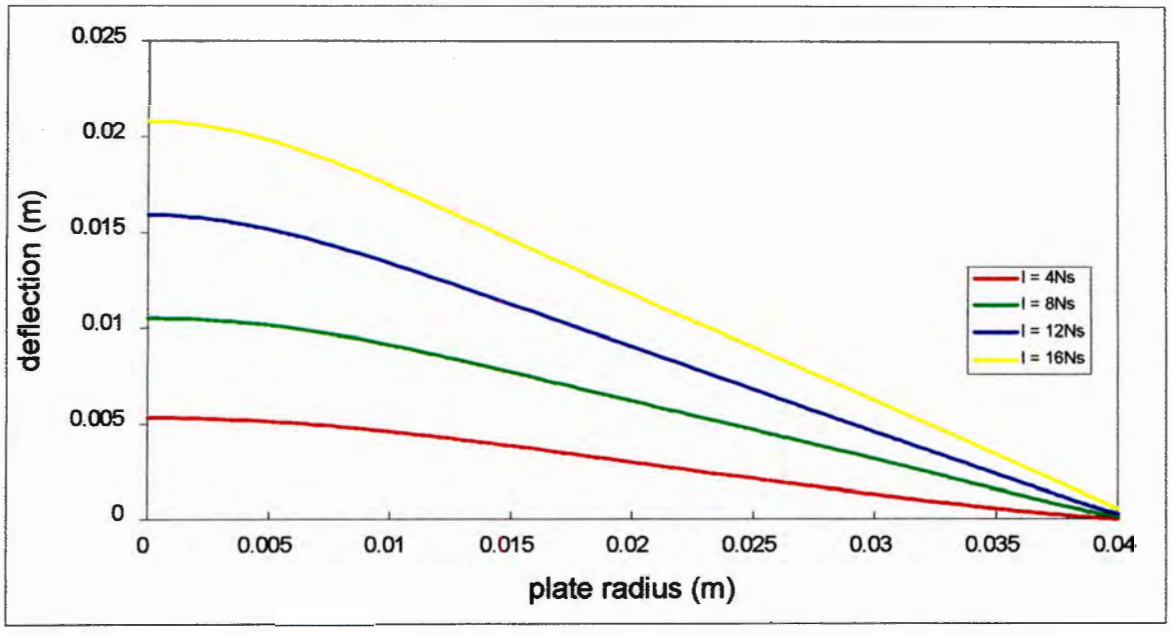

Figure {A2.5} Predicted plate profiles for 80mm clamped plates with no edge radius and thickness = 1.6mm.

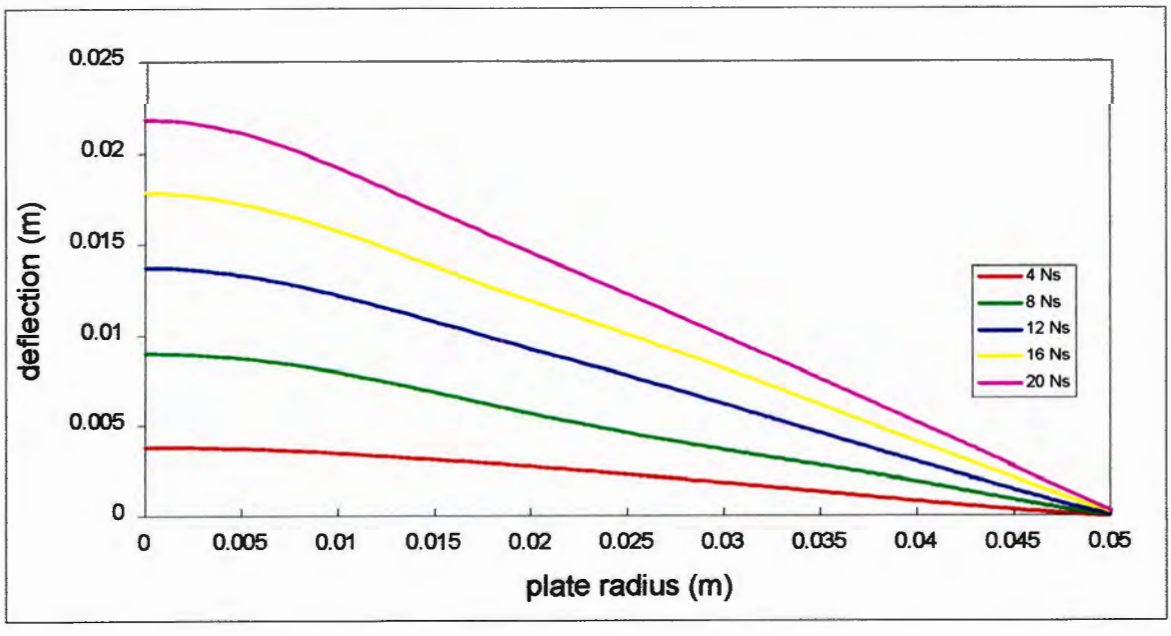

Figure {A2.6} Predicted plate profiles for 100mm clamped plates with no edge radius, and thickness = 1.6mm.

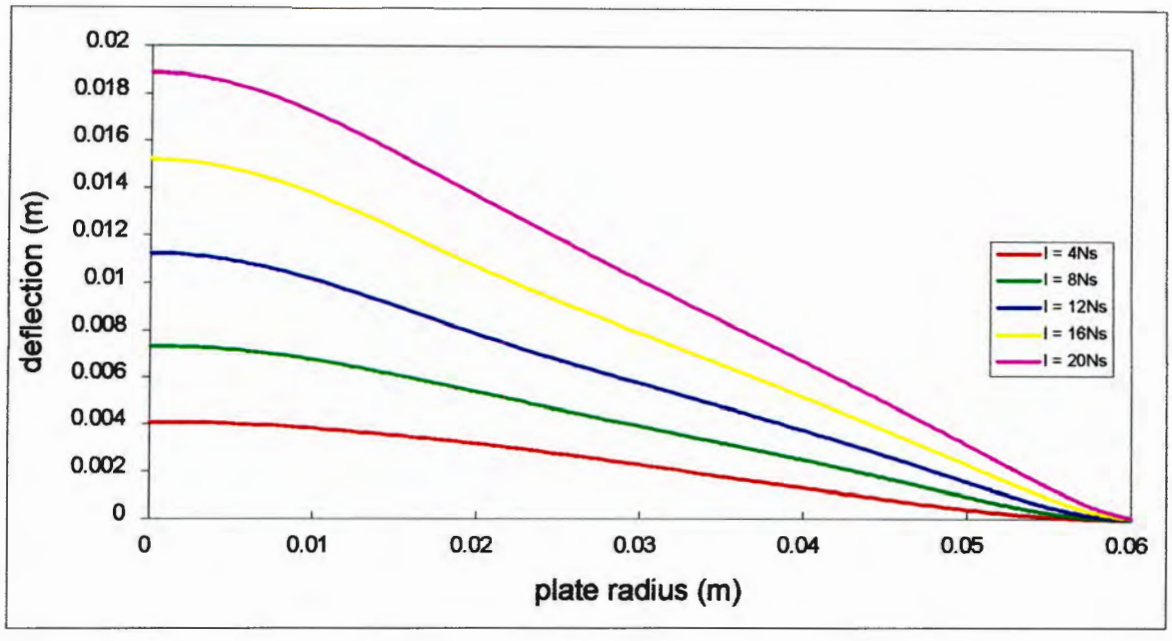

Figure {A2.7} Predicted plate profiles for 120mm clamped plates with no edge radius, and thickness = 1.6mm.

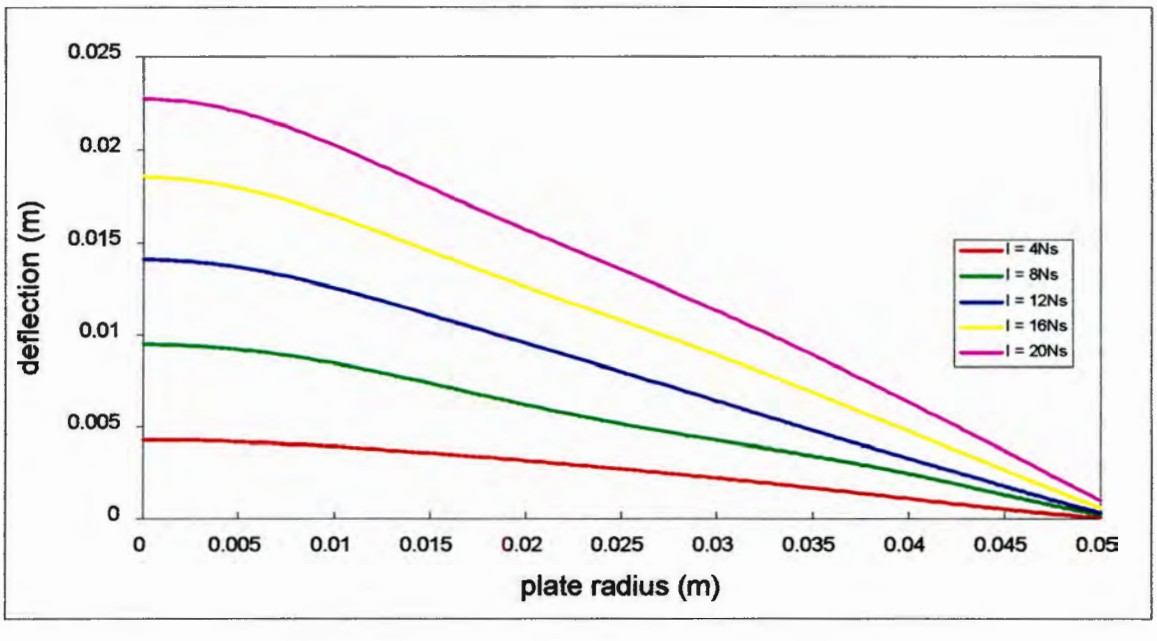

Figure {A2.8} Predicted plate profiles for 100mm clamped plates with an edge radius = 1.6mm and thickness = 1.6mm.

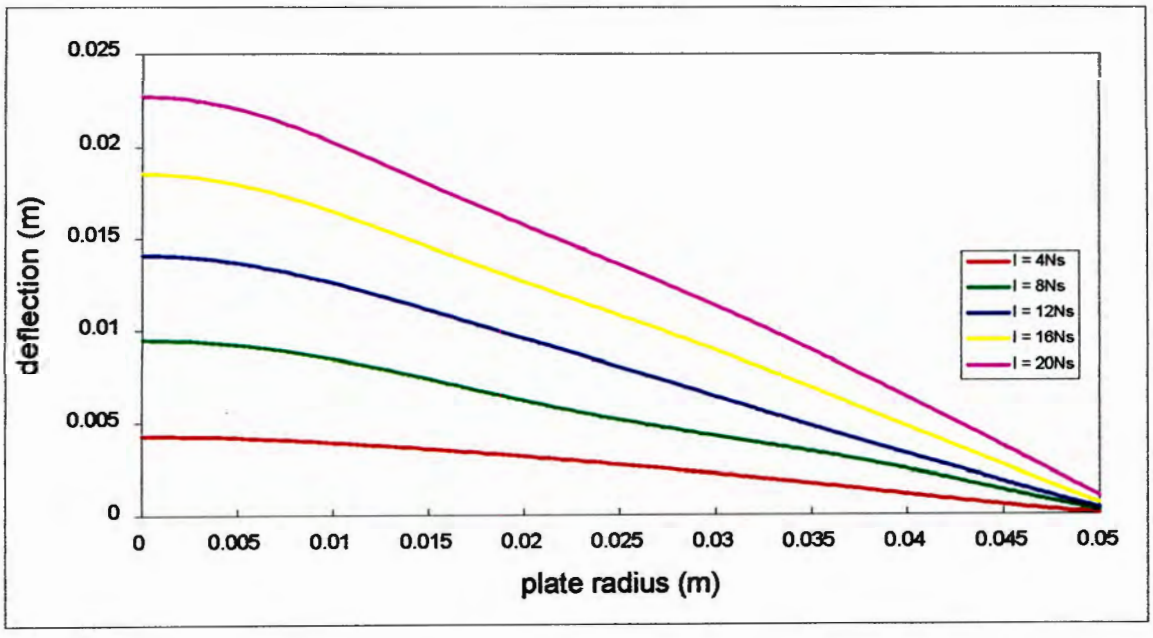

Figure {A2.9} Predicted plate profiles for 100mm clamped plates with edge radius = 3.2mm and thickness = 1.6mm.

APPENDIX 3: INPUT DECK

In this appendix, an example of a typical ABAQUS input deck is presented.

```
**********************************************************************
*HEADING
EXAMPLE INPUT DECK; CLAMPED PLATE WITH EDGE RADIUS
**********************************************************************
********** node and element definitions
*NODE
1, 0.0, 0.0
701, 0.07, 0.0
16001, 0.0, 0.0016
16701, 0.07, 0.0016
*NGEN, NSET=BOTTOM
1, 701, 1
*NGEN, NSET=TOP
16001, 16701, 1
*NFILL, NSET=ALL
BOTTOM, TOP, 16, 1000
*NSET, NSET=CENTRE
1, 1001, 2001, 3001, 4001, 5001, 6001, 7001, 8001 9001, 10001, 11001,
12001,
13001, 14001, 15001, 16001
*NSET, NSET=BOUND
501, 1501, 2501, 3501, 4501, 5501, 6501, 7501, 8501, 9501, 10501, 11501,
12501,
13501, 14501, 15501, 16501
*ELEMENT, TYPE=CAX4R
1, 1, 5, 4005, 4001
*ELGEN, ELSET=MODEL
1, 75, 4, 1, 4, 4000, 100
```

```
*ELEMENT, TYPE=CAX4R
1000, 301, 303, 2303, 2301
*ELGEN, ELSET=MODEL
1000, 75, 2, 1, 8, 2000, 1000
*ELEMENT, TYPE=CAX4R
10000, 451, 452, 1452, 1451
*ELGEN, ELSET=MODEL
10000, 50, 1, 1, 16, 1000, 1000
*ELEMENT, TYPE=CAX4R
50000, 501, 502, 1502, 1501
*ELGEN, ELSET=MODEL
50000, 50, 1, 1, 16, 1000, 1000
*ELEMENT, TYPE=CAX4R
75000, 551, 553, 2553, 2551
*ELGEN, ELSET=MODEL
75000, 75, 2, 1, 8, 2000, 1000
*ELSET, ELSET=BOT, ELSET=LOADED, GENERATE
1, 75, 1
1000, 1074, 1
10000, 10049, 1
*ELSET, ELSET=BOT, GENERATE
50000, 50049, 1
75000, 75074, 1
*ELSET, ELSET=TOP, GENERATE
301, 375, 1
8000, 8074,1
25000, 25049, 1
65000, 65049, 1
82000, 82074,1
*MPC
LINEA, 2301, 301, 4301
LINEA, 6301, 4301, 8301
```

LINEA, 10301, 8301, 12301

LINEA, 14301, 12301, 16301

LINEA, 1451, 451, 2451

LINEA, 3451, 2451, 4451

LINEA, 5451, 4451, 6451

LINEA, 7451, 6451, 8451

LINEA, 9451, 8451, 10451

LINEA, 11451, 10451, 12451

LINEA, 13451, 12451, 14451

LINEA, 15451, 14451, 16451

LINEA, 1551, 551, 2551

LINEA, 3551, 2551, 4551

LINEA, 5551, 4551, 6551

LINEA, 7551, 6551, 8551

LINEA, 9551, 8551, 10551

LINEA, 11551, 10551, 12551

LINEA, 13551, 12551, 14551

LINEA, 15551, 14551, 16551

********** meshing of the rigid clamps

*NODE

20003, 0.0516, 0.0

20001, 0.07, 0.0

20002, 0.06, -0.01

20013, 0.05, -0.0016

20100, 0.0516, -0.0016

30003, 0.0516, 0.0016

30001, 0.07, 0.0016

30002, 0.06, 0.0116

30013, 0.05, 0.0032

30100, 0.0516, 0.0032

*NGEN, LINE=C, SYSTEM=RC

20003, 20013, 1, 20100

```
30003, 30013, 1, 30100
*ELEMENT, TYPE=RAX2, ELSET=CLBOT
100000, 20003, 20001
*ELEMENT, TYPE=RAX2, ELSET=CLTOP
200000, 30003, 30001
*ELEMENT, TYPE=RAX2, ELSET=CLBOT
100010, 20013, 20012
*ELGEN, ELSET=CLBOT
100010, 10, -1, 1
*ELEMENT, TYPE=RAX2, ELSET=CLTOP
200010, 30013, 30012
*ELGEN, ELSET=CLTOP
200010, 10, -1, 1
*RIGID BODY, ELSET=CLBOT, REF NODE=20002
*RIGID BODY, ELSET=CLTOP, REF NODE=30002
********** boundary condition
*BOUNDARY
20002, ENCASTRE
********** material definition
*SOLID SECTION, ELSET=MODEL, MATERIAL=STEEL
*MATERIAL,NAME=STEEL
*ELASTIC
210.E9, 0.29
*PLASTIC
290.E6, 0.00
300.E6, 0.003
310.E6, 0.008
320.E6, 0.013
330.E6, 0.018
340.E6, 0.024
350.E6, 0.035
360.E6, 0.056
```

```
370.E6, 0.10
380.E6, 0.137
390.E6, 0.171
400.E6, 0.20
470.E6, 0.403
3779.E6, 10.0
*DENSITY
7850.
*RATE DEPENDENT
40.0, 5.0
******** clamping step
*RESTART, WRITE, NUMBER INTERVAL=1
*AMPLITUDE, NAME=CLAMPING, TIME=STEP TIME, VALUE=RELATIVE
0., 0., 0.0005, -1.0
*STEP
*DYNAMIC, EXPLICIT
, 0.00006
*SURFACE DEFINITION, NAME=BOTSURF
BOT, S1
*SURFACE DEFINITION, NAME=TOPSURF
TOP, S3
*SURFACE DEFINITION, NAME=CLAMPBOT
CLBOT, SPOS
*SURFACE DEFINITION, NAME=CLAMPTOP
CLTOP, SNEG
*CONTACT PAIR, INTERACTION=CLAMPING
TOPSURF, CLAMPTOP
BOTSURF, CLAMPBOT
*SURFACE INTERACTION, NAME=CLAMPING
*FRICTION
0.2
*BOUNDARY, AMPLITUDE=CLAMPING
```

```
30002, 2, 2, 0.000005
*END STEP
********** blast loading step
*STEP
*AMPLITUDE, NAME=STEP1
0.,0.,  0.,1.0,  1.5E-5,1.,  1.5E-5,0.,  .0125,0.
*DYNAMIC, EXPLICIT
, 0.0002
*DLOAD, AMPLITUDE=STEP1
LOADED, P1, 101.86E6
*END STEP
```

APPENDIX 4 : PHOTOGRAPHS

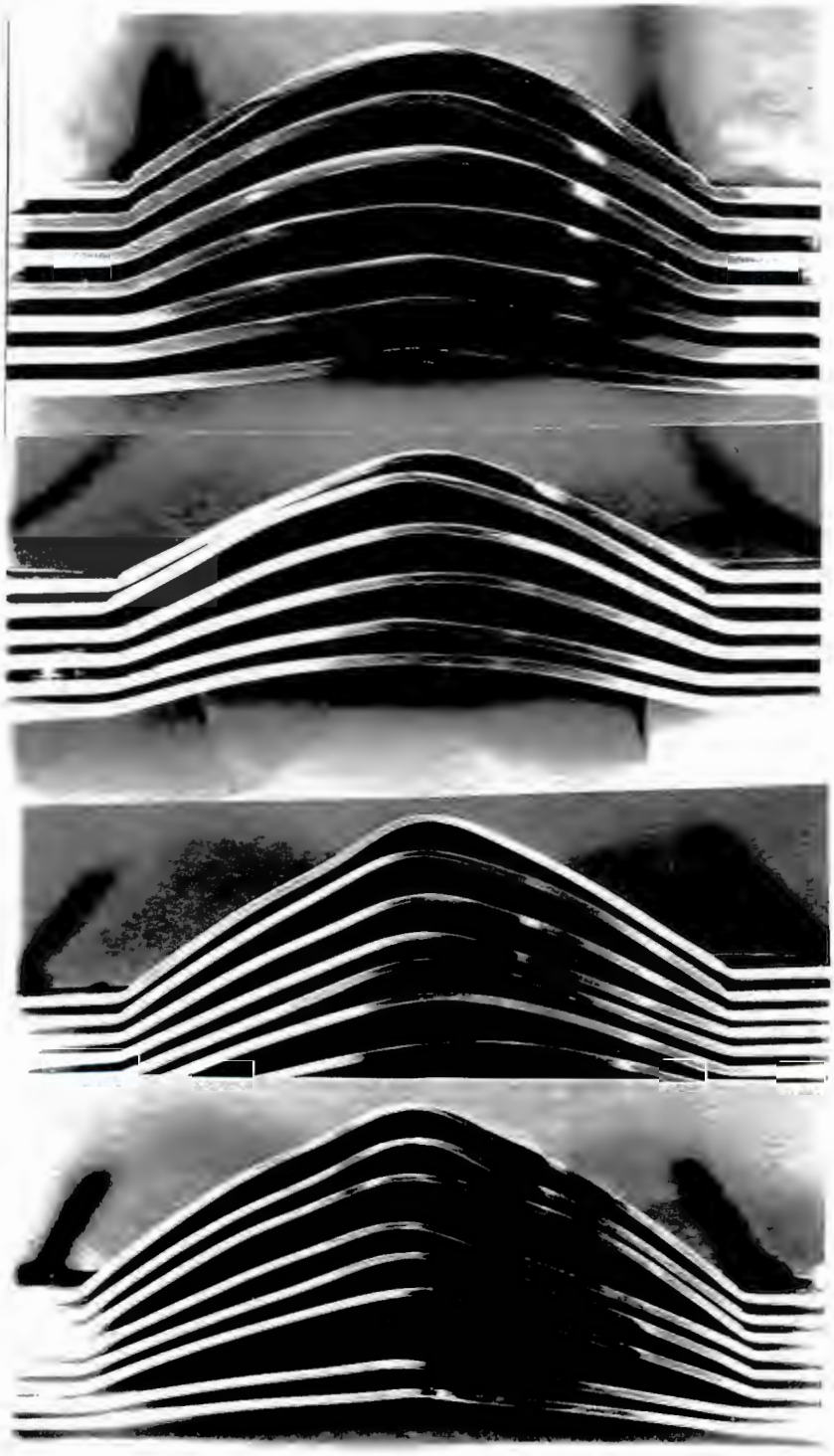

Figure {A4.1} Photographs of experiments for blast loaded clamped plates with sharp edged boundary conditions.

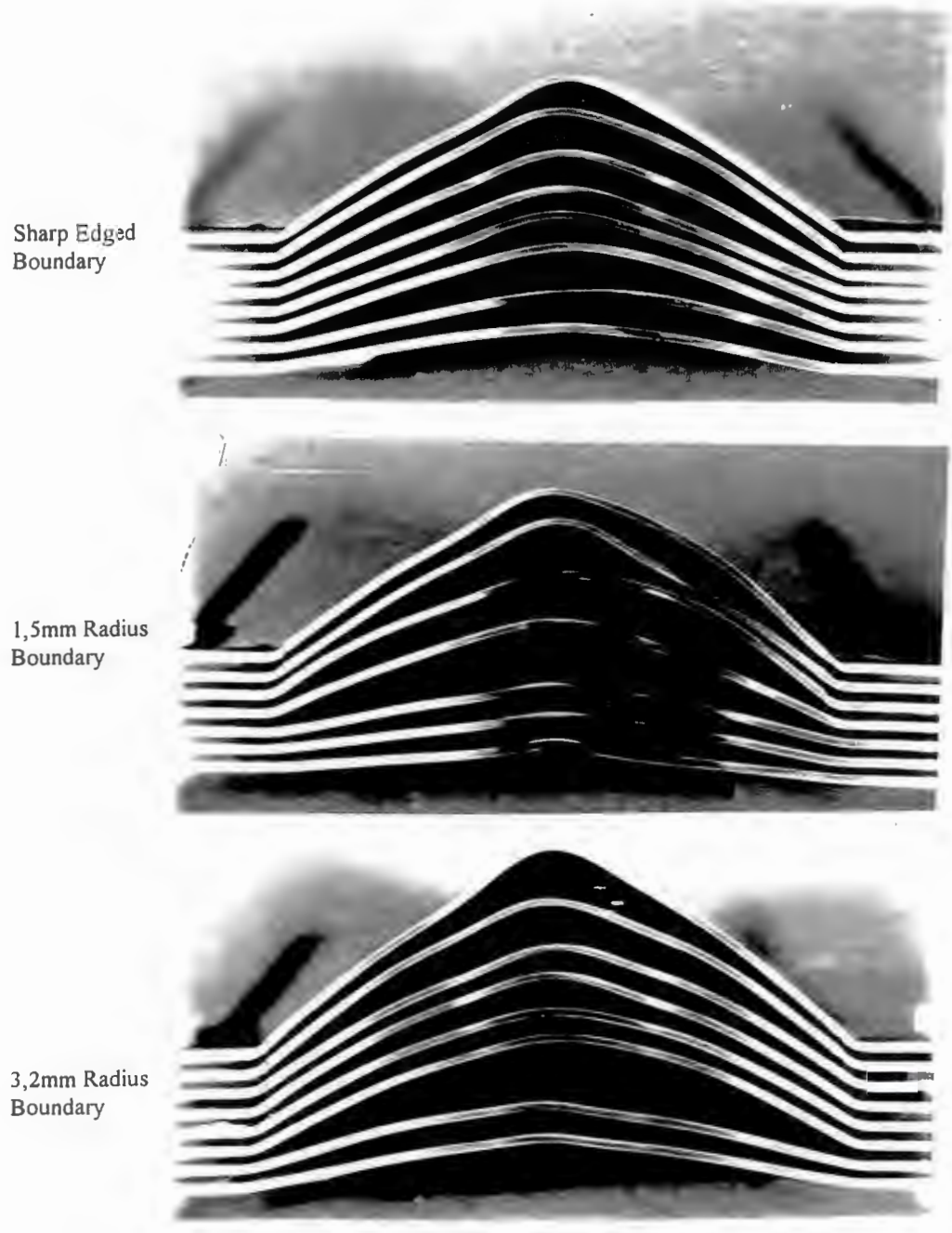

Figure {A4.2} Photographs of experiments for clamped 100mm plates with different clamp radii.

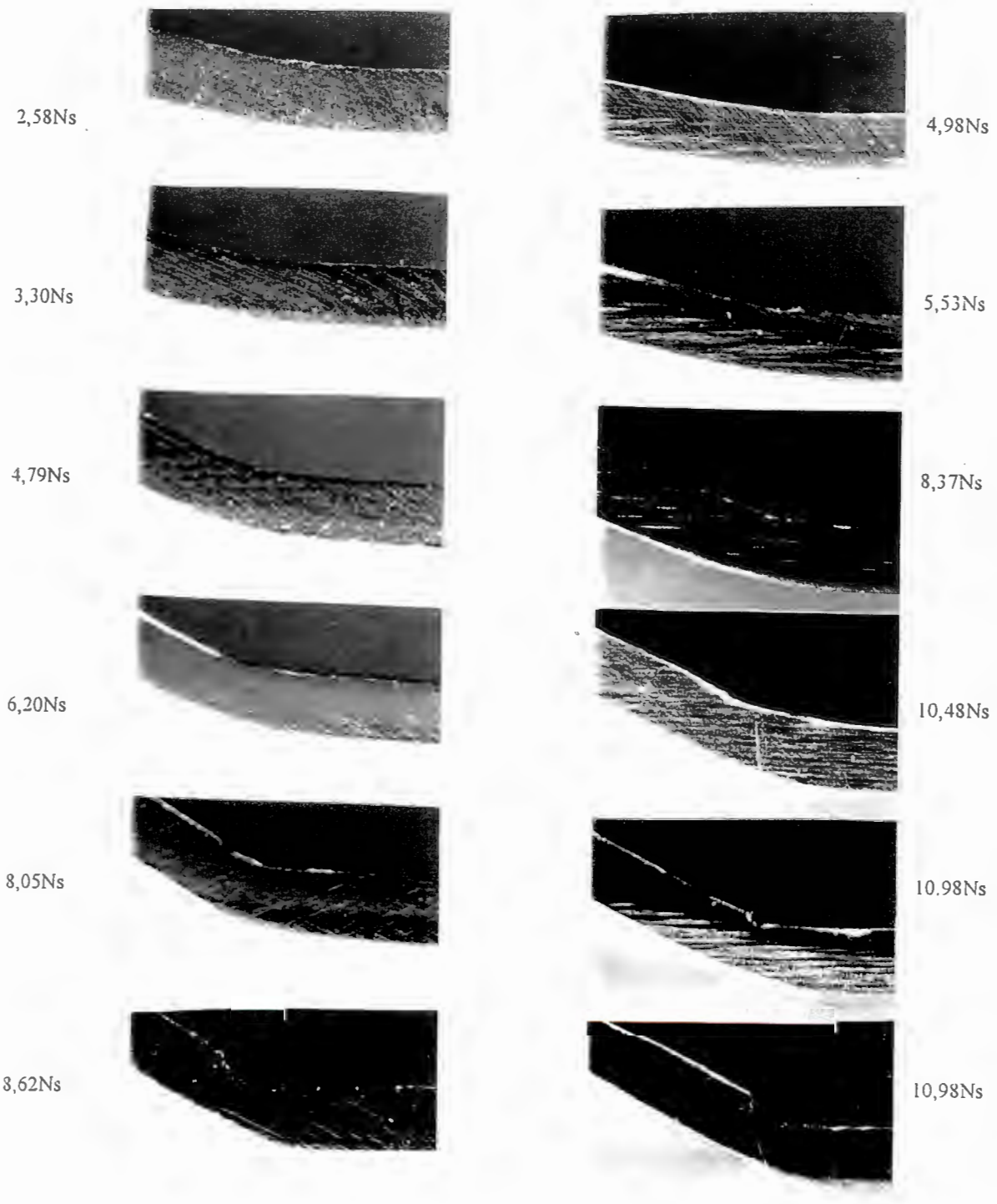

Figure {A4.3} Boundary detail of plate response for 60mm and 80mm clamped plates from figure {A4.1}.

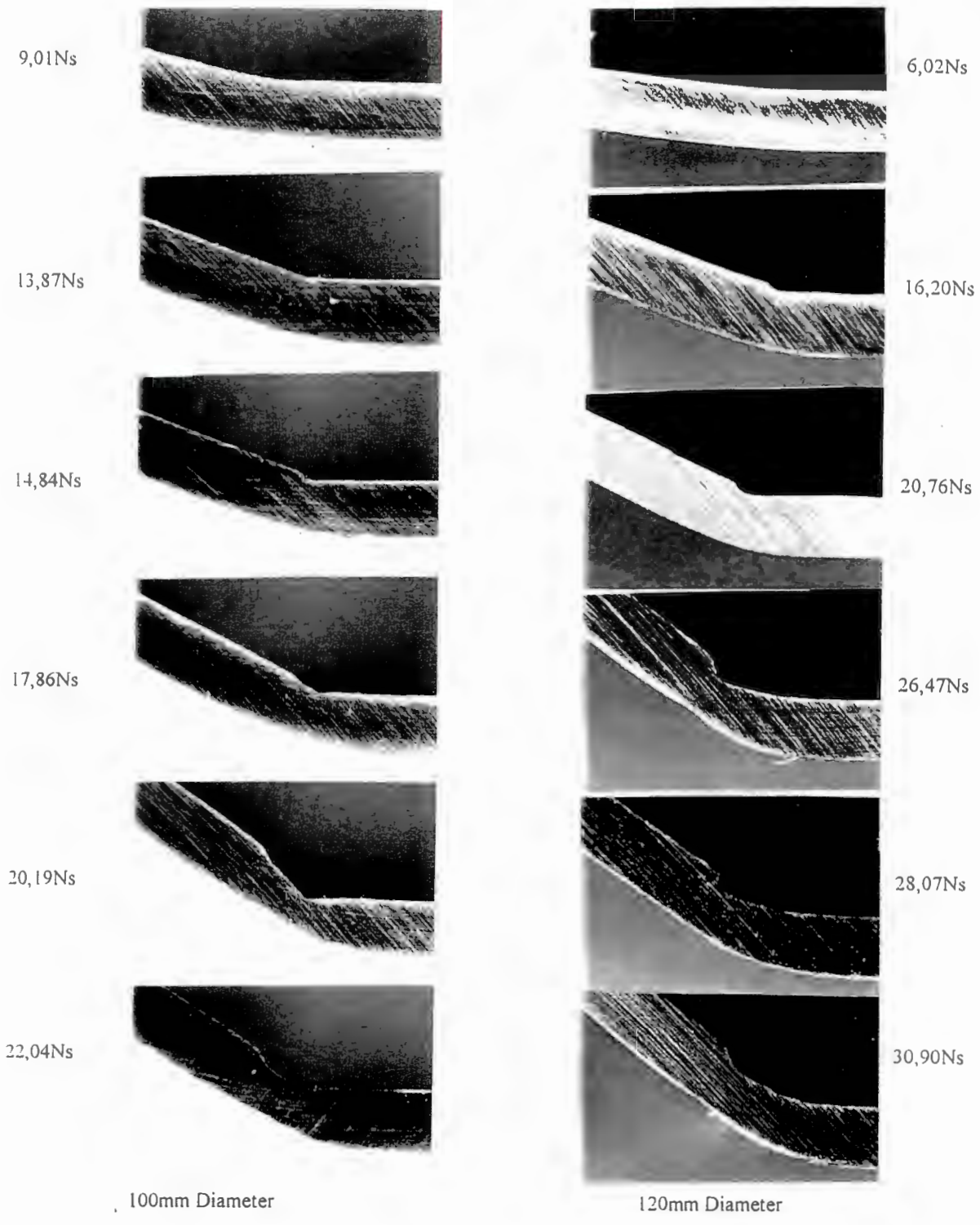

Figure {A4.4} Boundary detail of plate response for 100mm and 120mm clamped plates from figure {A4.1}.

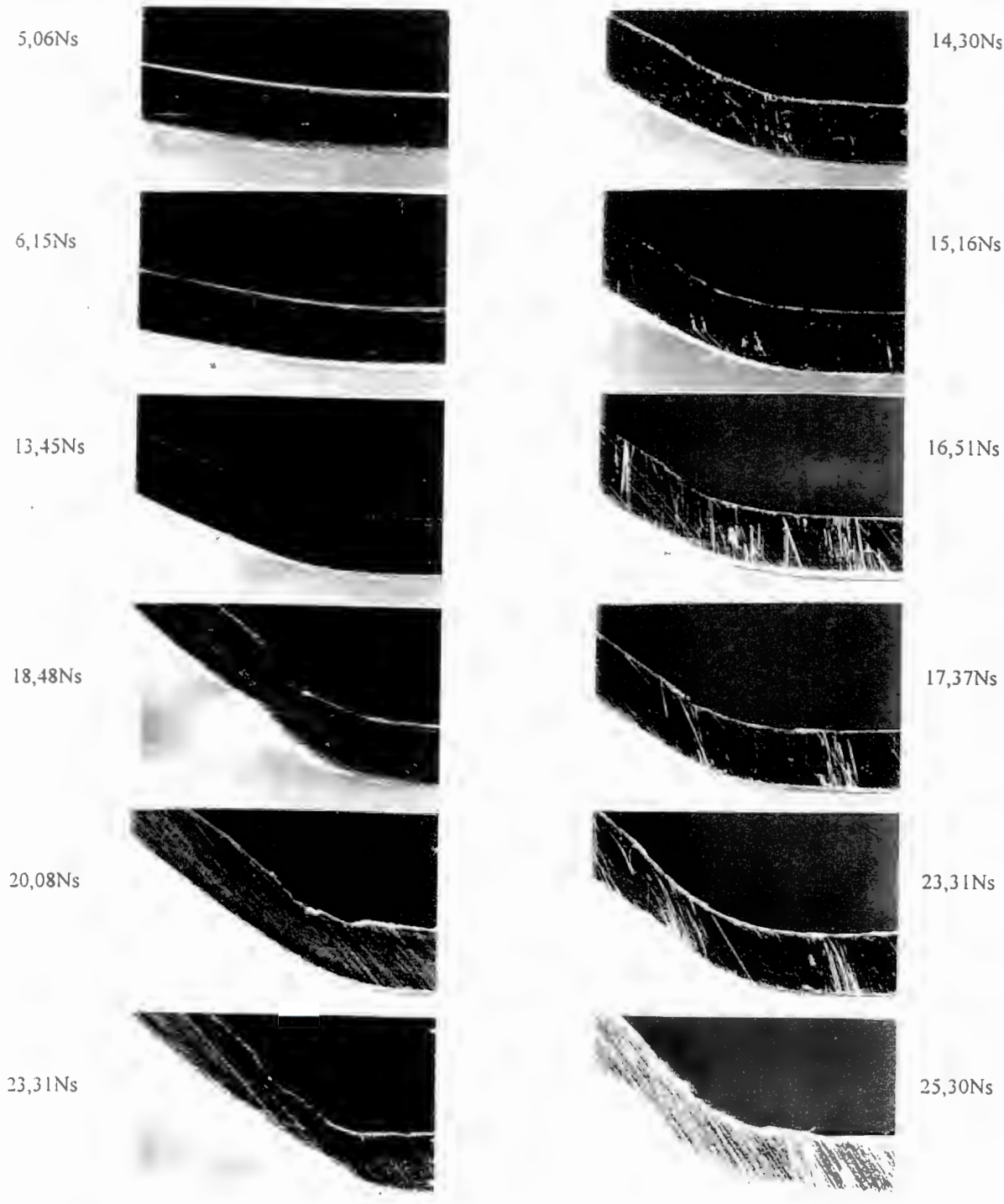

Figure {A4.5} Boundary detail of plate response for 100mm clamped plates with different clamp edge radii from figure {A4.2}.

APPENDIX 5 : TABULATED NUMERICAL PREDICTIONS

The numerical predictions for mid-point deflection from this investigation are tabulated below for reference.

diameter =	120mm		diameter =	100mm		diameter =	80mm
thickness =	1.6mm		thickness =	1.6mm		thickness =	1.6mm
boundary condition =	clamped		boundary condition =	clamped		boundary condition =	clamped
edge radius =	sharp		edge radius =	sharp		edge radius =	sharp
IMPULSE	MID-POINT DEFLECTION		IMPULSE	MID-POINT DEFLECTION		IMPULSE	MID-POINT DEFLECTION
4	4.1		4	3.9		4	5.4
8	7.4		8	9.1		8	10.6
12	11.3		12	13.8		12	16.0
16	15.3		16	17.9		16	20.9
20	18.9		20	21.9			
diameter =	100mm		diameter =	100mm			
thickness =	1.6mm		thickness =	1.6mm			
boundary condition =	clamped		boundary condition =	clamped			
edge radius =	1.6mm		edge radius =	3.2mm			
IMPULSE	MID-POINT DEFLECTION		IMPULSE	MID-POINT DEFLECTION			
4	4.4		4	4.4			
8	9.5		8	9.5			
12	14.2		12	14.2			
16	18.6		16	18.6			
20	22.8		20	22.8			
diameter =	100mm		diameter =	100mm		diameter =	100mm
thickness =	1.6mm		thickness =	2.0mm		thickness =	2.75mm
boundary condition =	fully built-in		boundary condition =	fully built-in		boundary condition =	fully built-in
fillet radius =	sharp		fillet radius =	2.0mm		fillet radius =	3.0mm
IMPULSE	MID-POINT DEFLECTION		IMPULSE	MID-POINT DEFLECTION		IMPULSE	MID-POINT DEFLECTION
4	3.9		4	2.0		4	0.3
8	9.2		8	6.4		8	3.4
12	13.3		12	10.0		12	6.9
16	17.7		16	13.6		16	9.2
20	21.9		20	16.7		20	11.2
			26	21.3		36	20.6
						50	28.3
diameter =	100mm						
thickness =	1.9mm						
boundary condition =	fully built-in from one side						
fillet radius =	2.0mm						
IMPULSE	MID-POINT DEFLECTION						
4	3.0						
8	7.7						
12	11.6						
16	15.4						
20	19.1						
30	27.6						

APPENDIX 6 : COURSES AND PAPERS

The following courses have been undertaken by the author for partial fulfillment of the requirements for the Degree of Master of Science:

CAM 500Z	Applied Mechanics A	3 credits
CAM 501Z	Applied Mechanics B	3 credits
CAM 502Z	An introduction to Finite Elements . .	3 credits
CAM 503Z	Finite Element Analysis . . .	4 credits
CAM 504Z	Engineering Software Design and Development	3 credits
MEC 536F	Managing for Performance Improvement .	5 credits
		total = 21 credits

Papers published or presented:

G. N. NURICK, M. E. GELMAN, N. S. MARSHALL, **Tearing of blast loaded plates with clamped boundary conditions,** *Int. J. Impact Engng.* **18**, (1996) [to appear].

M. E. GELMAN, G. N. NURICK, G. P. MITCHELL, **A numerical study of inelastic failure of impulsively loaded circular plates, with various boundary conditions,** *Proceedings of the 1st South African Conference on Applied Mechanics, Gauteng.* 223-234, (1996).